Key Points:
- Drylands are one of the most sensitive areas to climate change and human activities
- Attribution of major drivers and processes to dryland climate change has been summarized
- Enhanced warming, increasing aridity, and expanding drylands pose a threat to developing countries

Dryland climate change: Recent progress and challenges

J. Huang[1] iD, Y. Li[1,2] iD, C. Fu[3,4] iD, F. Chen[5], Q. Fu[1,6] iD, A. Dai[7] iD, M. Shinoda[8], Z. Ma[4], W. Guo[3] iD, Z. Li[9,10], L. Zhang[1] iD, Y. Liu[1], H. Yu[1], Y. He[1] iD, Y. Xie[1], X. Guan[1] iD, M. Ji[1], L. Lin[11] iD, S. Wang[12] iD, H. Yan[1], and G. Wang[1]

[1]Key Laboratory for Semi-Arid Climate Change of the Ministry of Education and College of Atmospheric Sciences, Lanzhou University, Lanzhou, China, [2]Agronomy College, Shenyang Agricultural University, Shenyang, China, [3]Institute for Climate and Global Change Research and School of Atmospheric Sciences, Nanjing University, Nanjing, China, [4]Key Laboratory of Regional Climate-Environment Research for Temperate East Asia, Institute of Atmospheric Physics, Chinese Academy of Science, Beijing, China, [5]College of Earth and Environmental Sciences and MOE Key Laboratory of Western China's Environmental Systems, Lanzhou University, Lanzhou, China, [6]Department of Atmospheric Sciences, University of Washington, Seattle, Washington, USA, [7]Department of Atmospheric and Environmental Sciences, University at Albany, Albany, New York, USA, [8]Graduate School of Environmental Studies, Nagoya University, Nagoya, Japan, [9]Department of Atmospheric and Oceanic Science and ESSIC, University of Maryland, College Park, Maryland, USA, [10]State Key Laboratory of Earth Surface Processes and Resource Ecology and College of Global Change and Earth System Science, Beijing Normal University, Beijing, China, [11]School of Atmospheric Sciences, Sun Yan-sen University, Guangzhou, China, [12]Key Laboratory of Arid Climatic Change and Reducing Disaster of Gansu Province and Key Open Laboratory of Arid Climatic Change and Disaster Reduction of CMA, Institute of Arid Meteorology, CMA, Lanzhou, China

Abstract Drylands are home to more than 38% of the world's population and are one of the most sensitive areas to climate change and human activities. This review describes recent progress in dryland climate change research. Recent findings indicate that the long-term trend of the aridity index (AI) is mainly attributable to increased greenhouse gas emissions, while anthropogenic aerosols exert small effects but alter its attributions. Atmosphere-land interactions determine the intensity of regional response. The largest warming during the last 100 years was observed over drylands and accounted for more than half of the continental warming. The global pattern and interdecadal variability of aridity changes are modulated by oceanic oscillations. The different phases of those oceanic oscillations induce significant changes in land-sea and north-south thermal contrasts, which affect the intensity of the westerlies and planetary waves and the blocking frequency, thereby altering global changes in temperature and precipitation. During 1948–2008, the drylands in the Americas became wetter due to enhanced westerlies, whereas the drylands in the Eastern Hemisphere became drier because of the weakened East Asian summer monsoon. Drylands as defined by the AI have expanded over the last 60 years and are projected to expand in the 21st century. The largest expansion of drylands has occurred in semiarid regions since the early 1960s. Dryland expansion will lead to reduced carbon sequestration and enhanced regional warming. The increasing aridity, enhanced warming, and rapidly growing population will exacerbate the risk of land degradation and desertification in the near future in developing countries.

Table of Contents

1. Introduction

Drylands are commonly defined as regions in which the annual potential evapotranspiration (PET) greatly exceeds annual precipitation (P); that is, the P/PET ratio is less than 0.65 [*Hulme*, 1996; *Safriel et al.*, 2005; *Feng and Fu*, 2013]. The P/PET ratio, termed as the Aridity Index (AI), reflects the scarcity of water supply relative to atmospheric demand for moisture. Based on this ratio, drylands can be further classified as hyperarid, arid, semiarid, and dry subhumid areas [*United Nations Convention to Combat Desertification (UNCCD)*, 1994; *Mortimore*, 2009; *Feng and Fu*, 2013; *Spinoni et al.*, 2015]. Over drylands, precipitation is scarce and highly variable [*Middleton and Thomas*, 1997; *Vallejo et al.*, 2012; *Ryan and Elsner*, 2016]. In contrast, PET, which represents the evaporative demand of the atmosphere, stays relatively high because of the high surface air temperature (SAT), low humidity, and abundant solar radiation over drylands [*Mortimore*, 2009; *Ji et al.*, 2015]. Globally, drylands occupy approximately 41% of terrestrial land surfaces [*White and Nackoney*, 2003] and account for approximately 40% of the global net primary productivity [*Grace et al.*, 2006; *Wang et al.*, 2012]. Drylands are home to 2.5 billion people (more than 38% of the world's population) [*Reynolds et al.*, 2007; *Mortimore*, 2009; *United Nations Development Programme (UNDP)*, 2014], and 90% of these people live in developing countries [*GLP*, 2005; *Safriel et al.*, 2005; *Armah et al.*, 2010]. Because of the low fertility of dryland soils, these areas are extremely sensitive to degradation induced by climate warming and human activities [e.g., *Scheffer et al.*, 2001; *Fu and An*, 2002; *Rietkerk et al.*, 2004; *MEA*, 2005; *Maestre et al.*, 2013; *J. Li et al.*, 2016; *Zhou et al.*, 2016]. Climate change in drylands strongly influences the economy and society especially in developing countries [*Huang et al.*, 2017a; *Fu and Mao*, 2017]. Therefore, improving our understanding of and ability to predict dryland climate and its change is a top priority for climate research [*Breshears and Barnes*, 1999; *Verstraete et al.*, 2008; *Qi et al.*, 2012]. The dryland study has been a major theme in a number of international research programs, such as Global Land Project (GLP, http://www.globallandproject.org), Global Water System Project (GWSP, http://www.gwsp.org), Integrated Land-Ecosystem-Atmosphere Processes Study (iLEAPS, http://www.atm.helsinki.fi/ILEAPS), and Monsoon Asia Integrated Regional Study (MAIRS) [*Fu and De Vries*, 2006].

The largest warming during the last 100 years was observed over drylands and accounted for more than half of the continental warming [*Huang et al.*, 2012, 2017b; *Ji et al.*, 2014]. Over the global semiarid regions, the warming of 1.53°C from 1901 to 2009 during the boreal cold season exceeded that for the annual-mean temperature increase of 1.13°C [*Huang et al.*, 2012]. Models project additional warming of over 2°C and 4°C in drylands by the end of the 21st century, respectively, for Representative Concentration Pathway (RCP) 4.5 and RCP8.5 scenarios [*Intergovernmental Panel on Climate Change (IPCC)*, 2013]. Additionally, models project that P will generally increase in drylands [*Bates et al.*, 2008; *Zhao et al.*, 2014] in the 21st century. PET, which is

crucial for the aridity index, is also projected to increase greatly [*Feng and Fu*, 2013; *Scheff and Frierson*, 2014; *Zhao and Dai*, 2015, 2016]. Both observations [*Dai et al.*, 2004; *Ma and Fu*, 2007; *Dai*, 2011a, 2011b, 2013b; *Feng and Fu*, 2013; *Huang et al.*, 2016a; *Trenberth et al.*, 2014; *Dai and Zhao*, 2016] and model simulations [*Dai*, 2011a, 2013b; *Feng and Fu*, 2013; *Fu and Feng*, 2014; *Zhao and Dai*, 2015, 2016] show that the aridity has increased globally since around 1950 and that this drying trend may continue in the 21st century because of global warming, especially over drylands, where enhanced warming is projected. Mainly because of the large PET increase associated with rising SAT, a drier climate is projected for a substantial portion of drylands [e.g., *Dai*, 2011a, 2013b; *Hughes*, 2011; *Cook et al.*, 2014a; *Scheff and Frierson*, 2015; *Huang et al.*, 2017a; *Fu and Mao*, 2017] and dryland expansion by 2100 is expected [*Feng and Fu*, 2013; *Fu et al.*, 2016; *Huang et al.*, 2017a]. These changes in temperature, precipitation, and PET may alter terrestrial ecosystems [*Osmond et al.*, 2004; *Kullman*, 2006; *Zeng and Yoon*, 2009; *Badreldin and Goossens*, 2015; *Sylla et al.*, 2015; *Yu et al.*, 2015; *Klein et al.*, 2017; *Seddon et al.*, 2016; *Sjögersten and Wookey*, 2016; *Wu et al.*, 2016], hydrology [*Ohmura and Wild*, 2002; *Cudennec et al.*, 2007; *Angeler et al.*, 2014; *Hu et al.*, 2015], and agricultural production [*El-Beltagy and Madkour*, 2012; *Valizadeh et al.*, 2014; *Hadgu et al.*, 2015] over drylands. Because of the drastic climate change and fragile ecosystems of drylands, a better understanding of dryland climate change and its impact is required for further research and policy making.

The causes of climate change in drylands have been investigated on different temporal and spatial scales [e.g., *Ma and Shao*, 2006; *Fu et al.*, 2008; *He et al.*, 2014; *Zhang et al.*, 2014; *Huang et al.*, 2016a; *Fu and Mao*, 2017]. These studies have addressed both natural (e.g., El Niño–Southern Oscillation (ENSO) [*Mullan*, 1995; *S. Wang et al.*, 2014]) and human-induced influences (e.g., increased greenhouse gas (GHG) emissions [*Rotenberg and Yakir*, 2010]). Atmospheric modeling studies with specified sea surface temperatures (SSTs) support an important role of oceans in controlling the dryland climates in the Sahel [*Bader and Latif*, 2003; *Lu and Delworth*, 2005; *Hoerling et al.*, 2006; *Lu*, 2009], Asia [*Fu et al.*, 2008; *Zhao and Zhang*, 2015], and North America [*H. Li et al.*, 2010]. In some dryland regions, climate change and human mismanagement have interacted to initiate the process of desertification (i.e., long-term land degradation) [*White and Nackoney*, 2003; *Winslow et al.*, 2004]. The concerns over the future of drylands are intensified by the expansion of human development into drylands as population growth continues and by the prospects of global and regional climatic change. Even more unsettling are claims that many other human activities, including land use, may induce climatic changes [*Taylor et al.*, 2002; *Gao et al.*, 2003; *Olson et al.*, 2008; *Li and Zhao*, 2012]. In recent decades, because of the population growth and migration and changes in land use practices, new burdens have been placed on the world's dryland ecosystems [*UNCCD*, 1994; *Nyamadzawo et al.*, 2009; *Hoover et al.*, 2015]. As a result of surface and soil water deficits, land degradation is becoming a serious threat to drylands [*Nahal*, 1995; *Qi et al.*, 2012; *Tarnavsky et al.*, 2013]. Dryland climate change is also increasing the challenges related to food security and water supply in these regions [*Kumar and Parikh*, 2001; *Asseng and Pannell*, 2013; *Zinyengere et al.*, 2014].

Driven by the underlying trend of global warming, what is the difference of the warming trend between drylands and humid regions? What are the mechanisms of the changes in temperature, precipitation, aridity index, and other climate variables in drylands over the world? What are the responses of dryland ecosystems to the changing climate? These are some of the questions facing dryland climate research. In recent years, dryland climate change has evolved from an environmental issue to a complex sustainable development issue. To develop appropriate strategies to cope with continued climate change in drylands and to maintain drylands as renewable resources, one critical need is to review the latest progress in dryland climate research. This article provides a general overview of recent dryland climate change studies with focuses on the following areas: (1) the difference in warming trends between drylands and humid regions, (2) different mechanisms driving climate change in different drylands, (3) the responses of dryland ecosystems to the changing climate, and (4) the feedbacks among the biological, hydrological and human systems over drylands.

This paper is organized as follows: We first present the dryland distribution and measures of aridity in section 2 and the temporal and spatial characteristics of dryland climate change in section 3. Then, we discuss some important mechanisms that may be responsible for dryland climate change, such as the impacts of dust-cloud interactions in section 4, atmosphere-dryland interactions in section 5, oceanic influences on drylands in section 6, and human activities in drylands in section 7. We also discuss dryland expansion, desertification and adaptation in section 8. A summary and discussions are given in section 9.
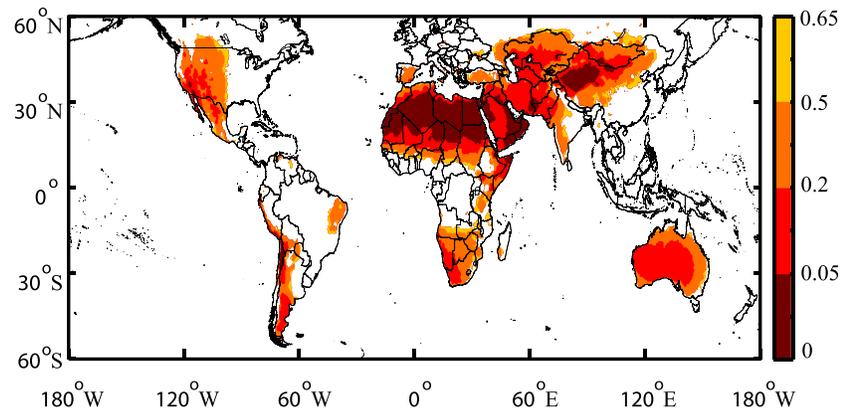
Figure 1. Global distribution of drylands for 1961–1990 climatology based on the aridity index (AI). Cited from *Huang et al.* [2016a].

2. Dryland Distribution and Measures of Aridity

2.1. Distribution of Drylands and Arid Climatology

The locations of drylands and arid climate are determined primarily by atmospheric general circulation (specifically, the subsidence of the Hadley circulation) and large-scale topography. The subtropical highs play an important role in the development of dryland climates in the middle to low latitudes because they are associated with the main factors promoting aridity (e.g., subsidence, divergent airflow, and thermal stability). The drylands over Australia, northern and southern Africa, the Middle East, and southwestern North America are strongly linked to the subtropical highs together with the descending branch of the Hadley cells [*Shin et al.*, 2012; *Scheff and Frierson*, 2012b]. Moreover, topography strongly impacts the aridity of some dryland regions in Asia, South America, the western United States, and the Horn of Africa because high terrains produce lee rain shadows and block the passage of rain-bearing disturbances. For example, huge drylands were formed in Asia at the time of rapid uplifting of the Tibetan Plateau as a natural process of Earth evolution [*An et al.*, 2001]. The dry climates in central Asia and the Sahara are also enhanced by their long distances from major sources of moisture. Furthermore, diabatic heating in monsoon regions can induce a Rossby wave response to the west, interacting with the midlatitude westerlies and producing a region of adiabatic descent [*Rodwell and Hoskins*, 1996, 2001]. According to this mechanism, desertification can also be influenced by remote changes in monsoon regions in addition to local effects. In summary, large-scale atmospheric circulations and regional topographic effects interact with synoptic-scale (e.g., cyclones, anticyclones, and tropical storms) and mesoscale systems (e.g., sea breezes and mountain winds) to control the essential components of dryland climates [*Nicholson*, 2011].

Over drylands, the air is almost always "thirsty" for water, but precipitation is not enough to meet this demand. A term associated with drylands is aridity, which implies a permanent water deficiency closely related to strong insolation, high temperature, strong PET, and low humidity [*Mainguet*, 1999]. Drylands defined by the P/PET ratio, also referred as the AI (see section 2.3 for details), are primarily distributed in middle and low latitudes (Figure 1). Major hyperarid (AI < 0.05) areas are located over the central and northern Sahara Desert, the Rub al Khali Desert, and Arab Plateau in the eastern and northwestern Arabian Peninsula, and the Taklimakan Desert in northwestern China. Arid (0.05 ≤ AI < 0.2) areas are located over the southern Sahara Desert, the Kalahari Desert in southwestern Africa, western and central Arabia Peninsula, central Asia, southwestern United States, eastern Patagonia, and much of Australia. Semiarid (0.2 ≤ AI < 0.5) and dry subhumid (0.5 ≤ AI < 0.65) regions mainly occur in the western United States, the west coast of South America, Central and East Asia, southern Africa, and a large portion of Australia outside of the central desert regions (Figure 1) [*Huang et al.*, 2016a].

2.2. Transitional Climate Zone (TCZ)

Early in the 1980s, Fu and colleagues raised the issue of the regionality of global change [*Fu*, 1989] and showed that certain regions are more sensitive to both natural and anthropogenic forcings, such as the transitional zones of climates and ecosystems. These regions are characterized by their instability, which is

related to strong gradients of climate and biological variables [*Di Castri et al.*, 1988; *Fu*, 1985, 1992; *Wen and Fu*, 2000], and are termed "transitional climate zones" (TCZs) [*Yeh and Fu*, 1984; *Fu*, 1992]. *Fu* [1992] described the three broad-scale TCZs in China and the related biome ecotones. The interaction between the East Asian summer monsoon (EASM) and the midlatitude westerlies [*Qian et al.*, 2009] and mixed agricultural-pastoral activities make these regions highly vulnerable to natural disasters [*Shi et al.*, 1994; *Shi*, 1996] and very sensitive to climate change and human activities [*Fu*, 1992; *Fu and Wen*, 2002]. Moreover, vegetation growth in these regions is relatively unstable [*Ou and Qian*, 2006].

For example, the semiarid region of northern China is a transitional zone between the inland arid region of northwestern China and the humid monsoon region of southeastern China. This region is very sensitive to both climate change and land use/land cover change. In the last century, the most significant aridity trend occurred over this region and other semiarid regions of the world [*Fu and Wen*, 2002; *Ma and Fu*, 2003; *Dai et al.*, 2004; *Dai*, 2011a, 2011b; *Dai and Zhao*, 2016]. Recent studies also highlighted more significant warming across all semiarid regions, relative to other parts of the world [*Huang et al.*, 2012, 2017b; *Ji et al.*, 2014; *Guan et al.*, 2015].

Wen and Fu [2000] analyzed normalized difference vegetation index (NDVI) data from satellite remote sensing and identified the locations of transitional climate and ecological zones in East China based on the variance contribution of the first empirical orthogonal function (EOF) mode and by matching it with divisions in previous studies. This result verifies the existing divisions of climate and ecological zones over this region. *Zhang and Zhang* [2005] examined the interannual variations and probability distributions of temperature and precipitation in the TCZ of northeastern China during 1951–2000. Results indicated that the probability distribution differences were closely related to the high frequency of extreme weather and climate events and the increasing probability of warm-dry winters and hot-drought summers.

Wang et al. [2016] examined the spatial and temporal variations of the TCZ in East Asia using observational data and model simulations. Results indicated that the TCZ edges shifted southeastward from 1961 to 2014 because of increasing aridity. Furthermore, most climate models can reproduce the shape and orientation of the TCZ. Indeed, the models project that the front edge of the TCZ will continue its southeastward displacement, whereas the rear edge will respond in an opposite direction under global warming scenarios in the 21st century. These projections imply that the TCZ will expand, the humid zone will contract, and the arid zone will retreat northwestward.

2.3. Measures of Aridity Changes

Drylands are not uniform and differ in terms of their degrees of aridity. *Wallén* [1967] identified three approaches for defining aridity: classical, index and water balance approaches. The classical approach mainly focuses on climatic variables, such as the amount, variability, and intensity of precipitation. The well-known index approach corresponds to the climate classification first proposed by *Köppen* [1884], which was based on annual temperature and precipitation. The water balance approach was initially explored by Thornthwaite and Penman, who both developed the concept of PET in 1948 [*Penman*, 1948; *Thornthwaite*, 1948]. PET reflects the atmospheric demand for moisture, which is the maximum amount of water that can be lost to the air from a surface with an unlimited supply of water under a given atmospheric condition. Over drylands, PET greatly exceeds P, and P/PET ratios are below 0.65 [*Hulme*, 1996; *Safriel et al.*, 2005; Feng and Fu, 2013].

Stadler [2005] and *Dai* [2011a] summarized several aridity indices for quantifying the degree of dryness or water deficiency at a given location. *Budyko* [1958] used the ratio of P to net radiation as a measure of aridity, which has been widely and effectively adopted in the hydrology and land surface communities over the last 50 years [*Blöschl et al.*, 2013]. The original Palmer Drought Severity Index (PDSI) created by *Palmer* [1965] is based on both precipitation and SAT, and it has been widely used in drought monitoring and research, including reconstructions of drought, particularly in the United States [e.g., *Dai et al.*, 1998, 2004; *Cook et al.*, 1999; *Heim*, 2002; *Dai*, 2011a, 2011b; *Cook et al.*, 2014b]. For assessing aridity changes under rising temperature [*Burke and Brown*, 2008; *Burke*, 2011; *Dai*, 2011a, 2011b; *van der Schrier et al.*, 2011; *Cook et al.*, 2014a; *Dai and Zhao*, 2016], the more realistic Penman-Monteith PET has been used to replace the Thornthwaite PET used in the original PDSI, and local calibrations have been used in the improved self-calibrated PDSI [*Wells et al.*, 2004]. The Standardized Precipitation Index (SPI) [*McKee et al.*, 1993] and

the Standardized Precipitation Evapotranspiration Index (SPEI) [*Vicente-Serrano et al.*, 2010, 2012] have been used widely to monitor moisture conditions. The Surface Wetness Index (SWI) [*Hulme et al.*, 1992] can be used to track meteorological drought and to define drylands [*Ma and Fu*, 2003, 2006, 2007]. Moreover, soil moisture can effectively reflect the local dry/wet conditions and therefore can serve as a measure of aridity changes and agricultural drought. However, the application of soil moisture is restricted by the scarcity of station observations and problematic results derived from remote sensing [*Kerr*, 2007]. Therefore, studies of soil moisture are usually based on the outputs from numerical models [*Keyantash and Dracup*, 2002; *Qian et al.*, 2007; *Li and Ma*, 2013], which contain large biases and require careful validation [*Qian et al.*, 2006].

The AI was adopted by the United Nations Environment Programme (UNEP) as a measure of aridity in their landmark world atlas on desertification [*Middleton and Thomas*, 1997], which is widely used for defining dry-lands and studying dryland climate change [e.g., *UNCCD*, 1994; *Hulme*, 1996; *Safriel et al.*, 2005; *Mortimore*, 2009; *Feng and Fu*, 2013; *Huang et al.*, 2016a, 2017a]. *Huang et al.* [2016a] compared three commonly used methods for identifying aridity changes and suggested that using the AI to identify aridity produces the most reasonable and reliable results among these three methods. Reconciling different measures of terrestrial arid-ity to address various environmental issues in a rapidly changing climate is an important topic that should be addressed in future research [*Fu et al.*, 2016].

3. Temporal and Spatial Characteristics of Dryland Climate Change

In this section, we will provide an overview of the temporal and spatial characteristics of dryland climate change on multiple time scales, ranging from annual to millennial, based on paleoclimatic reconstructed data, modern observational data, and model projections.

3.1. Analysis of Paleoclimatic Reconstructed Data

The climate records from instrumental observations roughly started 400 years ago, but these instrumental records in most drylands barely extend beyond one century. As a result, proxy records are utilized for climate reconstruction, including ice cores, ocean sediment cores, lake sediments, glacial deposits, pollen, and others. In drylands, sand dunes, aeolian sediments, and evaporite deposits have also provided a wealth of evidence for climate change [*Nicholson*, 2011].

Several large-scale temperature reconstructions have been performed [*Jones et al.*, 1998; *Esper et al.*, 2002a; *Mann and Jones*, 2003; *Moberg et al.*, 2005; *Mann et al.*, 2008]. These reconstructions show that the evolution of SAT in the Northern Hemisphere (NH) during the last millennium can be roughly divided into three major episodes: the Medieval Warm Period (MWP, from around 1000 to 1350 A.D.), the Little Ice Age (LIA, from around 1500 to 1850 A.D.), and the postindustrial warming. However, it is more difficult to reconstruct moisture or precipitation because of their heterogeneity on regional scales, which is due to differ-ences in atmospheric circulation patterns and topographic effects.

Many studies have examined the climate change over the drylands in the western United States based on var-ious paleoclimatic records from analyses of tree rings, sediments, pollen, and vegetation over the Holocene. They showed that the climate was warm and dry during the Middle Holocene (from around 6000 to 3300 B.C.) [*Grayson*, 2000; *Madsen et al.*, 2001; *Benson et al.*, 2002; *Jiang et al.*, 2007], and five extreme and persistent droughts in this period were identified by *Hughes and Graumlich* [1996], which occurred around 5970, 5881, 5591, 4058, and 3948 B.C. Moreover, a wide variety of evidence indicated that aridity in the western United States was intensified during the Medieval Climatic Anomaly (MCA, from around 900 to 1300 A.D., also known as the MWP) [e.g., *Stine*, 1994; *Cook et al.*, 2004; *Mason et al.*, 2004; *Cook et al.*, 2014b] and two centennial duration megadroughts in California were discovered by *Stine* [1994].

Arid Central Asia (ACA) is a unique dryland region. ACA is dominated by the midlatitude westerlies and strongly influenced by both North Atlantic sea surface temperature (SST) and high-latitude air temperature. Paleoclimatic data sets in this area are predominately derived from tree rings, ice cores, lake sediments, and archeological data related to lake level variations and glacier fluctuations from a wide variety of sites across ACA [e.g., *Thompson et al.*, 1995; *Esper et al.*, 2002b; *Solomina and Alverson*, 2004; *Sorrel et al.*, 2006; *Treydte et al.*, 2006; *Gates et al.*, 2008]. A synthesis of the available paleoclimatic records shows that ACA has experi-enced a relatively dry MWP and a wet LIA (Figure 2) and that precipitation and temperature over ACA are
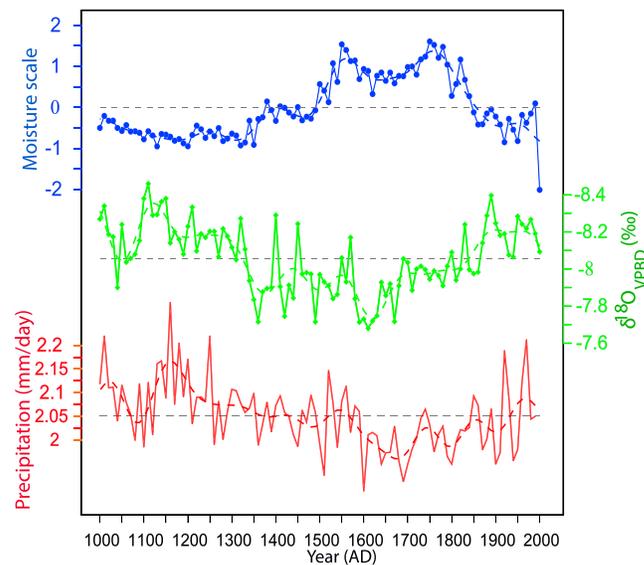
Figure 2. (top) The synthesized moisture anomaly over the last millennium with high (low) values indicating wet (dry) conditions from standardized high-resolution reconstructions of groundwater recharge rates based on chloride mass balance in the unsaturated zone over Arid Central Asia (ACA). Modified from *Chen et al.* [2010]. (middle) A 118 mm long stalagmite (WX42B) $\delta^{18}O$ record from Wanxiang Cave in the Asian monsoon controlled region. Modified from *Zhang et al.* [2008]. (bottom) The time series of May to August mean precipitation rate over extratropical Asian monsoon controlled region (36°N–50°N, 100°E–120°E) derived from the run that forced by three external forcing factors: solar variability, greenhouse gases in the atmosphere including CO_2 and CH_4, and an estimated radiative effect of stratospheric volcanic aerosols using an atmosphere-ocean coupled model ECHO-G which was implemented and developed at the Max-Planck Institute for Meteorology. Modified from *Liu et al.* [2011a].

negatively correlated on timescales ranging from annual to centennial over the last two millennia [*Yang et al.*, 2009; *Chen et al.*, 2010]. Other studies have shown that moisture variability in the ACA and the Asian monsoon-controlled region were out of phase during the early and late Holocene [*Chen et al.*, 2008], the last millennium (see Figure 2) [*Chen et al.*, 2010; *Liu et al.*, 2011a, 2014], and the past century [*Li et al.*, 2006, 2007; *Huang et al.*, 2013]. This is supported by the out-of-phase relationship of net snow accumulation changes in the northern and southern parts of the Tibetan Plateau on decadal to centennial timescales; these areas are controlled by the westerlies and the Indian monsoon, respectively [*Davis et al.*, 2005; *Wang et al.*, 2007]. Therefore, the spatial anomaly pattern over midlatitude Asia was arid in the west and central, but humid in the east during the MWP, and the opposite during the LIA.

Climate in the humid eastern part of Asia is controlled by monsoon circulation, which is largely driven by the land-sea thermal contrast caused by solar radiation [*Wang et al.*, 2005; *Jin et al.*, 2014]. *Zhang and Jin* [2016] used a coupled atmosphere–ocean general circulation model to explore the response of the Asian summer monsoon (ASM) to the solar forcing and oceanic feedbacks; they revealed that there was a circumglobal teleconnection (CGT) pattern in the summertime midlatitude circulation of the NH during the Holocene. This pattern is closely related to both the ASM and the climate of ACA and is probably responsible for the out-of-phase relationship in effective moisture between ACA and monsoonal Asia. *Chen et al.* [2010] also proposed that the wet climate of ACA during the LIA, which may have extended as far as the Mediterranean Sea and Western Europe, may have resulted from an increase in precipitation caused by frequent cyclone activity caused by an equatorward shift of the westerlies. This result could also be partially attributed to the predominately negative North Atlantic Oscillation (NAO) conditions at that time, coupled with decreased evapotranspiration due to colder temperatures.

Zhao et al. [2008] used pollen data from 30 sites to investigate changes in vegetation and climate over dryland areas of China and found that the vegetation responses suggested a drying trend during the late Holocene, although the responses were regionally diverse during the early Holocene. This conclusion is supported by several site-specific studies [*Hartmann and Wünnemann*, 2008; *Henderson and Holmes*, 2008; *X. Huang et al.*, 2008; *Sun et al.*, 2009; *Zhang et al.*, 2008]. Based on tree-ring width chronologies, *Chen et al.* [2015, 2016a, 2016b] developed new precipitation reconstructions for the Xinglong Mountains (1816–2010 A.D.), Helan Mountains (1760–2006 A.D.), and Mount Huashan (1482–2012 A.D.). The precipitation reconstructions for the Xinglong Mountains (Helan Mountains and Mount Huashan) explained 55.8% (52.1% and 55%) of the variance in precipitation during the period 1951–2010 (1953–2008 and 1953–2012). Thus, compared to observed gridded precipitation data, the tree-ring records were able to capture much of the interannual and decadal variability in the region. Moreover, *Cook et al.* [2010] used tree rings from more than 300 sites across Asian monsoon region to reconstruct summer PDSI. These reconstructions comprise the Monsoon Asia Drought

Atlas, which provides the spatiotemporal details of known historic monsoon failures and reveals the details of unknown megadroughts and their linkages to tropical Indo-Pacific SSTs.

3.2. Analysis of Modern Observational Data

Many studies have investigated historical precipitation changes over land using rain gauge records [e.g., *Diaz et al.*, 1989; *Dai et al.*, 1997; *IPCC*, 2013; *Xu et al.*, 2015]. As discussed in *Trenberth et al.* [2014] and *Dai and Zhao* [2016], some of the most widely used land precipitation data sets become unreliable after the 1990s due to a sharp drop in the number of rain gauges included in these data sets [*Schneider et al.*, 2014]. Nevertheless, many dryland areas show a drying trend beginning around 1950, including in parts of Africa, the Middle East, Central Asia, and South America. These trends are evident in historical precipitation and stream flow records as well as the observation-based PDSI (Figure 3). The recent drying over Africa, southern Europe, East Asia, and eastern Australia lead to a substantial increase in global aridity and drought areas [*Dai*, 2011a, 2011b, 2013b; *Dai and Zhao*, 2016; *Fu and Mao*, 2017]. A large part of this drying trend is related to precipitation decreases associated with natural decadal variability in the Pacific, and the rapid warming since the 1980s has also likely played a significant role [*Dai*, 2013b; *Dai and Zhao*, 2016].

Huang et al. [2016a] focused on global semiarid regions and obtained similar conclusions that a drying trend (a decrease in AI) from 1948 to 2008 occurred over East Asia, the Sahel in West Africa, southern Africa, and eastern Australia, whereas the semiarid regions over Central Asia, northern Australia, North America, and South America were getting wetter. The spatial distribution of precipitation trend is consistent with that of AI. *Cai et al.* [2012] also revealed that semiarid regions in the Southern Hemisphere, such as southern coastal Chile, southern Africa, and southeastern Australia, have experienced a drying trend in austral autumn since the late 1970s, predominantly during April and May.

Moreover, *Huang et al.* [2016a] analyzed variations in regionally averaged precipitation, PET, and AI over the semiarid regions in East Asia, Central Asia, and North America (see Figure 4). Considering that the newly formed semiarid regions transitioned from having a different climate, they are distinct from semiarid regions that have been presented for a long time; thus, each region is divided into old and newly formed semiarid regions. Figure 4 shows that there were consistent increasing and decreasing trends from 1948 to 2008 in annual precipitation, PET, and AI over the newly formed and old semiarid regions. Precipitation decreased in East Asia but increased in North America, and PET increased in East Asia but decreased in North America. Thus, the results for AI and precipitation are consistent, suggesting that climate is drying over East Asia but becoming wetter over North America, which are strongly associated with the weakened EASM and enhanced westerlies, respectively. The wetting trend since the 1950s over North America is largely related to multidecadal SST oscillations in the Pacific [*Dai*, 2013a].

From a global perspective, the continents in the Eastern Hemisphere have generally experienced drying but the American continents have become wetter [*Greve et al.*, 2014]. *Ma and Fu* [2007] analyzed the variations in the SWI from 1951 to 2002 and showed a drying trend in Africa and Eurasia during the period, but a wetting trend in North America during 1976–2002. They also identified a 30 year oscillation of dry-wet conditions in South America and Australia, with the latest one corresponding to a dry period. Moreover, this Southern Hemisphere dry-wet oscillation was closely related to large-scale SST variations in the Pacific. The out-of-phase relationship of the SWI between Africa/Eurasia and North America is correlated with the PDO; the interdecadal oscillation of SWI in South America and Australia is consistent with the interdecadal variation in the Southern Oscillation Index (SOI).

Many studies have examined climate changes over different parts of drylands [e.g., *Chen et al.*, 2011; *Y. Li et al.*, 2015]. For example, in central Asia, temperature was increasing (0.18°C per decade) during 1901–2003 [*Chen et al.*, 2009] and the increase rate is twice that in the NH [*Jones and Moberg*, 2003]; precipitation generally increased during 1930–2009 [*Chen et al.*, 2011], which was supported by the evidence of increasing moisture from tree-ring reconstructed PDSI [*Li et al.*, 2006]. Moreover, *Y. Li et al.* [2015] showed that there was a "wet-west and dry-east" anomaly pattern over the expanded drylands in northern China based on changes in precipitation and AI, consistent with the results from previous studies through analyses of daily rain gauge records in this region [*Gong et al.*, 2004; *Zhai et al.*, 2005; *Wang et al.*, 2013]. *Shi et al.* [2007] also showed that arid northwestern China has shifted to wetter conditions since the mid-1980s.
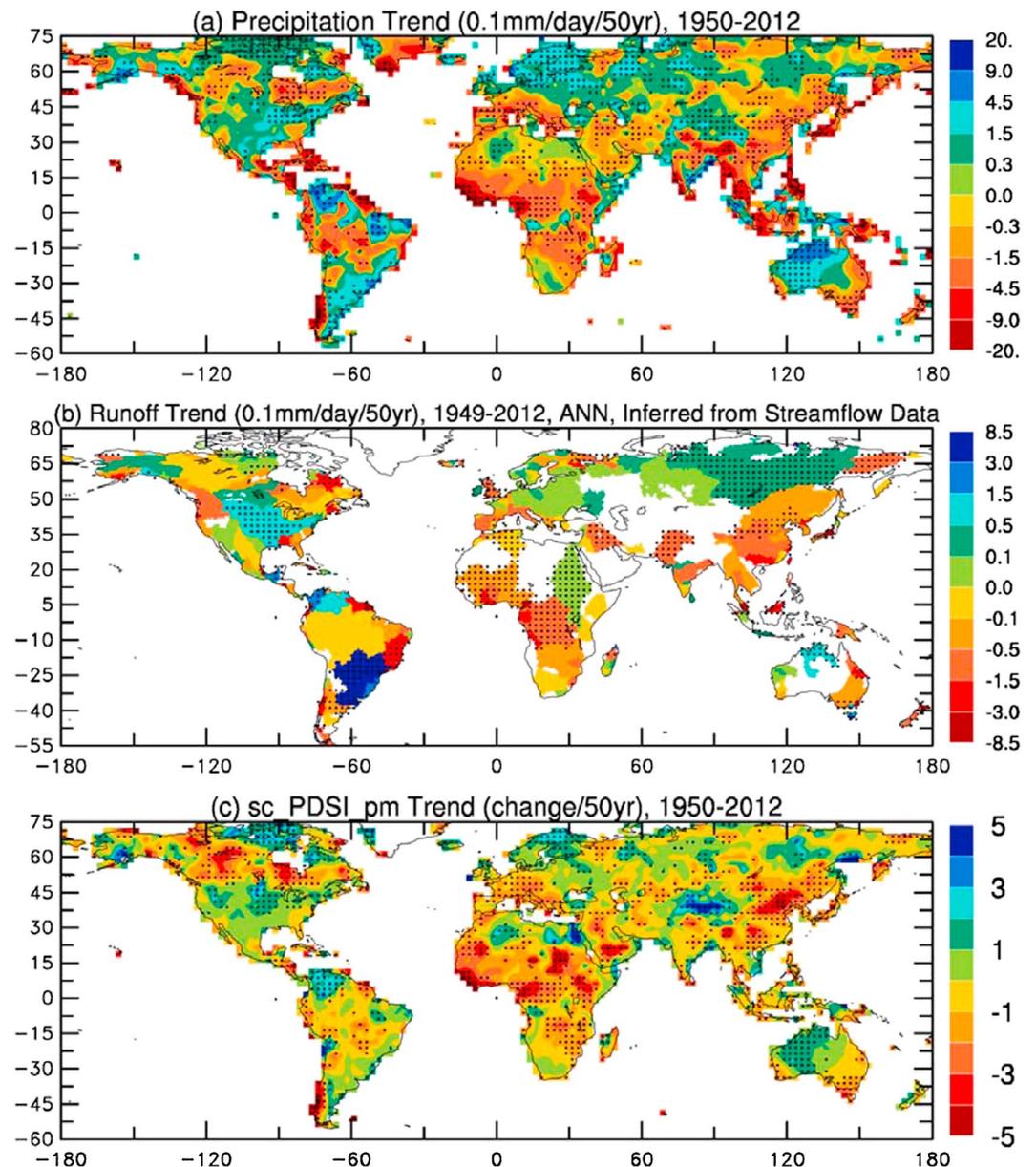
Figure 3. Long-term trend in annual (a) precipitation, (b) basin-mean runoff (inferred from streamflow gauge records for the water year from October of the previous year to September of the current year), and (c) self-calibrated PDSI with Penman-Monteith PET (sc_PDSI_pm) from 1950 to 2012. Blank land areas in Figure 3b do not have runoff into the oceans or do not have sufficient observations. A negative trend in sc_PDSI_pm indicates drying. Stippling indicates the trend is a statistically significant trend at the 5% level. Cited from *Dai and Zhao* [2016].

Purely based on their calculated PDSI changes, *Sheffield et al*. [2012] argued that the global drying trend during 1950–2008 is small and statistically insignificant. This is in sharp contrast to the significant drying trends since the 1950s over many land areas found by a number of studies as discussed above, in which the broad drying patterns are evident and consistent among different measures of aridity (Figure 3). Further analyses [*Trenberth et al*., 2014; *Dai and Zhao*, 2016] revealed that the small drying trend of *Sheffield et al*. [2012] likely resulted from their use of biased precipitation data since the 1990s and other issues in their analyses. Furthermore, *Dai and Zhao* [2016] showed that a large part of the historical drying trend is attributable to decreasing precipitation associated with multidecadal SST changes in the Pacific and the Atlantic Ocean; rapid warming since the 1980s has become an increasing important cause of the recent global drying trend.
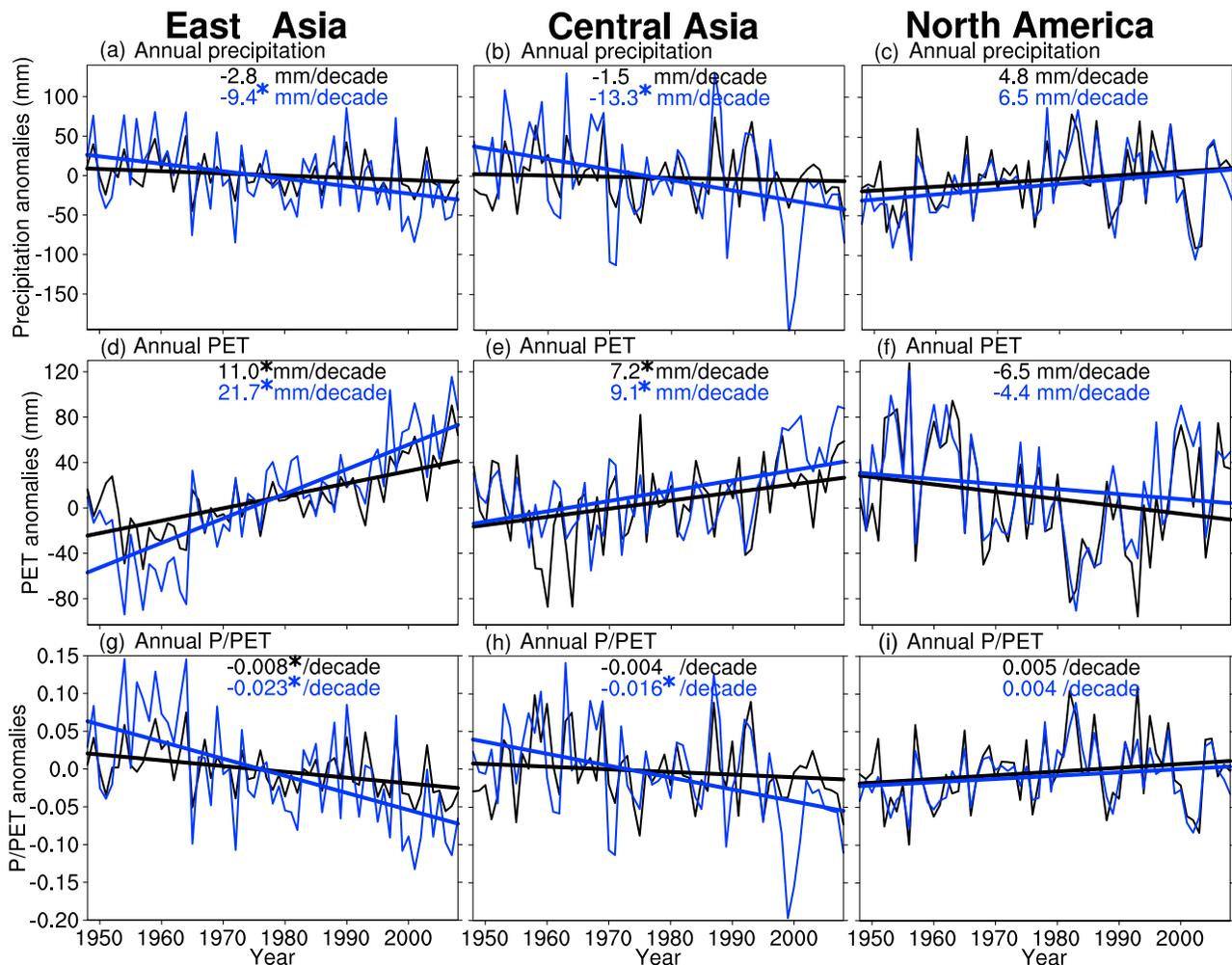
Figure 4. Variations in the regionally averaged annual (a-c) precipitation, (d-f) PET, and (g-i) AI in semiarid regions over East Asia, Central Asia, and North America from 1948 to 2008. The blue curves indicate newly formed semiarid regions, and the black curves denote old semiarid regions. The thick blue (black) lines show the linear trend for the curves. Asterisks indicate a trend that exceeds the 99% confidence level. Cited from *Huang et al.* [2016a].

Floods are among the worst weather-related hazards. Many hydrological approaches have been developed to investigate floods in humid areas; however, the hydrology of drylands differs from that of humid areas and it raises important scientific, technical, and logistical challenges [*Saber et al.*, 2015]. For example, there is a serious lack of data on many key hydrological processes in drylands, which makes it difficult to understand the hydrological processes in these regions [*McMahon*, 1979; *Pilgrim et al.*, 1988]. Although drylands are characterized by very low mean annual precipitation, due to their poor ability to retain water, drylands may still experience severe flooding (especially flash floods) following intense storms, which can cause widespread damages. In the hydrological literature, regional flood frequency analysis studies have seldom been applied to arid regions due to limited data availability [*Zaman et al.*, 2012].

3.3. Analysis of Model Simulations and Projections

Model-projected future changes in precipitation are more uncertain than those for temperature (Figures 5a and 5c), partly because of the large internal climate variability in regional precipitation [*Dai*, 2013a; *Dong and Dai*, 2015; *Zhao and Dai*, 2016]. For example, *Ji et al.* [2015] compared the observational data with Coupled Model Intercomparison Project phase 5 (CMIP5) simulations over the period 1948–2005 and found that the simulated mean precipitation on the global scale was too high over drylands, especially over the semiarid and dry subhumid regions. An analysis of multimodel projections shows that changes in annual precipitation ranged from −30% to 25% over drylands [*Bates et al.*, 2008]. Climate model projections suggested that under
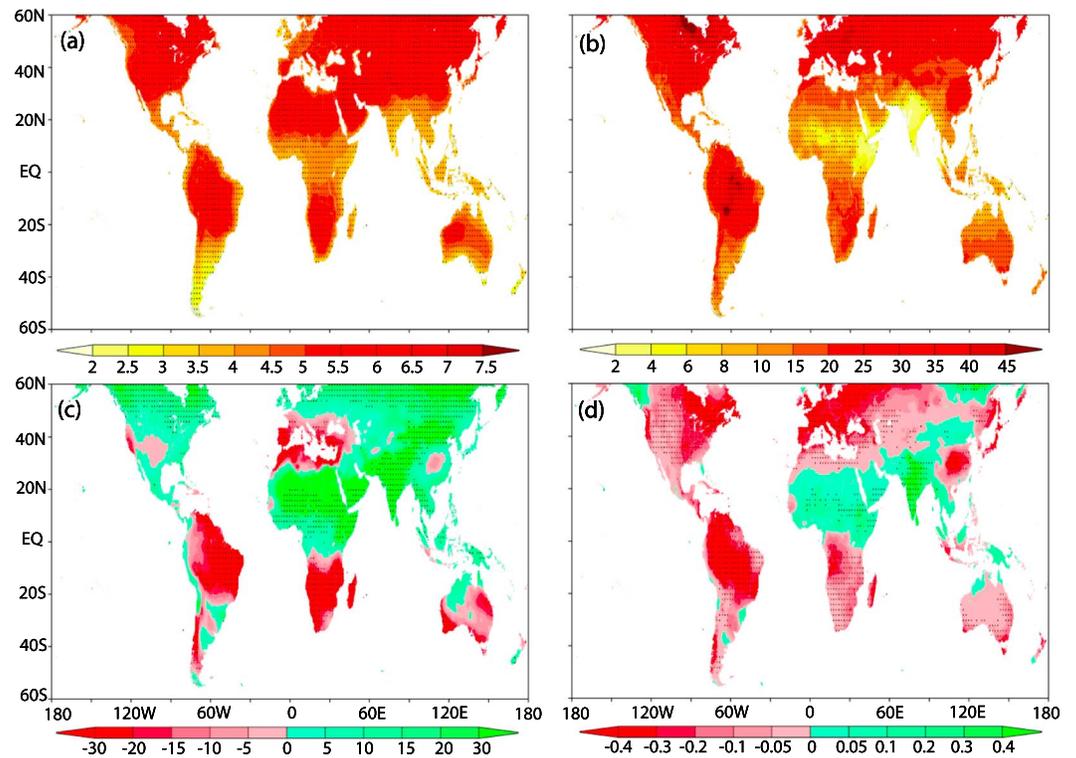
Figure 5. Projected changes in annual (a) SAT (°C), (b) PET (%), (c) precipitation (%), and (d) P/PET for 2071–2100 relative to 1961–1990 under the RCP8.5 scenario from 27 CMIP5 climate models. Grid points are stippled where more than 80% of the models agree on the sign of change. Cited from *Feng and Fu* [2013].

the RCP4.5 and RCP8.5 scenarios, precipitation is expected to increase by more than 40% over central Asia and the Sahara and Sahel but decrease by approximately 20% over southern Africa and northeastern South America [*Zhao et al.*, 2014; *Zhao and Dai*, 2016]. Partly due to large internal variability, the projected regional changes in seasonal and annual precipitation vary substantially among the CMIP5 model simulations [*Feng et al.*, 2014].

However, annual precipitation (Figure 5c) is generally projected to increase over most of Eurasia, tropical Africa, and the extratropical North America but to decrease in the subtropical regions, including areas near the Mediterranean Sea, southwestern North America, southern Africa, and most of Australia and South America [*Feng and Fu*, 2013; *Feng et al.*, 2014; *Zhao et al.*, 2014; *Zhao and Dai*, 2016]. *Scheff and Frierson* [2015] further argued that precipitation over land does not change uniformly in response to greenhouse warming, except for high latitudes. The response of precipitation to global warming (Figure 5c) can be partially explained by the poleward expansion of the Hadley cells [*Scheff and Frierson*, 2012a] and the "dry-get-drier, wet-get-wetter" thermodynamic mechanism [*Chou et al.*, 2009].

PET, which represents the evaporative demand of the atmosphere, is projected to increase over most land areas (Figure 5b) [*Feng and Fu*, 2013; *Scheff and Frierson*, 2014; *Zhao and Dai*, 2015]. The PET increase, estimated using the Penman-Monteith equation, results primarily from the increased water vapor deficit near the surface as temperature rises [*Scheff and Frierson*, 2014; *Sherwood and Fu*, 2014; *Zhao and Dai*, 2015]. Because of the large PET increase and the decreased precipitation over subtropical land areas, a drying trend is expected to occur in a large portion of drylands [*Zhao and Dai*, 2015, 2016], with an approximately 10% increase in world's desert areas [*Zeng and Yoon*, 2009] and an approximately 10% expansion in global dryland areas [*Feng and Fu*, 2013] (see also section 8.1).

Changes in global aridity are affected by changes in precipitation and temperature through their impact on PET. The PET increases greatly in North and South America, as well as the middle and high latitudes in the Eastern Hemisphere, with smaller increases over Africa, Australia, and India by the end of the 21st century

(Figure 5b) [*Feng and Fu*, 2013]. This PET change pattern is consistent with other studies [e.g., *Solomon et al.*, 2007; *Scheff and Frierson*, 2014; *Zhao and Dai*, 2015]. The projected changes in P/PET (Figure 5d) shows decreases in most of the global land surface, except for northern China, India, the southern Saharan, and eastern equatorial Africa regions; this finding is consistent with the shrinking drylands in these regions and expansion in others [*Feng and Fu*, 2013]. In summary, most of the model simulations show that drying is much more widespread than wetting in the low and middle latitudes because of ubiquitous PET increases and decreased precipitation over many subtropical regions [*Feng and Fu*, 2013; *Scheff and Frierson*, 2015; *Zhao and Dai*, 2015].

Many other studies [e.g., *Wang*, 2005; *Burke and Brown*, 2008; *Sheffield and Wood*, 2008; *Dai*, 2011a, 2013b; *Cook et al.*, 2014a; *Fu and Feng*, 2014; *Prudhomme et al.*, 2014; *Sherwood and Fu*, 2014; *Zhao and Dai*, 2015, 2016] have also analyzed climate model-projected changes in precipitation, soil moisture, runoff, and the off-line calculated PDSI (with Penman-Monteith PET) and P/PET ratio. All these studies found increased aridity and frequency of drought in the latter part of 21st century under moderate-to-high emissions scenarios. In particular, *Zhao and Dai* [2015] analyzed the off-line-calculated PDSI, and the top-10 cm soil moisture content and runoff directly from 14 CMIP5 models, of which at least nine of them included the effect of stomatal closure under increasing CO_2 levels; they found that all three measures of aridity show increased frequency of drought in the 21st century under a low-moderate emissions scenario, with the soil moisture-based estimates being the largest. Moreover, runoff-based drought frequency increases mainly due to the flattening of the probability density function for runoff, despite the increases in the mean runoff over many of these areas.

However, some studies have argued that the drying trends and increased drought stress may be considerably weaker and less extensive in the future than those indicated by AI or PDSI. *Swann et al.* [2016] indicated that in contrast with PDSI, only 37% of global land areas have increasing drought stress based on precipitation minus evapotranspiration (P-E), which is a measure of atmospheric moisture convergence. However, actual evapotranspiration is often limited by moisture availability in the soil (thus affected by aridity) and therefore is not a good measure of aridity or drought, especially under rising temperatures which lead to increased atmospheric demand for moisture. *Milly and Dunne* [2016] showed that the Penman-Monteith PET overestimates the evapotranspiration changes over nonwater-stressed land areas computed in CMIP5 models. They suggested that this may be because the calculations of the Penman-Monteith PET often neglect the stomatal conductance reductions induced by increasing CO_2 concentrations [*Roderick et al.*, 2015; *Swann et al.*, 2016] and water vapor demand [*Byrne and O'Gorman*, 2016; *Novick et al.*, 2016; *Parkes et al.*, 2017]. In fact, some models have already included the above plant physiological responses to elevated CO_2 [*Zhao and Dai*, 2015], implying that the projections of soil moisture and RH are reasonable. However, the projections of off-line-computed PET, AI, and PDSI may be overestimated because the r_s is assumed to be constant in the calculations. Moreover, soil moisture changes directly from the global climate models also suggest a severe drying trend and increased frequency of drought [*Wang*, 2005; *Sheffield and Wood*, 2008; *Zhao and Dai*, 2015]. Soil moisture projections from CMIP5 identify a robust vertical gradient of projected mean soil moisture changes, with more negative changes located near the surface [*Berg et al.*, 2017]. This is consistent with a surface drying trend induced by increased evaporative demand (i.e., PET), which would reduce the near-surface soil moisture more quickly than that in the deeper layers. However, the deep soil layer could become increasingly dry during the growing season in temperate drylands [*Schlaepfer et al.*, 2017]. The soil moisture and temperature feedback contribute significantly to the amplified warming on the hottest days [*Vogel et al.*, 2017; *Kala et al.*, 2016] and to the frequency of extreme daily precipitation [*May et al.*, 2016], as previously observed [*Donat et al.*, 2016; *Fischer and Knutti*, 2016].

4. Impacts of Dust-Cloud Interactions

Large amounts of mineral dust particles are emitted from dryland regions worldwide and play a very important role in local energy balance through direct [e.g., *Evan et al.*, 2009; *J. Huang et al.*, 2009; *Z. Li et al.*, 2010], indirect effects [e.g., *Twomey*, 1977; *Albrecht*, 1989; *DeMott et al.*, 2003; *Su et al.*, 2008; *Li et al.*, 2011; *Yan et al.*, 2014], and semidirect effects [e.g., *Huang et al.*, 2006a; *J. Huang et al.*, 2010]. Indeed, these particles modify the hydrological cycle via radiative forcing (RF) [e.g., *Andreae et al.*, 2004; *Huang et al.*, 2014] and affect clouds' microphysical properties [*Huang et al.*, 2006a, 2006b; *J. Huang et al.*, 2010]. Additionally, dust aerosols can act as a vehicle for the long-range transport of nutrients to oceans [e.g., *Okin et al.*, 2011] and terrestrial
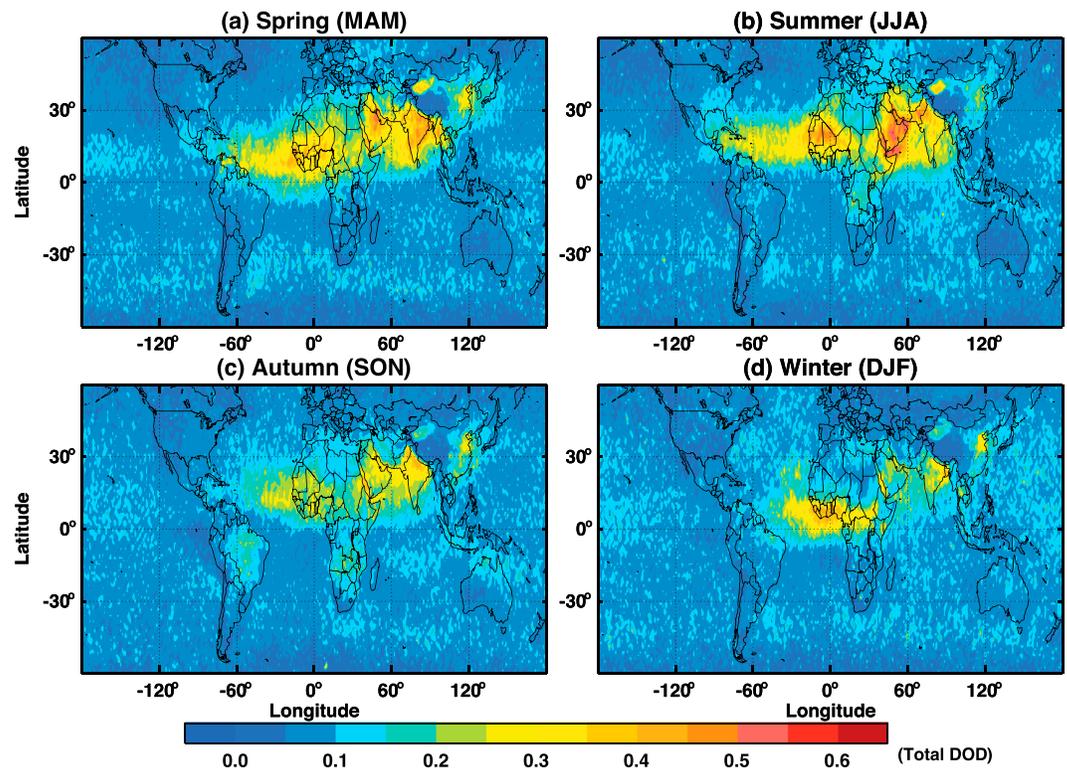
Figure 6. Seasonal distributions of total dust (including pollution-derived dust) optical depth from CALIPSO measurements from 2007 to 2010 for (a–d) spring-winter. Cited from *Huang et al.* [2015].

land surfaces [e.g., *Das et al.*, 2013]. In this section, we will review the source and transportation of dust aerosols and their direct, indirect and semidirect effects on dryland climate change.

4.1. Dust Source and Transportation

Drylands account for one third of the Earth's continental areas and are the primary sources of dust storms. Figure 6 shows the long-term seasonally averaged dust optical depth (proportional to the column-integrated dust amount from the surface to the top of the atmosphere (TOA)) at 0.55 μm over a 3 year period (2007–2010) obtained from the Cloud-Aerosol Lidar and Infrared Pathfinder Satellite Observation (CALIPSO) instrument [*Huang et al.*, 2015]. The most important sources of dust aerosols are located in the NH, primarily over the Sahara and Sahel in North Africa, the Middle East, and Southwest and East Asia [*Prospero and Lamb*, 2003; *Ginoux et al.*, 2012; *Choobari et al.*, 2014]. Each year, roughly 1,000 to 3,000 trillion grams (Tg) of dust are entrained into the atmosphere from dryland regions [*Penner et al.*, 2001; *J. F. Huang et al.*, 2010]. North Africa is the world's largest dust source, accounting for more than 55% of global dust emissions [*Engelstaedter et al.*, 2006; *Ginoux et al.*, 2012], and nearly 60% of the dust transported off that continent is deposited in the Atlantic Ocean [*Kaufman et al.*, 2005]. Over Asia, approximately 800 Tg yr^{-1} of dust is injected annually into the atmosphere, of which approximately 30% is redeposited onto deserts, 20% is transported over regional scales, and the remaining approximately 50% is transported to the Pacific Ocean and beyond [*X. Zhang et al.*, 1997; *Liu et al.*, 2008; *Uno et al.*, 2009]. *Allen et al.* [2016] studied a suite of state-of-the-art climate models and found that 74% of the models yielded a positive change in dust amount in a warmer world, largely because of a decrease in wet deposition associated with decreased large-scale precipitation over land.

African dust emission and transport exhibit variability on diurnal [*Chaboureau et al.*, 2007] to decadal [*Evan and Mukhopadhyay*, 2010] timescales that is correlated with seemingly disparate atmospheric phenomena, including the ENSO [*DeFlorio et al.*, 2016; *Prospero and Lamb*, 2003], the North Atlantic Oscillation [*Moulin et al.*, 1997], the meridional position of the intertropical convergence zone [*Doherty et al.*, 2012, 2014], Sahelian rainfall [*Prospero and Lamb*, 2003], and surface temperatures over the Sahara Desert [*Wang et al.*, 2015]. The key processes in the atmosphere that are associated with dust emissions cover a range of
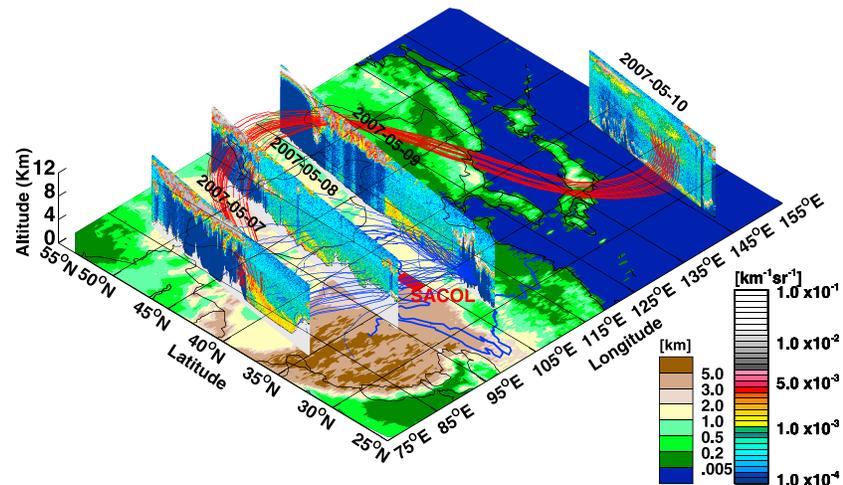
Figure 7. Illustration of a dust event that originated in the Taklamakan Desert on 7 May 2007; the dust was transported to the Pacific Ocean. Red lines represent back trajectories initialized over the Eastern Pacific. Blue lines represent back trajectories initialized over central China. Total attenuated backscatter profiles at 532 nm from CALIPSO are shown in the vertical images. The Color scale on the left shows the topographical elevation in units of kilometers, and the color scale on the right shows the 532 nm total attenuated backscatter in units of $km^{-1}\ sr^{-1}$. Cited from *J. Huang et al.* [2008].

scales—from synoptic-scale, mesoscale to microscale—and the most important challenge is to represent the effects of smaller-scale meteorological features in the models [*Knippertz and Todd*, 2012].

African dust emission is highly sensitive to vegetation changes in this narrow transitional zone. *Wang et al.* [2015] found that interannual variability in both Sahelian rainfall and surface wind speeds over the Sahara's major emitting regions, which lie to the north of the Sahelian vegetated zone, results from changes in the lower tropospheric air temperatures over the Saharan heat low—a region with local surface and lower tropospheric temperature maxima and surface pressure minima in the western Sahara Desert from June to August.

Asian dust often originates from the Taklimakan and Gobi Deserts. This dust is transported long distances by the prevailing westerlies, which pass over northeastern Asia and the Pacific Ocean and reach North America (Figure 7) [*J. Huang et al.*, 2008]. Compared to African dust emission, dust aerosols from the Taklimakan Desert can be lofted vertically up to 10 km and transported to the Tibetan Plateau and even eastern China because of the unique topography and northeasterly winds associated with certain synoptic conditions [*Huang et al.*, 2007; *Ge et al.*, 2014]. Dust from China's deserts seems to have increased most significantly from the 1960s to 1990s but has generally decreased since the 1990s and fluctuated, with mixed ups and downs, in recent years [*Che et al.*, 2015; *Xia et al.*, 2016]. Such dust could warm the atmosphere [*Liu et al.*, 2011b] and affect atmospheric stability and even the monsoon system [*Huang et al.*, 2007].

B. Fan et al. [2014] examined the relationship between recorded spring dust storm outbreaks and satellite-derived vegetation green-up dates in Inner Mongolia, Northern China, from 1982 to 2008 and found a significant dampening effect of advanced vegetation growth on spring dust storms, with each 1 day earlier shift in the green-up date corresponding to a 3% decrease in annual spring dust storm outbreaks. However, *Kurosaki et al.* [2011a] noted that the frequency of April dust outbreaks has increased from the 1990s to 2000s, whereas the frequency of strong winds has either decreased or shown little change in Mongolia, eastern Inner Mongolia, and northeastern China. The threshold wind speed has also decreased in these subregions. These results suggest that changes in land surface conditions have increased the vulnerability to dust outbreaks, resulting in their increased frequency. In some areas of the Mongolian grasslands, decreased precipitation has caused a reduction in the amount of summer vegetation, ultimately leading to reductions in the amount of brown, dead leaves and thus dust outbreaks during the following spring [*Kurosaki et al.*, 2011b; *Nandintsetseg and Shinoda*, 2015].

4.2. Direct, Indirect and Semidirect Effects

The presence of suspended dust can affect the local energy balance and hydrologic cycle over drylands through direct [e.g., *Evan et al.*, 2009; *J. Huang et al.*, 2009; *Ge et al.*, 2014], indirect effects
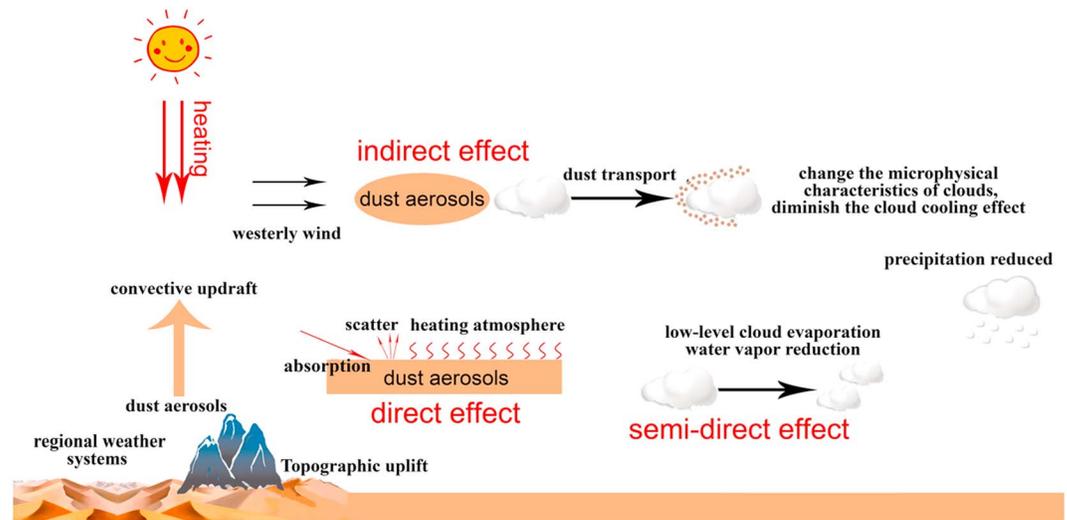
Figure 8. A schematic diagram summarizing dust-cloud-precipitation interactions in arid/semiarid and downwind (wet) regions. Modified from *Huang et al.* [2014].

[e.g., *DeMott et al.*, 2003; *Su et al.*, 2008], and semidirect effects [e.g., *Huang et al.*, 2006a; *J. Huang et al.*, 2010] (Figure 8).

Dust aerosols can change the radiative budget by scattering and absorbing radiation directly. The instantaneous change in the radiative budget with and without dust aerosols is defined as the direct RF. Dust can generate local heating, thereby changing the relative humidity (RH) and atmospheric stability and, thus, influencing the cloud lifetime and cloud liquid water content [*Hansen et al.*, 1997; *Huang et al.*, 2006a, 2006b]. This effect is referred to as the semidirect effect, which has been considered to consist of rapid adjustments that contribute to the aerosol direct effect in the fifth Intergovernmental Panel on Climate Change (IPCC) report [*IPCC*, 2013]. Also, in *IPCC* [2013], the terms in describing various types of aerosol effects on radiation and cloud have been rephrased as aerosol-radiation interaction and aerosol-cloud interaction, respectively.

Dust aerosols are one of the most common types of ice nuclei (IN) [*Heintzenberg et al.*, 1996; *Sassen*, 2002; *Sassen et al.*, 2003; *DeMott et al.*, 2003; *Teller and Levin*, 2006; *Barahona et al.*, 2010] and also efficient cloud condensation nuclei (CCN) when they have a soluble coating, such as sea salt, anthropogenic pollutants, or secondary organic aerosols [*Gibson et al.*, 2007; *Levin et al.*, 2005; *Seisel et al.*, 2005]. Dust aerosols can modify cloud macrophysical and microphysical properties in many different ways [*Twomey*, 1977; *Albrecht*, 1989; *Andreae et al.*, 2004]. Such aerosol-mediated changes in cloud parameters alter the cloud RF, which is a component of the aerosol RF. To differentiate it from the aerosol RF exerted under clear-sky conditions, it is often referred to as the aerosol indirect RF or the aerosol indirect effect.

An increase in the number of dust particles competing for limited water resources in air will result in smaller cloud droplets and higher droplet number concentrations, thereby increasing the total surface area and cloud albedo [*Twomey*, 1977]. A dust-polluted cloud reflects more solar radiation back to space, resulting in a negative RF at the TOA [*Lohmann and Feichter*, 2005]. More numerous but smaller cloud droplets collide less efficiently with each other, reducing the precipitation efficiency of polluted clouds and presumably prolonging their lifetime [*Albrecht*, 1989]. This also implies that more solar radiation will be scattered back to space, thus reinforcing the cooling effect [*Lohmann*, 2006; *Takemura et al.*, 2007]. However, for a warm-based mixed-phase cloud, delaying precipitation would allow more small cloud particles to ascend above the freezing level and begin the initial ice process, releasing more latent heat and, hence, invigorating the vertical development of clouds [*Andreae et al.*, 2004; *Koren et al.*, 2005; *Li et al.*, 2011; *Yan et al.*, 2014]. The climatic impact of this effect is likely positive forcing [*Koren et al.*, 2010; *Rosenfeld et al.*, 2013].

The RF of dust may be near zero over North Africa because the shortwave cooling is approximately balanced by the longwave warming [*Yoshioka et al.*, 2007], and dust transported over the tropical North Atlantic cools the surface via direct [*Evan and Mukhopadhyay*, 2010; *Evan et al.*, 2009] and indirect [*Doherty and Evan*, 2014]

radiative effects. Therefore, a reduction in dust would act as a positive feedback to GHGs-induced warming in the tropical North Atlantic. This feedback may also enhance the warming of the tropical North Atlantic [*Evan et al.*, 2009], which would make the basin more suitable for hurricane formation and growth [*Dunion and Velden*, 2004].

In West Africa, large amounts of mineral dust from the Sahel and Sahara are transported across the region, which, combined with human-induced biomass burning, leads to persistent haze because of the lack of wet removal. The particles from these two regions have been suggested to reduce cloud frequencies and height [*Konaré et al.*, 2008; *J. F. Huang et al.*, 2009; *Solmon et al.*, 2012].

Same as the Sahel and Sahara, dust aerosols over Asian drylands have a warming effect within the atmosphere but a cooling effect at the surface. Unlike dark surfaces, the total effect of dust aerosols is usually warming or nil at the TOA in Asian arid and semiarid regions [*J. Huang et al.*, 2009; *Ge et al.*, 2010] because of their higher surface albedo. The dust aerosols over Asia are more absorptive than those from all other dust source regions, such as the Sahara Desert. Both satellite and ground-based observations [*J. Huang et al.*, 2009; *Ge et al.*, 2010] suggested a single scattering albedo (SSA) of about 0.8 ~ 0.9 at a wavelength of 0.67 μm for dust in northwestern China. *Costa et al.* [2006] found that the SSA of Asian dust can be as low as 0.76, whereas *Fouquart et al.* [1987] reported that the mean SSA of African dust was 0.95. *Haywood et al.* [2003] found that the SSA at 0.55 μm ranged from 0.95 to 0.99 during the Saharan Dust Experiment (SHADE). The largest forcing values were found over or near dust source areas. *J. Huang et al.* [2009] combined the radiative transfer model with satellite observations to derive the maximum daily mean of the radiative heating rate over the Taklimakan Desert, which can reach 5.5 K d^{-1} at the location of the dust layer. The temperature changes caused by the dust direct effect may result in a horizontal temperature gradient, thus modify near-surface winds. Because the surface wind threshold determines the uptake of dust from the surface [e.g., *Ge et al.*, 2016], a feedback loop could be established for the total emission flux [*Huang et al.*, 2014].

Huang et al. [2006a, 2006b] compared the cloud properties under dusty and dust-free conditions in the same meteorological environment over northwestern China and found that dust aerosols injected into clouds would decrease ice cloud effective particle size and the optical depth of cirrus clouds via the semi-direct effect by 11% and 32.8%, respectively [*Huang et al.*, 2006a]. *W. Wang et al.* [2010] also studied the dust aerosol effect on cloud properties over the dust source region (the Taklimakan Desert) and dust transported region (the Western Pacific Ocean) and found similar results. Other studies [*Kawamoto et al.*, 2004; *Su et al.*, 2008; *J. Huang et al.*, 2010] also revealed similar trends over arid and semiarid regions in Asia and further confirmed the conclusion that dust aerosols can reduce cloud effective particle size. *W. Wang et al.* [2010] found that dust aerosols caused an instantaneous net cloud cooling effect in northwestern China. Other works also indicated that dust aerosols caused a cloud cooling effect at the TOA [*Huang et al.*, 2006a, 2006c].

Sakaeda et al. [2011] used a 20 year run of the Community Atmospheric Model (CAM) coupled with a slab ocean model to investigate the direct and semidirect effects of aerosols, including anthropogenic sulfate, sea salt, organic and black carbon (BC), and dust, over southern Africa. Over the ocean, where the aerosol layers are primarily located above clouds, negative TOA semidirect radiative effects associated with increased low cloud cover dominated over the weaker positive all-sky direct radiative effect (DRE). In contrast, over the land, where the aerosols are often below or within cloud layers, reductions in the cloud liquid water path led to a positive semidirect radiative effect that dominated over the near zero DRE. *Koren et al.* [2005, 2010] also elucidated the invigoration effect of Saharan dust over the eastern Atlantic Ocean.

The effect of anthropogenic aerosols on cloud droplet concentrations and radiative properties is the source of one of the largest uncertainties in the RF of climate during the industrial period. This uncertainty affects our ability to estimate the sensitivity of the climate to GHG emissions. *Carslaw et al.* [2013] performed a sensitivity analysis using a global model to quantify the uncertainty in cloud RF over the industrial period resulting from uncertainties in aerosol emissions and processes. The results demonstrated the importance of understanding pristine preindustrial-like environments, (i.e., with natural aerosols only) and suggested that improved measurements and evaluation of simulated aerosols in polluted present-day conditions will not necessarily result in commensurate reductions in the uncertainty of forcing estimates. Thus, we should pay much more attention to natural aerosols, which contribute substantially to the uncertainty in indirect forcing.

4.3. Impact on Precipitation

Dust aerosols can suppress or enhance precipitation depending on many factors, such as the spatial distribution of dust aerosols, humidity in the atmosphere, atmospheric circulation, geography, and cloud types.

In West Africa, several studies [*Konaré et al.*, 2008; *J. F. Huang et al.*, 2009; *Solmon et al.*, 2012; *Zhao et al.*, 2015] have suggested that mineral dust can reduce precipitation by altering the atmospheric circulation. Moreover, atmospheric aerosols may also impact oceanic cyclones by modifying thermodynamic and microphysical conditions [*Rosenfeld et al.*, 2012; *Dunstone et al.*, 2013; *Y. Wang et al.*, 2014]. Studies of mineral dust have revealed that the Sahara Desert strongly influences the formation and development of Atlantic hurricanes [*Dunion and Velden*, 2004; *Zhang et al.*, 2007].

Ault et al. [2011] reported that the mineral dust aerosols often observed over California, which are associated with long-range transport from Asia, can serve as IN particles and increase the riming rate. *Creamean et al.* [2013] further supported this speculation by examining in situ aircraft- and ground-based data. Similarly, IN particles emitted from the Sahara were also found to contribute to precipitation over the Amazon basin [*Prenni et al.*, 2009]. Local anthropogenic pollution in California, in contrast, was shown in previous observational and modeling studies to reduce precipitation from orographic clouds because of the slow conversion of cloud droplets into raindrops [*Lynn et al.*, 2007; *Lowenthal et al.*, 2011; *J. Fan et al.*, 2014]. In fact, intensified land use and climatic change will likely increase the future emissions of IN particles associated with wind-blown soil dust [*Conen and Leifeld*, 2014].

Lau et al. [2006] and *Lau and Kim* [2006] suggested that the absorption of elevated dust aerosols accompanied by BC led to an earlier onset and intensification of the Indian Monsoon through an "elevated heating pump" mechanism. This mechanism of dust aerosols also enhanced the West African Monsoon in boreal summer, leading to increased precipitation over the West Africa/Eastern Atlantic intertropical convergence zone (ITCZ) and decreased precipitation over the Western Atlantic and Caribbean regions [*Lau et al.*, 2009].

Based on the International Center for Theoretical Physics-Regional Climate Model (ICTP-RegCM4), *Islam and Almazroui* [2012] suggested that dust aerosols would increase the wet season precipitation and intensify the hydrological cycle over the Arabian Peninsula; additionally, *Sun et al.* [2012] suggested that dust aerosols tend to increase summer precipitation around the source areas and suppress it over the downwind areas in East Asia.

Compared to the local impact of aerosols on precipitation at monthly to seasonal timescales, *Vinoj et al.* [2014] used satellite data to conclude that dust and precipitation over the Arabian Sea, West Asia, and the Arabian Peninsula varied in concert over timescales of approximately 1 week. Analyzing global climate model simulations, they demonstrated that by heating the atmosphere, dust aerosols induce large-scale convergence over North Africa and the Arabian Peninsula and can increase the flow of moisture over India within a week. Moreover, dust-induced atmospheric heating over North Africa and West Asia rapidly modulates monsoon rainfall over central India. Diabatic atmospheric heating and surface cooling induced by dust, which vary with latitude [*Nair et al.*, 2013], can establish a positive feedback loop with dynamics in the Indian summer monsoon system and significantly contribute to the interannual to decadal variations in precipitation in this region [*Solmon et al.*, 2015].

Han et al. [2013] applied an online-coupled regional climate-chemistry-aerosol model to investigate the dust direct radiative feedback affecting the dust deflation, transport, and meteorological elements of a severe dust storm in East Asia. The dust RF decreased precipitation in the middle reaches of the Yangtze River and large areas of North China by 0.1–0.6 mm d^{-1}.

A positive feedback loop exists in the dust aerosol-cloud-precipitation interactions over drylands. A decrease in precipitation leads to an increase in the occurrence of dust storms, which decreases the low cloud cover and relative humidity via the semidirect effect and further contributes to decreasing precipitation [*Huang et al.*, 2014]. Thus, more dust storms can occur in arid and semiarid regions, which may have contributed to the desertification observed in recent decades and the accelerated development of the arid conditions over the drylands in Asia [*Huang et al.*, 2014].

Miller et al. [2004] noted that dust aerosols could reduce global evaporation and precipitation by reducing the surface temperature but reported that, overall, these aerosols contribute to a negative feedback loop for

desertification. *Z. Li et al.* [2016] provided an extensive review of aerosol and monsoon interactions over Asia, including dust aerosols in China and India. Similarly, *Zhao et al.* [2015] used an aerosol-climate-coupled system to study the direct climatic effects of dust aerosols on global arid (including hyperarid) and semiarid regions and suggested that the effects of dust aerosols are indiscernible in the expansion of arid and semiarid regions.

5. Impacts of Atmosphere-Land Interactions

Atmosphere-land interactions control the energy balance, water cycle, and carbon cycle through turbulence at the planetary boundary layer (PBL) and play an important role in climate change, especially in arid and semiarid regions.

Although many proposed mechanisms for the climate changes that occur in drylands emphasize the driving role of oceanic warming and associated atmospheric processes, it should be emphasized that the aridity index response is substantially amplified by atmosphere-land feedbacks that respond to climate changes [*Berg et al.*, 2016]. The land surface changes induced by droughts in arid, semiarid, and subhumid regions can induce some positive feedbacks that reinforce and prolong the droughts. Clearly, understanding the response of the energy cycle, water cycle, and carbon cycle to global warming is crucial for understanding and predicting future dryland climate changes.

5.1. Enhanced Semiarid Warming

Recently, some studies have shown that the warming of drylands over the last century has been most significant [*Huang et al.*, 2012; *Ji et al.*, 2014; *Guan et al.*, 2015]. As shown in Figure 9a, the temperature increase in semiarid regions (with a precipitation range of 200–600 mm yr^{-1} over 20–60°N) is more significant than that in other regions, especially in the cold season (November to March), whereas for the wet regions (with a precipitation of >1000 mm yr^{-1} over 20–60°N), there is no significant difference in the warming trend between the cold and warm seasons. The results also showed that the cold season temperature has increased by 1.89°C in the semiarid regions over 20–60°N during 1901–2009, and that the contribution of semiarid regions to continental warming reaches is approximately 50% [*Huang et al.*, 2012]. This indicates that the warming is enhanced in semiarid regions in the cold season, and that temperature change in semiarid regions is more sensitive to climate change than in other regions. However, the semiarid regions identified by a precipitation range of 200–600 mm yr^{-1} over 20–60°N may include some areas of subhumid or humid northern forests, such as southern Siberia and northeastern China.

Further, *Ji et al.* [2014] demonstrated that the strongest and fastest warming occurs in the NH midlatitudes, by analyzing the evolution of the global land SAT trend from 1901 to 2009 using a spatial-temporally multidimensional ensemble empirical mode decomposition (MEEMD) method (Figure 9b). *Guan et al.* [2015] investigated the driving factors of the enhanced semiarid warming (ESAW) by using a recently developed method that can identify and separate the temperature change into dynamically induced and radiatively forced changes [*Wallace et al.*, 2012; *Smoliak et al.*, 2015]. The results showed that the warming trend on the global and regional scales is mainly due to radiatively forced temperature (RFT) changes as a result of GHGs, land cover change, clouds, aerosols, and human activities.

In addition, *Zhou et al.* [2015, 2016] also found that the warming rate observed for the period 1979–2012 increased dramatically with decreasing vegetation greenness over land between 50°S and 50°N, with the strongest warming rate observed over the driest regions, including the Sahara desert and the Arabian Peninsula; this is consistent with the idea of ESAW. Moreover, *Zhou et al.* [2015, 2016] found that the mechanisms are likely to be attributable primarily to enhanced longwave radiative forcing that is associated with stronger water vapor feedback over drier ecoregions in response to the positive global-scale GHG forcing. Drylands are dry regions and are mostly cloud free because of the subsiding air that rises over the tropics. The air in these regions can be warmed efficiently by the powerful greenhouse effect in which the water vapor content of the air increases with the increasing temperature of the air but the latent heat cannot be released because the descending air inhibits condensation. This heating effect is radiative in nature and is manifested as enhanced downward longwave radiation [*Zhou et al.*, 2016]. Further, this group also found that the ESAW could be reproduced in historical simulations using anthropogenic and natural forcings but that
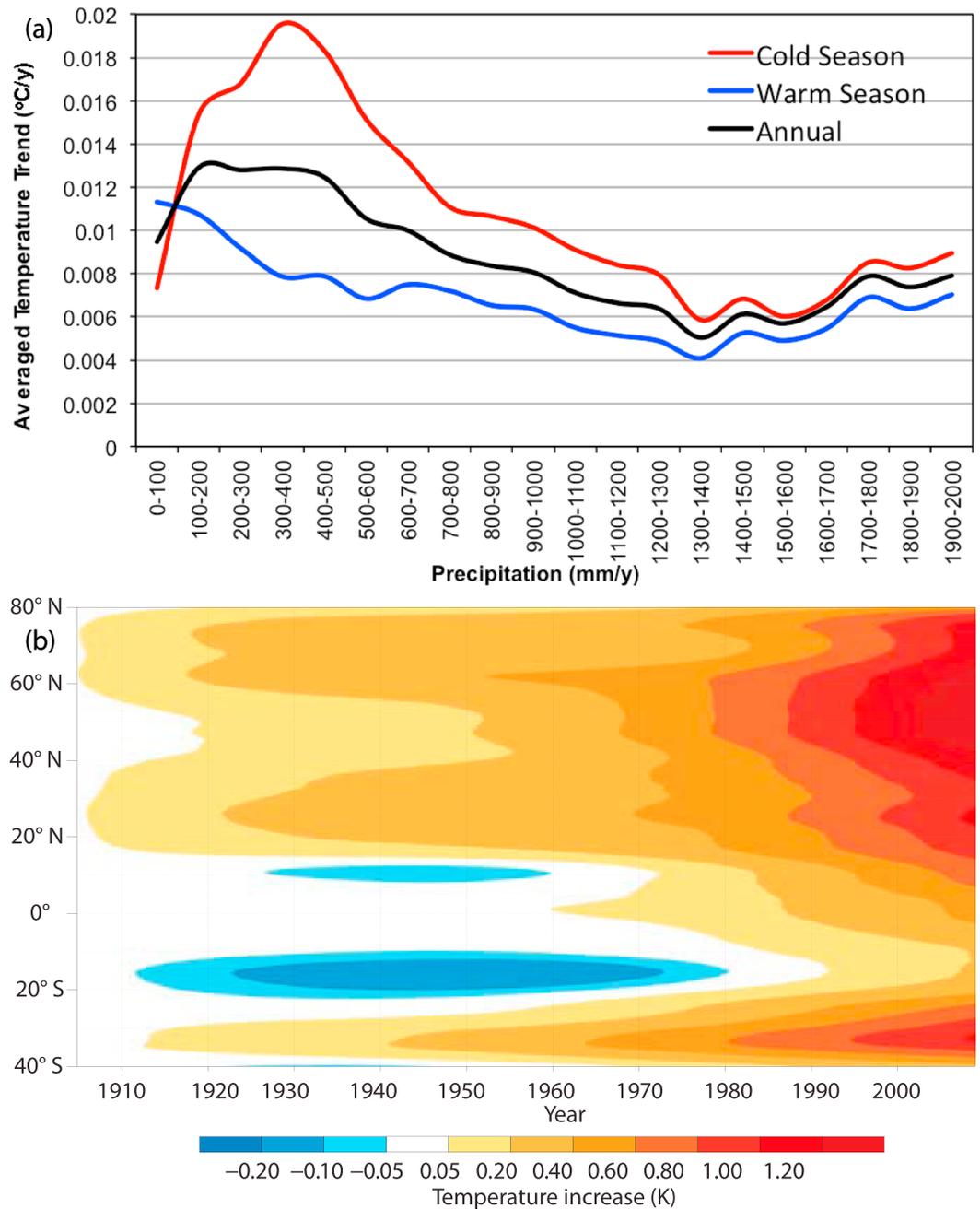
Figure 9. (a) Comparison between the regionally-averaged linear temperature trend over 20–60°N as a function of clima-tological mean precipitation for the entire year, and the cold and warm seasons. The precipitation interval is 100 mm/yr. Cited from *Huang et al.* [2012]. (b) Evolution of the zonally averaged trend in SAT. Note that color intervals are uneven. Cited from *Ji et al.* [2014].

they are absent if only natural forcings are considered, suggesting new potential fingerprints for anthropogenic warming.

The phenomenon of enhanced warming has important implications in interpreting global warming patterns and assessing the impacts of climate change. Climate models project drying over many areas in low and mid-dle latitudes based on PDSI and SPEI with increasing GHG concentrations [*Cook et al.*, 2014a]. Moreover, enhanced warming may accelerate over dry areas in the context of a warming climate and thus have impor-tant societal and economic consequences [*Zhou et al.*, 2016]. However, the SAT trend in semiarid area is
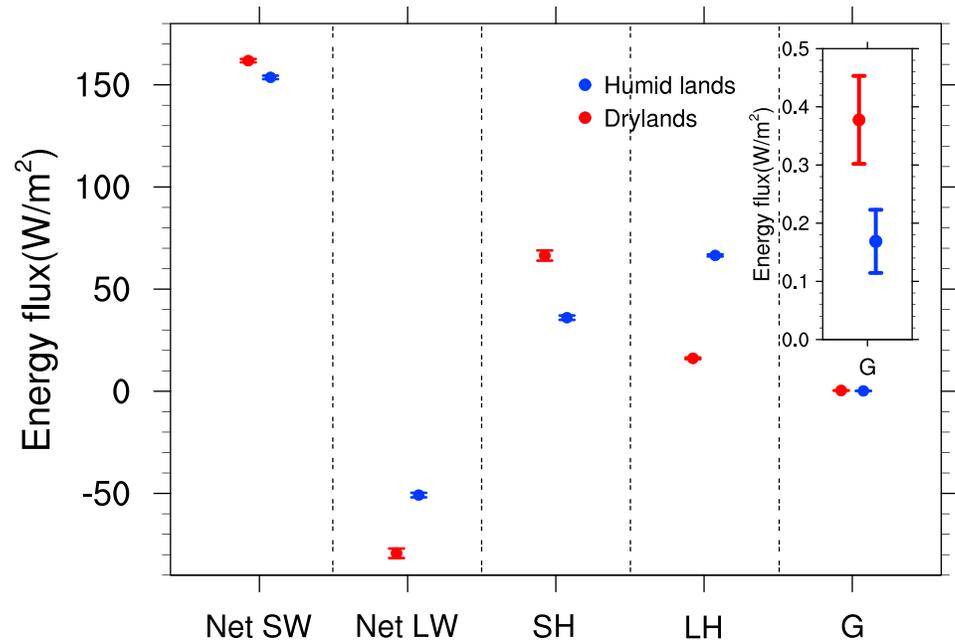
Figure 10. Comparison between the mean surface energy fluxes for drylands and humid lands based on GLDAS data, including net shortwave radiation (Net SW; downward positive), net longwave radiation (Net LW; downward positive), sensible heat flux (SH), latent heat flux (LH), and ground heat flux (G). Error bars denote the ±1 standard deviation range of temporal variations from 1948 to 2010. Cited from *Huang et al.* [2017b].

underestimated in the CMIP5 simulations and the SAT trend in humid area is overestimated, which means that there is large uncertainty in the response of SAT to global warming in CMIP5 simulations [*Huang et al.*, 2017a].

5.2. Energy Balance

The energy balance should be satisfied in atmosphere-land interaction. At a given location, the net radiative heat gain, which is expressed as the net radiation, must be balanced by other forms of heat transfer. This heat balance is expressed as [*Burba et al.*, 1999]

$$R\mathrm{n} = \mathrm{LH} + G + \mathrm{SH} \tag{1}$$

where LH is the latent heat flux, G is the conduction to or from the subsurface, and SH is the sensible heat flux [*Nicholson*, 2011].

The partitioning of the surface contribution to atmospheric heating into sensible and latent heat depends on the nature of the surface [*Malone et al.*, 2014; *Zhu et al.*, 2014; *Jia et al.*, 2016; *Kool et al.*, 2016]. Under increasing atmospheric water demand, the availability of surface moisture has a decisive influence on this partitioning because of the characteristic properties of water [*Koster et al.*, 2004; *Sherwood and Fu*, 2014].

In principle, the available energy ($R_n - G$) is theoretically balanced by the sensible heat flux (SH) and the latent heat flux (LH), which is the basic principle of all the atmospheric models, and large closure errors are unacceptable. However, the energy partitioning of the net radiation (R_n) between SH and LH depends on the land cover conditions and atmospheric evaporative demand [*G. Wang et al.*, 2010; *Liu et al.*, 2015; *Guo et al.*, 2016]. In general, both SH and LH generally increase with surface solar radiation in humid areas, but LH increases more under warm conditions. By contrast, LH is limited by the soil water supply and SH accounts for a higher proportion of R_n in arid or semiarid regions [*Wang and Dickinson*, 2013].

Over drylands, low precipitation and soil moisture content, which are the inputs to dryland water cycles, limit the evaporation and transpiration associated with low vegetation cover [*Yin et al.*, 2014], resulting in a low mean latent heat flux of 16.12 W/m^2 over drylands compared with 66.49 W/m^2 over humid lands (Figure 10). To release the heating from solar and infrared radiation through sensible heat fluxes, surface

temperatures over drylands must rise sharply to create a large land-air temperature difference. This difference leads to a large sensible heat flux of 66.44 W/m^2 compared with that of 36.02 W/m^2 over humid lands. The high upward net longwave radiation over drylands of 79.33 W/m^2 (versus 50.82 W/m^2 over humid lands) also indicates a large land-air temperature difference over drylands. By contrast, additional heat resulting from increased GHGs can be used to evaporate more moisture over humid lands [*Neelin et al.*, 2003], thus decreasing the resultant surface warming. Therefore, the high sensitivity of surface temperatures to extra heating from increased GHGs over drylands primarily occurs from a lack of evapotranspiration because of limited soil moisture and vegetation.

5.3. Water Cycle

The water cycle, which describes the continuous movement of water through the climate system, is a key process in atmosphere-land interactions and is mediated by the variation of soil moisture, ET, P, and runoff. Global warming and anthropogenic activities have altered global ET, P, and runoff, suggesting a general intensification or acceleration of the global water cycle [*Huntington*, 2006; *Wentz et al.*, 2007]. However, asynchronous changes in these components may lead to hydrological deficits and adverse ecological consequences.

Soil moisture, a key participant in many hydrologic and atmosphere-land interactions, is affected by the changes in precipitation and evapotranspiration and shows an observable downward trend over East Asia from 1948 to 2010 compared with the global mean (Figure 11a) [*Cheng et al.*, 2015]. The most obvious drying occurred over transitional areas between dry and wet regions [*Cheng and Huang*, 2016]. Above all, global warming through soil moisture-temperature feedback caused enhanced soil drying in these transitional regions (Figure 11c). In East Asia, a region of pronounced drying, soil drying is driven primarily by decreasing precipitation (Figure 11d) and is enhanced almost twofold by increasing temperatures. At the same time, soil suction increases with decreasing soil moisture, and the remaining soil moisture becomes less accessible for uptake by plant roots; thus, evapotranspiration may be reduced, possibly leading to an increase in the sensible heat flux and a further temperature increase. The increased temperature, decreased evapotranspiration, and soil water loss form a positive feedback loop, which can continue until the soil is completely dry, and desertification results [*Seneviratne et al.*, 2010].

Many Global Land-Atmosphere Coupling Experiments have demonstrated that the coupling between soil moisture and precipitation, which is measured as the omega difference, is strongest in transitional regions (such as semiarid and semihumid regions) because the surface climate in such regions is the most sensitive to soil moisture (Figure 11b) [*Koster et al.*, 2004; *Song et al.*, 2009; *Seneviratne et al.*, 2010]. Only in such transitional zones is the precipitation amenable to soil moisture influence. Indeed, soil moisture can trigger moist convection, and evaporation is suitably high but still sensitive to soil moisture. Simultaneously, in transitional climate regions, soil moisture controls the near-surface temperature and evapotranspiration through the partitioning of sensible and latent heat fluxes. The increased local surface temperature resulting from large-scale circulations can decrease the soil moisture and, thereby, induce a significant decrease in precipitation through the strong coupling relationship in transitional zones and further induce an increase in temperature by increasing the energy partitioning to sensible heat. These processes could enhance the drying trend and interactions, making drylands even drier. Therefore, the observational and projected warming and drying trends are most severe in transitional climate regions. Additionally, transitional regions are normally agricultural districts with large populations. Their ecosystems tend to be fragile and sensitive to climate change; a slight disturbance in the climate is likely to cause devastating consequences. The most serious warming and drying would pose a great challenge to the ecosystem as well as human survival. Therefore, strict management and rational schemes to use water resources are in urgent need to alleviate the enormous impact from drying.

In addition, vegetation-atmosphere interactions and dust-climate feedbacks are also important processes in local atmosphere-land interactions, despite their impacts on each other. Decreased soil moisture can markedly enhance dust outbreaks under certain wind conditions [*Kim and Choi*, 2015]. The ability of atmospheric dust to suppress precipitation can contribute to a positive desertification feedback whereby plant mortality and enhanced dust emissions result from the reduced vegetation cover [*Rosenfeld et al.*, 2001; *Huang et al.*, 2014]. This would destroy the ecological environment, depress crop production, and cause dust and drought. Changes in the water cycle are projected to occur in a warming climate. Regional to global-scale projections of soil moisture and drought remain relatively uncertain compared to other aspects of the water cycle.
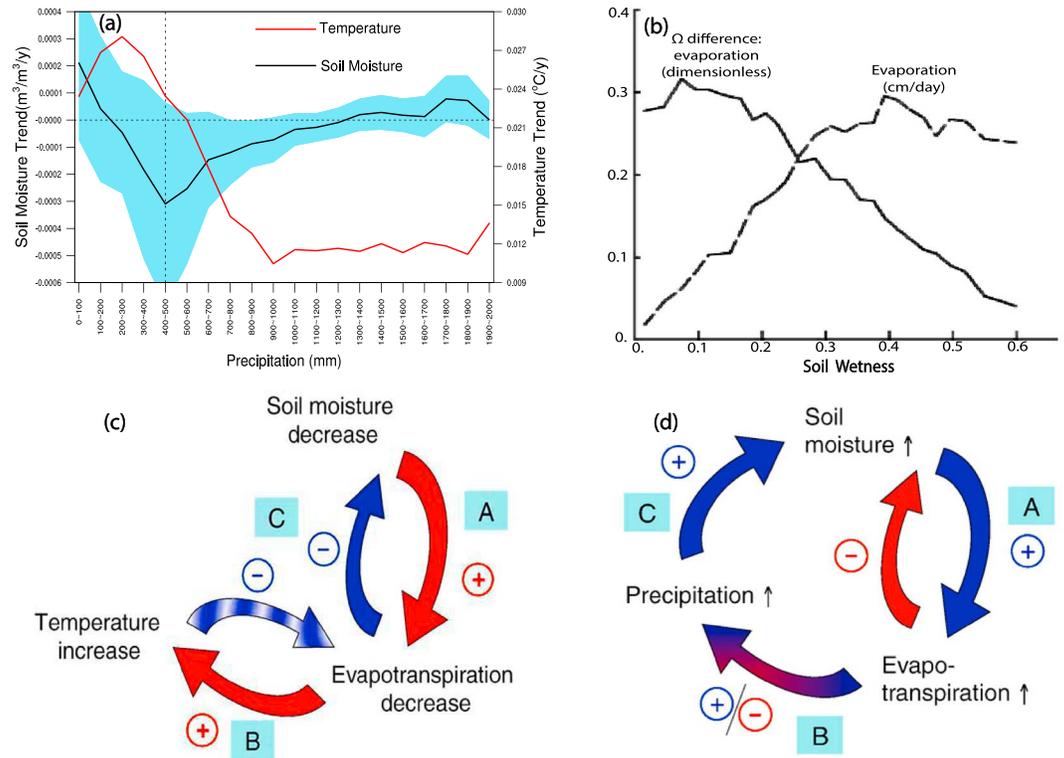
Figure 11. Linear trends in annual-mean temperature and soil moisture as a function of climatological mean precipitation over East Asia. The black line denotes the domain average for various climatic regions, and shaded bands denote one standard deviation of the soil moisture trend. Cited from *Cheng et al.* [2015]. (b) Average relationship between soil wetness (the degree of saturation in the soil) and two separate aspects of the land-surface energy budget: the Ω difference for evaporation (a dimensionless measure of soil moisture-precipitation coupling, solid curve) and the average evaporation rate (dashed curve; in cm/d). Cited from *Koster et al.* [2004]. (c) Processes contributing to soil moisture-temperature coupling and feedback loop. Positive arrows (red) indicate processes that lead to a drying/warming in response to a negative soil moisture anomaly and blue arrows denote potential negative feedbacks. Cited from *Seneviratne et al.* [2010]. (d) Processes contributing to soil moisture-precipitation coupling and feedback loop Positive arrows (blue) indicate processes leading to a positive soil moisture-precipitation feedback (wetting for positive soil moisture anomaly, drying for negative soil moisture anomaly). The negative arrow (red) indicates a negative feedback damping the original soil moisture anomaly, and the red-blue arrow denotes both positive and negative feedbacks between evapotranspiration and precipitation anomalies. A, B, and C show the different steps of the feedback loop. Cited from *Seneviratne et al.* [2010].

Nonetheless, drying in the Mediterranean, southwestern United States, and southern African regions is consistent with projected changes in the Hadley Circulation. Thus, drying in these regions as global temperatures increase is likely for several degrees of warming under RCP8.5 [*IPCC*, 2013].

5.4. Carbon Cycle

One of the greatest sources of uncertainty for future climate predictions is the response of the global carbon cycle to climate change [*Ballantyne et al.*, 2012]. Dryland ecosystems, which include landforms from deserts to dry shrublands, play an important driver role in the global carbon cycle. Drylands cover about 41% of the terrestrial land surface and account for approximately 40% of global net primary productivity [*Wang et al.*, 2012]. Semiarid areas are not only the recipients of the most enhanced climate changes induced by increasing CO_2 [*Huang et al.*, 2017a] but also the biggest contributor to the trend and interannual variability of the terrestrial carbon sink [*Poulter et al.*, 2014; *Ahlstrom et al.*, 2015]. Semiarid forests maintained substantial carbon sequestration levels in large semiarid regions (with annual precipitation from 200 to 600 mm) by shifting peak photosynthetic activities from summer to early spring [*Rotenberg and Yakir*, 2010; *Seddon et al.*, 2016]. Estimates on the basis of data for savannas show the huge potential for harnessing these ecosystems for carbon sequestration, if savannas were protected from burning and grazing so that an accumulation of carbon could occur [*Grace et al.*, 2006]. The higher turnover rates of carbon pools in semiarid biomes are

an increasingly important driver of global carbon interannual variability [*Poulter et al.*, 2014]. It is now recognized that the quantitative importance of terrestrial carbon cycles match those of atmosphere-ocean interactions in global climate models [*Osmond et al.*, 2004]. Although approximately one half of the total CO_2 emissions are removed by combined land and ocean sink, coupled climate-carbon feedback models have predicted decreased carbon uptake by land sinks that is induced by the diminishing productivity and increased respiration associated with high temperatures. However, recent observations show that the evolution of the terrestrial carbon sink over the past 30 years presents a trend of increasing strength in the land carbon sink, which may be due to a range of possible factors, such as the fertilization effect of increased CO_2 and atmospheric nitrogen deposition on plant growth, changes in growing season length, and land management [*Ballantyne et al.*, 2012; *Poulter et al.*, 2014]. *Wu et al.* [2016] found that increased tree cover and leaf area index (LAI) associated with a CO_2 and climate-driven increase in net primary productivity. However, this phenomenon is likely to disappear in the near future since the vegetation greening associated with CO_2 fertilization in semiarid areas could increase the evapotranspiration and decrease the soil moisture [*Zhao et al.*, 2011; *Forzieri et al.*, 2017]. As the soil moisture continues to decrease and cannot support the existing ecosystem, the gross primary production will decrease abruptly because of desertification [*Wu et al.*, 2013].

Enhanced dryland warming may aggravate the dryland expansion by causing a higher vapor pressure deficit and evaporative demand. In addition, the decreased soil moisture may lead more energy to SH than to LH [*Seneviratne et al.*, 2010; *Sherwood and Fu*, 2014], leading to an even stronger impact on temperature extremes [*Seneviratne et al.*, 2014; *Hirschi*, 2011; *Vogel et al.*, 2017]. Changes in temperature and moisture resulting from climate change are likely to modify strongly the ecosystem carbon sequestration capacity in high latitude areas, both through vegetation shifts and via direct warming effects on photosynthesis and decomposition [*Sjögersten and Wookey*, 2016]. Furthermore, soil organic carbon (SOC) storage decreases with increasing temperature and increases with increasing soil water content [*Sharma et al.*, 2012]. The capacity of drylands to sequester atmospheric CO_2 will decrease with other warming-induced effects, such as the increase in soil CO_2 efflux and the changes in microbial communities to alter C cycling in drylands and to reduce soil C stocks in the mid to long term [*Maestre et al.*, 2013]. Erosion-induced land degradation may also lead to the emission of carbon [*Lal*, 2003]. Therefore, against the background of global warming, the expansion of drylands will reduce the SOC storage and emit CO_2 into the atmosphere. Additionally, the soil degradation and reduced soil moisture severely constrain the gross primary production (GPP) [*Peng et al.*, 2013] and affect the photosynthesis rate of plants that can absorb CO_2 and store carbon [*Hoover et al.*, 2015]. As shown in Figure 12a, the GPP is positively correlated with the AI, and the GPP in arid regions is approximately one fifth of that in humid regions. By these two processes, dryland soils store less carbon and emit more CO_2 into the atmosphere, aggravating global warming. These processes result in a positive feedback cycle, with the warming and drying reinforcing each other (Figure 12b). However, during the warming hiatus, a recent pause in the growth rate of atmospheric CO_2 was reported [*Keenan et al.*, 2016] and attributed to an increase in the terrestrial sink [*Ballantyne et al.*, 2017] during the last decade. This increase was associated with the effects of increasing atmospheric CO_2 on vegetation and those of the slowdown in global warming on global respiration. Unfortunately, CMIP5 cannot reproduce this pattern without large uncertainty because global carbon cycle processes are not included in some CMIP5 models [*Huang et al.*, 2017a]. However, the carbon concentration still has a large uncertainty even in state-of-the-art models coupled with the global carbon cycle. Many new discoveries concerning the response of vegetation to global warming were identified from ecosystem scale to leaf scale, although the processes are too complex to fully parameterize the processes in the model [*Yu et al.*, 2015; *Klein et al.*, 2017]. For example, earlier spring leaf unfolding of plants in response to climate warming could be counteracted because many deciduous trees require chilling for dormancy release and warming induces reductions in chilling [*Fu et al.*, 2015]. Further, 80% of the expected increase in leaf respiration may be eliminated by the acclimation of leaf respiration to climate warming [*Reich et al.*, 2016].

Recent studies [*Delgado-Baquerizo et al.*, 2013; *Wardle*, 2013] have revealed that for dryland ecosystems worldwide, the balance among carbon, nitrogen, and phosphorus will become increasingly disrupted as ecosystems become drier. As the aridity increases, available soil carbon (C) and nitrogen (N) decline because of the impairment of biological processes, whereas available soil phosphorus (P) increases because of the increased role of abiotic processes (Figure 12c). Adverse ecological consequences will arise not only through the direct effects of moisture limitations but also through the indirect effects of decoupled elemental cycling and reduced organic matter in soil. *Wardle* [2013] demonstrated that this decoupling of elemental cycles
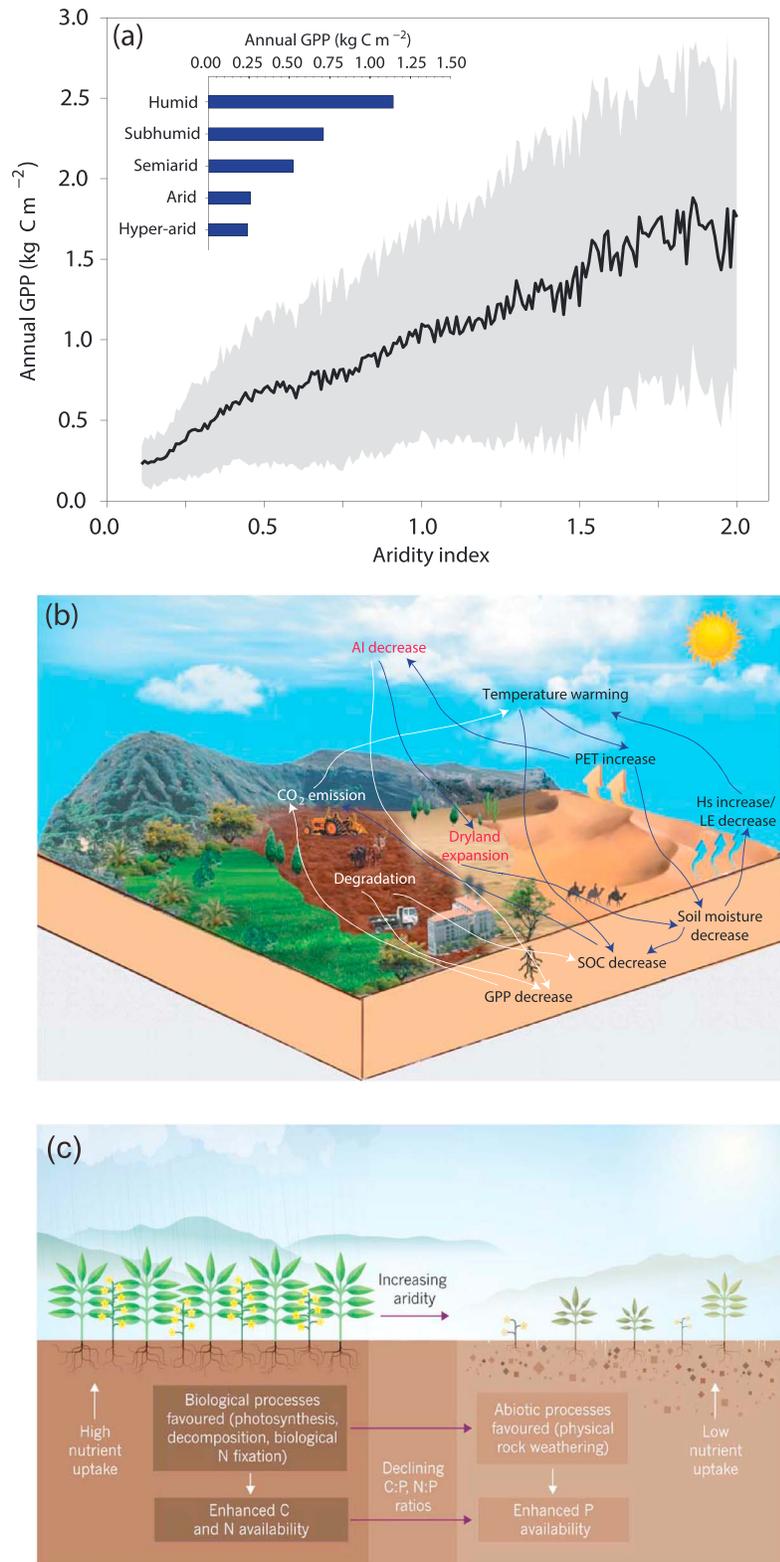
Figure 12. (a) Annual GPP as a function of the AI; the black line denotes the regional mean from 2000 to 2010, the grey shading denotes one standard deviation; the regional mean annual GPP of each subtype is shown in the inset by the blue bars. Cited from *Huang et al.* [2017a]. (b) A schematic diagram of positive feedback cycles, including processes of global warming, dryland expansion, and carbon emissions from soils. Cited from *Huang et al.* [2017a]. (c) Aridity causes elemental cycles to decouple. Cited from *Wardle* [2013].

accelerates in a nonlinear manner as the aridity increases, suggesting that the ecosystem properties of many drylands could pass a tipping point that will be difficult or impossible to reverse.

6. Impacts of Atmosphere-Ocean Interactions

Many studies have shown that oceanic conditions, especially the SSTs in the Pacific, Atlantic, and Indian basins strongly influence precipitation around the globe, particularly over fragile drylands [e.g., *Ting and Wang*, 1997; *Y. Zhang et al.*, 1997; *Seager et al.*, 2005; *Mo et al.*, 2009; *Zhong et al.*, 2011; *Dai*, 2013a; *Trenberth et al.*, 2014; *Dong and Dai*, 2015]. During 1998–2002, extensive droughts with prolonged below-normal precipitation and above-normal temperatures affected the NH midlatitudes, including the United States, southern Europe, the Mediterranean, and Southwest and Central Asia [*Lawrimore et al.*, 2001; *Waple et al.*, 2002]. These droughts were thought to have originated from the distant tropical Pacific Ocean based on atmospheric general circulation model (AGCM) simulations forced by observed global SSTs [*Hoerling and Kumar*, 2003]. *Trenberth et al.* [2014] suggested that tropical Pacific SST variations are the primary cause of many episodic droughts around the world via "the atmospheric bridge." In this section, we will focus on the influence of the atmosphere-ocean interactions on dryland climate changes from the perspectives of the impacts of oceanic oscillations, land-sea thermal contrast, and the Hadley Circulation expansion.

6.1. Oceanic Oscillations and SST Anomalies

Decadal to interdecadal variability of SSTs in different ocean basins can cause overlying atmospheric circulation anomalies at the corresponding timescales and, thus, impact the climate over various regions via atmospheric teleconnections. For example, AGCM simulations forced by observed SSTs support the notion that oceans play a crucial role in the semiarid climate in the Sahel, and that the warming over the tropical Atlantic and Indian Ocean is the major cause of the severe drought during the 1970s and 1980s in the Sahel [*Giannini et al.*, 2003; *Bader and Latif*, 2003; *Lu and Delworth*, 2005; *Hoerling et al.*, 2006, 2010]. For North America, many studies have shown that persistent SST anomalies in the Pacific and Atlantic basins strongly influence precipitation over the contiguous United States (CONUS) by impacting atmospheric circulations [*Ting and Wang*, 1997; *Schubert et al.*, 2009; *Mo et al.*, 2009; *Hu and Feng*, 2012; *Dai and Wigley*, 2000; *Dai*, 2013a; *Dong and Dai*, 2015]. More than half (52%) of the spatial and temporal variance in the interdecadal drought frequency over the CONUS is attributable to the PDO and AMO [*McCabe et al.*, 2004]. Specifically, the Pacific Ocean plays a more important role in controlling precipitation over arid and semiarid regions in the western United States. Additionally, persistent La Niña-like SST anomalies or a cold PDO or interdecadal Pacific oscillation (IPO) phase can cause below-normal precipitation and often drought over southwestern North America [*McCabe et al.*, 2004; *Dai*, 2013a; *Dong and Dai*, 2015; *Coats et al.*, 2016]. Additionally, climate changes over arid/semiarid regions in Asia are associated with the PDO. For example, North China, a typical semiarid agricultural region, is prone to drought during warm phases of the PDO as shown in Figure 13 [*Ma and Shao*, 2006; *Ma and Fu*, 2003, 2006; *Ma*, 2007; *Qian and Zhou*, 2014]. This phenomenon explains the robust drying trend and dry episode that lasted for approximately 30 years in the late twentieth century in this region [*Ma and Fu*, 2003, 2006; *Ma and Dan*, 2005].

Moreover, the interdecadal variability of the PDO can exert a modulating effect on ENSO teleconnections over many parts of the world [*Dong and Dai*, 2015], such as the United States [*Gershunov and Barnett*, 1998; *Gutzler et al.*, 2002; *Hu and Huang*, 2009], South America [*Andreoli and Kayano*, 2005], Mexico [*Pavia et al.*, 2006], Australia [*Power*, 1999], East Asia [*Wang et al.*, 2008; *Kim et al.*, 2013], and even globally [*S. Wang et al.*, 2014]. These studies show that the interannual relationship between ENSO and regional climate is not stationary and can be modulated by the phase of PDO. When the ENSO is in phase with the PDO, ENSO-induced dry-wet changes are magnified relative to the canonical pattern (Figure 14a). Conversely, when the ENSO is out of phase with the PDO, these dry-wet variations weaken or even disappear (Figure 14b). For example, the arid and semiarid climates over the Sahel, southern Africa, and China worsen, whereas those over central Asia improve, although these conditions lead to concerns regarding flooding. Figure 14c shows that when the ENSO is in phase with the PDO, approximately 28% of the global land area is affected by significantly abnormal dryness or wetness that far exceeds the canonical pattern. All of these effects of the ENSO on global dry-wet changes during transitions of the interdecadal PDO phase warrant attention in the coming decades, especially over fragile dryland regions.
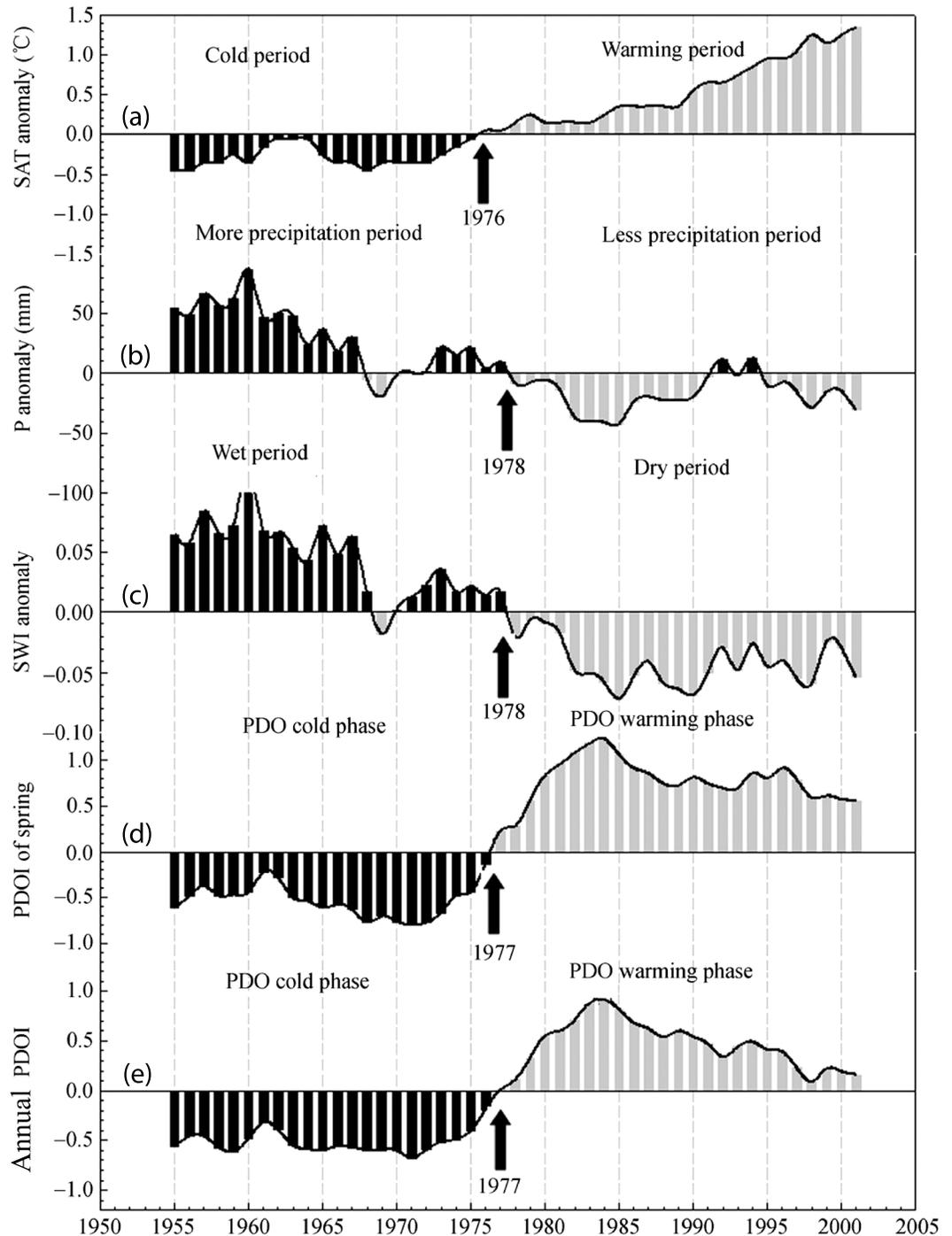
Figure 13. Anomalies of regional mean annual (a) SAT, (b) precipitation, (c) surface wetness index (SWI) in North China. (d) Spring PDO index (PDOI) and (e) annual PDOI. Modified from *Ma* [2007].

Recently, *Dong and Dai* [2015] investigated the influence of the IPO, which includes the PDO of the North Pacific but extends to the tropical and South Pacific, on temperature and precipitation over the globe, including its modulating effect on regional influences of ENSO. The results show that the interdecadal variability of the Pacific SSTs explains more than half of the interdecadal variations in temperature and precipitation over many regions. Moreover, the IPO also modulates the influence of the ENSO on local temperature and precipitation over most of these regions. Many of these IPO-affected regions are drylands, such as western North
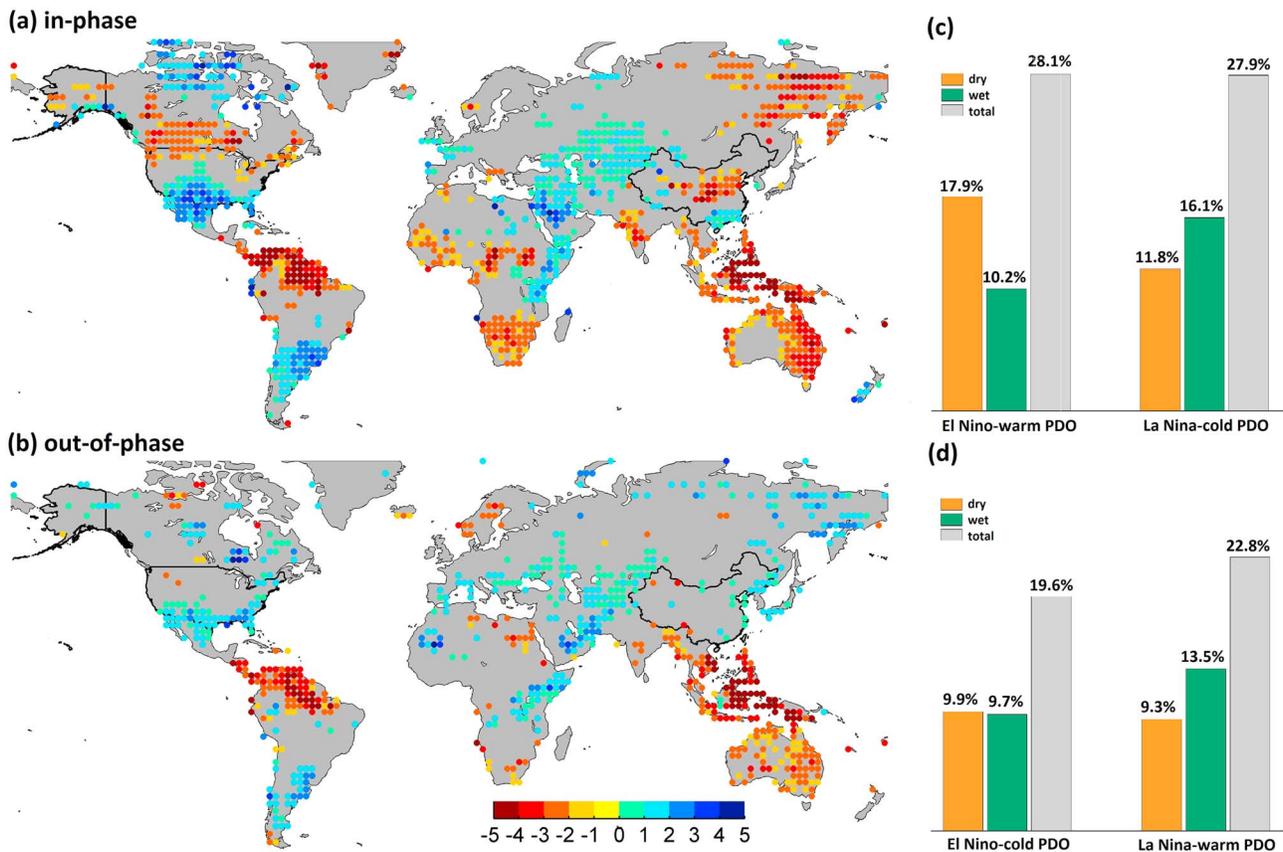
Figure 14. Differences in sc_PDSI_pm between El Niño and La Niña states during (a) an in-phase combination and (b) an out-of-phase combination of ENSO and PDO. Colored circles indicate aridity changes exceeding the 90% confidence level. Cited from *S. Wang et al.* [2014]. (c) Fractions of the global land area with significant drying and wetting induced by ENSO when in phase with PDO, which is El Niño during warm PDO regimes and La Niña during cold PDO regimes; (d) the same as Figure 14c but for the out-of phase combination, that is, El Niño during cold PDO regimes and La Niña during warm PDO regimes. The significant drying and wetting indicates the areas that exceed the 90% confidence level based on a two-tailed Student's *t* test. Modified from *S. Wang et al.* [2014].

America and southern Africa. The IPO-induced precipitation anomalies can be explained by the associated atmospheric anomaly circulation, which is characterized by a high-pressure center and anticyclonic flows over the North Pacific and negative pressure anomalies and increased wind convergence over the Indonesia and western Pacific region during the IPO cold phases. Furthermore, these observed influences of the IPO on regional temperature and precipitation are generally reproduced by an atmospheric model forced by observed SSTs, confirming the influences of the SSTs [*Dong and Dai*, 2015]. Therefore, it is important to predict the phase change of the IPO for decadal climate predictions.

6.2. Land-Sea Thermal Contrast

To investigate the mechanisms influencing winter temperature over the NH, many studies have examined the influence of atmospheric circulations and its forcings, especially asymmetric thermal forcing associated with the land-sea thermal contrast, Arctic changes, and other oceanic forcings. At a regional scale, the monsoon is associated with the land-sea thermal contrast, e.g., variations in East Asian winter monsoon (EAWM) intensity affect wintertime temperature and precipitation over Asian dryland regions. The EAWM has also been shown to have a close relationship to the Siberian high, which is mainly caused by the cold land temperatures during the winter [*Gong and Wang*, 1999; *Xie et al.*, 2016]. In recent decades, the Siberian high has strengthened, leading to stronger cold surges from the Arctic and generating winter cooling over East Asian dryland regions [*Xie et al.*, 2016; *Huang et al.*, 2017a]. On a hemispheric scale, *Wallace et al.* [1996] named the second EOF pattern in the 500 hPa geopotential height anomalies the "cold ocean-warm land" (COWL) pattern. This pattern accounts for 65% of the SAT variance during the cold season, and *Wallace et al.* [1996] noted that the anomalous warming in winter during the 1980s could be attributed to strong positive bias in the
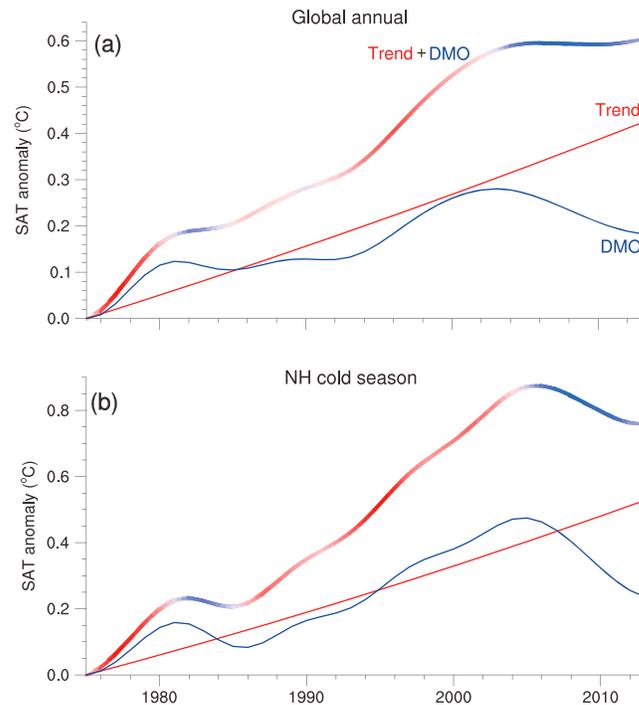
Figure 15. (a) The EEMD decomposed global annual mean SAT anomalies for the long-term trend component (red), the DMO component (blue), and the trend plus DMO (red-blue). (b) Same as Figure 15a but for the NH cold season. Cited from *Huang et al*. [2017a].

COWL pattern. *Wu and Straus* [2004] compared the pattern using traditional and modified COWL definitions and found that the midtropospheric temperature trend was largely determined by the COWL pattern, with the Arctic oscillation only accounting for local cooling over Greenland.

Those components of global SAT that are modulated by internal climate variability on a decadal to interdecadal timescale can be referred as decadal modulated oscillation (DMO) (Figure 15) [*Huang et al*., 2017a]. The DMO significantly affect hemispheric climate changes, including the temperature changes over dryland regions in the middle and high latitudes of the NH. Based on the Charney's multiple equilibrium theory [*Charney and DeVore*, 1979], zonal asymmetric thermal forcing can alter the equilibrium of atmospheric circulation, causing abrupt shifts between high-index and low-index circulation patterns. To quantitatively measure changes in asymmetric zonal thermal forcing (ZTF), *He et al*. [2014]

defined a land-sea index (LSI) as a linear combination of the average surface temperature anomaly in key areas of the COWL pattern. They found that a negative LSI, as well as stronger ZTF, followed the warm ocean-cold land (WOCL) pattern, indicating a larger land-sea thermal contrast during the winter, which would favor the formation and persistence of synoptic atmospheric blocking. During the second half of the twentieth century, the LSI shifted from negative to positive anomaly in around 1980 [*He et al*., 2014]. Consequently, blocking over Eurasian and North American also decreased, which was caused by the change in surface thermal forcing, namely, a decrease in ZTF. This decreased blocking would further increase inland temperatures, giving rise to a positive feedback. This feedback would help to accelerate global warming during the accelerated warming period, as well as generate a cooling trend over the Eurasian continent during the recent warming hiatus period. Many studies have shown that Eurasian blocking increased during the warming hiatus of 1998–2012 [*C. Li et al*., 2015a; *Xie et al*., 2016; *Huang et al*., 2017a], which supports the above proposed mechanism.

In addition to ZTF, the meridional thermal forcing (MTF) can also affect temperature in the middle and high latitudes. MTF results from the meridional temperature gradients between the middle and high latitudes. *Huang et al*. [2017a] found that the effect of DMO on SAT was strongest during periods of simultaneous weaker (stronger) MTF and stronger (weaker) ZTF. They suggested that the current hiatus resulted from a downward DMO with a weaker MTF and stronger ZTF together; these effects gave rise to a weaker polar vortex and westerly winds along with amplified planetary waves as well as facilitated an Arctic cold air invasion and blocking formation. The weaker MTF followed a pattern of "warm Arctic and cold land" (WACL) pattern [*Overland et al*., 2011; *Mori et al*., 2014; *Huang et al*., 2017a]. The weakened MTF, or the WACL, induced positive geopotential height anomalies over the Arctic, which correspond to a weakened polar vortex. Some recent studies have suggested that Arctic amplification might be related to Ural blocking (UB) [*Luo et al*., 2016b, 2016a, 2017; *Yao et al*., 2017]. UB could amplify Arctic warming, although this mechanism depends on the phase of NAO [*Luo et al*., 2016a]. On the other side, a weakening MTF caused by Arctic warming can induce a weakening westerly winds and increased quasi-stationarity and persistence of the UB, leading to more Eurasian cold events and further enhancing Arctic warming via blocking-induced amplification [*Luo et al*.,

2017; *Yao et al.*, 2017]. Together, the weaker MTF and stronger ZTF favor weaker westerlies over the high latitudes and enhanced southward flow over many regions of Eurasia and North America [*Huang et al.*, 2017a]. Both the meridional (between Arctic and the Northern Hemisphere middle to high latitudes) and zonal (between the midlatitude continents and oceans) land-sea thermal contrast can induce the abrupt shift in thermally forced atmospheric circulations such as synoptic blocking. Thus, the meridional and zonal land-sea thermal contrast significantly influences the climate changes over the Northern Hemisphere continents, including the dryland regions of Eurasia and North America [*He et al.*, 2014; *Huang et al.*, 2017a].

However, there is significant controversy concerning the relative contributions of zonal and meridional thermal forcing. Recent studies have shown that GHGs and SSTs warming outside the Arctic could explain nearly all terrestrial warming [*Wu et al.*, 2011; *Sun et al.*, 2016] and that the observed cooling over central Eurasia related to an increase in cold winters was not due to Arctic sea ice loss [*McCusker et al.*, 2016; *Sun et al.*, 2016; *Woollings et al.*, 2014]. In addition, the different responses of summer and winter blocking to the land-sea thermal contrast could also contribute to the asymmetric warming trends between seasons. These concepts require further investigations.

6.3. Hadley Circulation Expansion

In recent decades, the change in the Hadley cell has been given significant attention because it can transport energy and angular momentum poleward and organize the three-dimensional tropical atmospheric circulation. Moreover, it plays a crucial role in the global climate system, especially in the subtropical dry zone [e.g., *Hu and Zhou*, 2009; *Fu et al.*, 2006; *Lu et al.*, 2007]. Observational evidences have indicated that the Hadley cell has widened over both hemispheres since 1979 [*Fu et al.*, 2006; *Hu and Fu*, 2007; *Seidel et al.*, 2008; *Johanson and Fu*, 2009; *Fu and Lin*, 2011]. It is shown that the tropical belt has widened by approximately 2° of latitude according to atmospheric temperature trends [*Fu et al.*, 2006]. *Birner* [2010] used four different reanalysis data sets and found that the widening trends of the tropical belt are particularly sensitive to changes in the tropopause height threshold. Additionally, the widening disappears in the NH and becomes nonrobust in the Southern Hemisphere if the width of the tropical belt is calculated more fairly and consistently. Moreover, *Davis and Birner* [2016] found that models and reanalyses are consistent to exhibit robust historical and future expansions of Hadley Cell.

The causes for the Hadley cell expansion is complex [*Seidel et al.*, 2008; *Hawkins and Sutton*, 2009] and is influenced by many factors including atmospheric stability [e.g., *Schneider*, 1977], tropical heating processes [e.g., *Mitas and Clement*, 2006], total atmospheric moisture [e.g., *Frierson et al.*, 2006], and large-scale atmospheric eddy dynamics [e.g. *Walker and Schneider*, 2006; *Levine and Schneider*, 2011]. Many studies have shown that the Hadley cell expansion is closely related to the changes in SSTs [*Lu et al.*, 2008], ozone depletion [*Hudson et al.*, 2006; *Polvani et al.*, 2011], and aerosols [*Allen et al.*, 2012]. Among them, the SST changes are important for the Hadley cell expansion in the NH, whereas the stratospheric ozone changes are important for the Southern Hemisphere [*Garfinkel et al.*, 2015]. It is well known that the descending branch of the Hadley cell can greatly affect the majority of the Earth's arid and semiarid regions [*Seager et al.*, 2007; *Cai et al.*, 2012; *Nguyen et al.*, 2013, 2015]. Such widening of the Hadley cell is always accompanied by expanding large-scale sinking that suppresses convection, which results in shifts in precipitation and temperature patterns, causing serious consequences for inhabitants who are accustomed to established precipitation patterns [e.g., *Lu et al.*, 2007; *Seidel et al.*, 2007, 2008]. For example, *Seager et al.* [2007] has indicated that the Hadley cell expansion is partially responsible for the projected aridity and water shortage changes in the subtropical land areas of the NH (e.g., arid/semiarid regions in the American Southwest and Mediterranean Europe). Since the late 1970s, semiarid regions of the Southern Hemisphere have experienced a drying change that is attributable to the poleward expansion of the Southern Hemisphere Hadley cell [*Cai et al.*, 2012]. Recently, *Nguyen et al.* [2015] noted that the Hadley cell expansion is strongly associated with the poleward shift of the subtropical dry zone, which explains the increasing trends of droughts in subtropical areas such as Australia, Africa, and South America.

To date, advances in modeling have suggested that the widening of the zonal mean circulations related to the Hadley cell is associated with global warming [e.g., *Yin*, 2005; *Frierson et al.*, 2007; *Lu et al.*, 2007; *Previdi and Liepert*, 2007; *Lau and Kim*, 2015]. A robust characteristic of anthropogenic climate change is a poleward expansion of the Hadley cells [*Lu et al.*, 2007; *Seager et al.*, 2007], resulting in a poleward expansion of subtropical dry zones [*Scheff and Frierson*, 2012a]. Although the climate model simulations offer a strategy

to assess the Hadley cell response to global warming, a number of problems remain unknown. Thus far, attempts to understand the recent changes in the Hadley cell width have focused on comparing observations to GCM simulations of 21st century climate [*Lu et al.*, 2007] and idealized GCMs [*Frierson et al.*, 2007]. Some other studies have focused on the poleward shifts in zonal mean circulations related to the Hadley cell solely as projected changes during the 21st century [*Yin*, 2005; *Previdi and Liepert*, 2007]. Although all of these studies suggest a widening of the Hadley cell over the 21st century that is associated with global warming, the model projected rate is much smaller than the observations [e.g., *Lu et al.*, 2007; *Johanson and Fu*, 2009].

In addition to the width of the Hadley cell, changes in its intensity also represent a crucial factor in climate variations. Even small changes in the Hadley cell may have a profound impact on the position and variability of the tropical rain belt, Asian monsoon, and subtropical drylands [*Feldl and Bordoni*, 2016]. The Hadley cell may also have strengthened, although evidences for a significant strengthening are ambiguous [*Quan et al.*, 2004; *Mitas and Clement*, 2006]. In model simulations, the weakening of the Hadley cell is one of the robust responses of many global climate models to a warming Earth [*Held and Soden*, 2006; *Lu et al.*, 2007; *Vecchi and Soden*, 2007], but this is not consistent among all models [*Tanaka et al.*, 2005]. Therefore, these results should be taken seriously when considering the influences of Hadley cell variation on the climate changes over subtropical drylands.

7. Impacts of Human Activities

Anthropogenic activities play an important role in dryland climate change. Salinization, desertification, the loss of vegetative cover, the loss of biodiversity, and other forms of environmental deterioration are partly a result of anthropogenic activities [*Huang et al.*, 2016a, 2017a]. As economic development has progressed rapidly, more fossil fuels have been consumed, producing substantial GHG emissions and energy [*Barnett and O'Neill*, 2010]. The released GHGs and energy have strongly influenced the spatial distribution of temperature in recent years [*Li and Zhao*, 2012; *Zhang et al.*, 2013], especially in developing countries, where economic policies lead to the inefficient use of resources and, thus, increased energy wastage. The enhanced warming that has occurred in drylands [*Huang et al.*, 2012] is closely related to the effects of human activities, especially in higher density GHG scenarios [*Huang et al.*, 2017a]. In this section, we will provide an overview of the latest progress in the impacts of increased GHG emissions, anthropogenic aerosols, and land use and urbanization on dryland climate change.

7.1. Increased GHG Emissions

Regarding the influence of GHGs on climate change, climate models have robustly predicted an increase in the global mean precipitation in response to increased GHG emissions [*Mitchell et al.*, 1987; *Allen and Ingram*, 2002; *Held and Soden*, 2006; Lambert and Webb, 2008; *Stephens and Ellis*, 2008; *Pendergrass and Hartmann*, 2014]. *Sherwood and Fu* [2014] found that overall, the terrestrial climate become drier in the future because of an obvious increase in PET in a warming climate. Based on global climate model output from the CMIP5, many studies [*Feng and Fu*, 2013; *Dai*, 2013b; *Cook et al.*, 2014a; *Scheff and Frierson*, 2015; *Lin et al.*, 2015; *Huang et al.*, 2017a] have projected drying trends over land during the 21st century, with high GHG emissions.

Fu and Feng [2014] examined the terrestrial-mean aridity index, which is defined as the ratio of P to PET (i.e., P/PET), in respond to GHG forcing using CMIP5 transient CO_2 increase to $2 \times CO_2$ simulations. They found that the increase in the P averaged over land is approximately 1.7%/°C of the ocean-mean SAT increases, whereas PET increased at a rate of 5.3%/°C; thus, P/PET decreases by approximately 3.4%/°C, leading to a drier climate. A framework for understanding the change in P/PET has been created and suggests that a drier terrestrial climate is caused by (1) enhanced land warming relative to the ocean, (2) decreased RH over land but increased RH over the ocean, (3) a partial increase in net downward surface radiation into the deep ocean, and (4) different responses of PET over land and ocean to given changes in atmospheric conditions (Figure 16). The relative contributions of these four factors to changes in the terrestrial-mean aridity index are approximately 35%, 35%, 15%, and 15%, respectively.

A decrease in the terrestrial-mean aridity index of 2.7%/°C (approximately 3.2%/°C) global-mean (ocean-mean) SAT increase was calculated by *Lin et al.* [2016a] using the Community Earth System Model (CESM) ensemble simulations to isolate the impact of GHGs. Using the GCM output from CMIP5, *Cook*
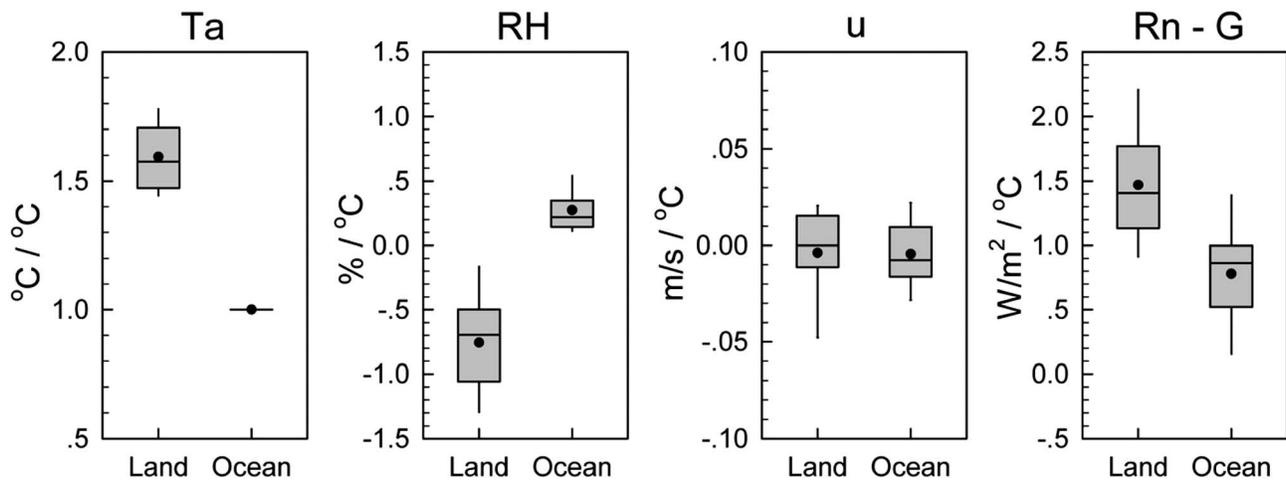
Figure 16. Changes in SAT (first panel, T_a), relative humidity (second panel, RH), wind speed (third panel, u), and available energy (fourth panel, R_n-G) averaged over land and ocean and scaled by ocean-mean SAT increases, from the CMIP5 1pctCO2 simulations. The results are plotted with box and whisker diagrams representing percentiles of changes computed from the 25 models. The central line (black dot) within each box represents the median (mean) value of the model ensemble. The top and bottom of each box indicate the 75th and 25th percentiles, and the top and bottom of each whisker indicate the 95th and 5th percentiles of the ensemble, respectively. Cited from *Fu and Feng* [2014].

et al. [2014a] investigated projected 21st century drying and wetting trends under the RCP8.5 scenario according to PDSI SPEI. Their results showed that robust cross-model drying occurs in western North America, Central America, the Mediterranean, southern Africa, and the Amazon, whereas robust wetting occurs in the NH high latitudes and east Africa (PDSI only). The SPEI is more sensitive to PET changes than the PDSI, especially in arid regions such as the Sahara and Middle East. *Seager et al.* [2010] analyzed 15 coupled climate models and revealed that the climate of southwestern North America will become drier throughout the 21st century because of rising GHG emissions. The regional discrepancies observed in this previous work are consistent with the result reported by *Scheff and Frierson* [2015]. They found that with greenhouse warming, land P does not systematically increase or decrease, except at high latitudes. Therefore, because of moderate, ubiquitous PET increases, P/PET decreases (drying) are much more widespread than increases (wetting) in the tropics, subtropics, and midlatitudes in most models; this finding confirms and builds on those of earlier studies.

Greve and Seneviratne [2015] assessed the future changes in hydroclimatological conditions based on an ensemble of 30 models from CMIP5 using P-Ep (i.e., precipitation-potential evaporation) as a measure of aridity instead of P/PET used in the above studies. A robust increase in aridity was detected in several subtropical regions and their adjacent humid regions, further confirming the previous findings of dryland expansion. By affecting the precipitation and the fertilization effect, increases in GHGs, such as CO_2, may further influence dryland vegetation. *Lu et al.* [2016] hypothesized that elevated level of CO_2 drive global drylands greening by affecting plant water savings and available soil water and tested this hypothesis using meta-analytic techniques, analyzing 1705 field measurements from 21 distinct sites. A strong response of the availability of soil water to the elevated CO_2 was observed in drylands. *Ukkola et al.* [2015] also observed that an elevated atmospheric CO_2 level altered the vegetation and hydrology across Australia based on the NDVI and evapotranspiration data of the period 1982–2010. Therefore, the biological effects of vegetation adaptations to GHG changes should be evaluated in future studies.

7.2. Anthropogenic Aerosols

In addition to the GHGs, aerosols are also key forcing agents associated with human activities [*IPCC*, 2013, 2014]. The aerosol declines relative to the present levels that are expected to occur in the 21st century would lead to additional warming of the system, which could aggravate the climate impact caused by GHG-induced warming. Therefore, it is important to investigate and understand the response of terrestrial aridity to aerosols.

Lin et al. [2016a] examined the changes in terrestrial aridity index forced by aerosols, using three sets of ensemble simulations from the CESM. They found that aerosol reductions exert a small impact on global
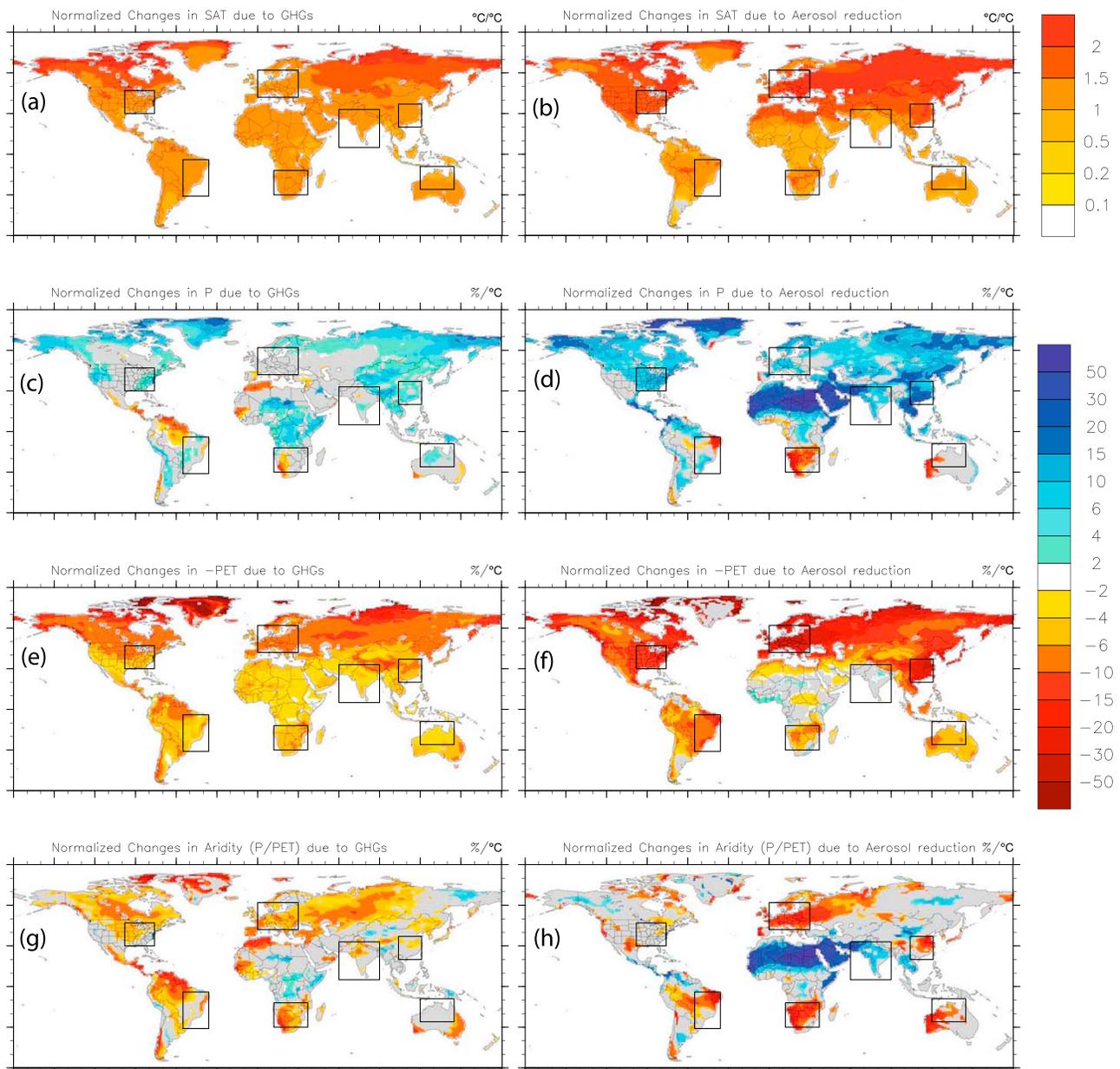
Figure 17. Changes in surface air temperature (SAT), precipitation (P), potential evapotranspiration (PET) and P/PET due to (a, c, e, and g) GHGs and (b, d, f, and h) aerosols, scaled by global-mean SAT changes. Gray regions do not have statistically significant changes based on a 95% confidence interval from a two-sided *t* test. Cited from *Lin et al.* [2016a].

aridity index because of offsetting effects of P and PET but can significantly affect regional aridity index. Additionally, they discovered that aerosol-induced AI changes are caused by different factors over different regions (Figure 17). *Fu et al.* [2016] showed that although anthropogenic aerosols have small effects on terrestrial-mean aridity index, they could largely alter its attributions from the temperature change to precipitation change. This might make the detection and attribution of aridity change due to GHG increases difficult when aerosols also exert a forcing because the precipitation has much larger natural variability than temperature.

C. Li et al. [2015b] investigated the effects of anthropogenic aerosols on temperature changes in the arid-semiarid region and humid-semihumid regions of China using model outputs from CMIP5. In general, anthropogenic aerosols reduced the temperature and exhibited greater contributions over the humid-semihumid regions than over the arid-semiarid regions.

Meehl et al. [2012] examined time series of annual-mean globally averaged SAT data from 1850 to 2005for sulfate (SO_4) aerosol forcing using the Community Climate System Model, versions 4 (CCSM4). Their results indicated that the negative RF of SO_4 aerosols decreased the temperature by $-0.25 \sim -0.40$°C by the end of the twentieth century. *Levy et al.* [2013] concluded that both direct and indirect effects of SO_4 aerosols dominate the strong precipitation response and the their indirect effects strongly enhance the impacts of aerosols on the surface temperature based on the Geophysical Fluid Dynamics Laboratory's (GFDL's) fully coupled chemistry-climate model CM3.

Positive BC RF enhances the direct radiative heating of the atmosphere and increases the global mean SAT [e.g., *Bond et al.*, 2013]. The warming surface tends to increase the longwave cooling, which leads to increased precipitation [*Held and Soden*, 2006]. However, the atmospheric solar absorption caused by BC suppresses P [*O'Gorman et al.*, 2012]. In CESM and GFDL models, the suppression of P outweighs the surface warming effects of BC, resulting in a net decrease in the global mean precipitation [*Ocko et al.*, 2014; *Lin et al.*, 2016b]. Moreover, BC decreases the solar radiation that reaches the surface, leading to decreased PET. In contrast, BC-induced surface warming tends to increase PET. Interestingly, the surface warming effect outweighs the radiation effect in terms of the effect on PET, resulting in a net increase in the global mean PET, which combines with the above P suppression to lower the AI (increasing aridity) [*Lin et al.*, 2016a, 2016b].

Lin et al. [2016b] further explored the terrestrial aridity index responses to anthropogenic BC and SO_4 aerosols using CESM simulations. Positive BC RF decreases P/PET by 1.9%/°C of warming (i.e., drying), with P decreasing by 0.9%/°C and PET increasing by 1.0%/°C. Negative SO_4 forcing has a small effect on terrestrial-mean P/PET (drying of 0.4%/°C cooling) because of the cancelation effect of decreased P (6.7%/°C) and decreased PET (6.3%/°C). Despite their opposite effects on global-mean temperature, BC and SO_4 both contributed to drying in the twentieth century.

The impacts of natural dust aerosols on climate change have been reviewed in section 4, and here we focus on the impacts of anthropogenic dust. *Guan et al.* [2015] found a positive relationship between regional warming and anthropogenic dust aerosols in drylands. By using CALIPSO dust, PBL height retrievals, and a land use data set, *Huang et al.* [2015] revealed that local anthropogenic dust aerosols originating human activities, such as agriculture, industrial activity, transportation, and overgrazing, account for about 25% of the global continental dust load. *Xi and Sokolik* [2016] quantified the anthropogenic dust emission in Central Asia by using the Weather Research and Forecasting-Chem-DuMo model system and indicated that anthropogenic dust emission and land cover change contributed 18.3–56.5% of dust emission in Central Asia during 2000 and 2014. *Zhao et al.* [2014] used an aerosol-climate coupled system (BCC_AGCM2.0.1_CAM) and found that dust aerosols can cause surface cooling over arid and semiarid regions and that precipitation is decreased (increased) over these regions in the NH (SH) through the different effects of dust aerosols on evaporation and circulation. Additionally, PET is decreased over most of these regions, primarily because of the changes in net radiation flux. As a net effect, dust aerosols do not exacerbate the aridity or enlarge the areal extents of arid and semiarid regions globally. Additionally, a sequence of GCM experiments showed that dust aerosol forcing and land surface changes likely contributed to the intensity and persistence of the U.S. Central Plains megadroughts because dust increases the shortwave planetary albedo, thereby reducing energy inputs to the surface and boundary layer. Energy deficits also increase atmospheric stability, inhibiting convection and reducing cloud cover and precipitation over the central plains [*Cook et al.*, 2013].

7.3. Land Use and Urbanization

Nature and human activities have modified and will continue to modify the Earth's surface. Land use/cover change (LUCC) has a prominent impact on regional climate and environment by altering energy, momentum, and moisture exchange between atmosphere and land surface [*Findell et al.*, 2007; *IPCC*, 2013, 2014]. More attention and efforts are required to improve our understanding of the processes and mechanisms that control the interactions among LUCC, regional climate, and socio-ecosystems over drylands [*Fu and Mao*, 2017].

Negative LUCC can dry the climate and lead to land degradation, particularly over semiarid regions. For example, in the Sahel, positive feedbacks between degraded land and regional climate were found. Dry

soil and smaller leaf area would increase the surface albedo and reduce transpiration, further intensify drought [*Charney*, 1975; *Xue and Shukla*, 1993; *Taylor et al.*, 2002]. *Olson et al.* [2008] found a similar positive feedback over arid/semiarid regions in East Africa and revealed that the projected large expansion of cropping into natural savannas would lead to drier conditions in this region.

Using a climate model coupled with a land surface scheme, *Avila et al.* [2012] demonstrated that anthropogenically induced changes in temperature extremes are not merely affected by increasing CO_2; instead, land use-induced land cover change (LULCC) may regionally mask or amplify the impact of increasing CO_2. However, the influence of LULCC on extreme temperature indices has a smaller magnitude and is more local than that of doubling CO_2. *Junkermann et al.* [2009] indicated that changes in surface properties constitute key factors contributing to observed reduction of precipitation.

Fu et al. [2016] examined the impact of land use on the SAT, P, PET, P/PET, and other meteorological variables averaged over land by using CESM simulations forced with the transient evolution of land use conditions [*Otto-Bliesner et al.*, 2015]. The land use resulted in a slight decrease in both precipitation (nonsignificant) and PET (significant), leading to nonsignificant changes in P/PET. A decrease in PET associated with land use resulted from the combined effects of decreases in SAT and available energy and increases in RH and surface wind (Figure 18).

Mahmood et al. [2014] recommended that several observational platforms should be used to better detect the climate impacts of land use change; more accurate vegetation and management data are also needed to continually improve the simulations of the climatic impacts of land cover change.

Extreme climatic events can have disproportionate effects on ecosystems. Drought-induced forest die-off in a region may increase the biogeophysical climate impacts of deforestation, resulting in a large uncertainty in regional climate-ecosystem interactions and carbon-cycle feedbacks within the global climate [*McAlpine et al.*, 2010]. *Sterling et al.* [2013] demonstrated that land cover change reduces annual terrestrial evapotranspiration and alters annual runoff to a similar or greater extent than other major drivers, which can further affirm that land cover change plays an important role in the Earth system.

Human influences on drought and potential feedbacks between drought and society remain uncertain. Drought management is inefficient because feedback between drought and human activities is incompletely understood. In this human-influenced era, we must reformulate the concept of drought to include the humans' roles in mitigating and enhancing drought [*Van Loon et al.*, 2016]. Indeed, *Cook et al.* [2016] suggested that land surface change might generate megadroughts in North America.

8. Dryland Expansion, Desertification and Adaptation

Studies have indicated that global drylands as defined by the AI have expanded over the last 60 years and will continue to expand in the 21st century [*Feng and Fu*, 2013; *Huang et al.*, 2016a, 2017a]. The rising temperature, increasing aridity, and expanding drylands along with extensive land use and other human activities may lead to desertification, which will pose a severe threat to the ecosystems and inhabitants of drylands and exacerbate local tensions [*Winslow et al.*, 2004; *Jones*, 2011; *Milesi et al.*, 2010; *Shinoda*, 2017]. Therefore, proactive planning and adaption strategies should be developed, and management and adaptation actions must be taken for global drylands with careful consideration of region-specific characteristics of a nature-society system. This section will summarize the recent progress in research on dryland expansion, desertification, and adaptation.

8.1. Dryland Expansion in Observations and Simulations

Many studies using observational data have reported that dryland expansion is a result of global warming. *Huang et al.* [2016a, 2017a] analyzed the temporal variations in the areal coverage of drylands as defined by the AI and its subtypes from 1948 to 2008 and found that global drylands have expanded because the area of drylands from the more recent 15 years (1990–2004) is 2.6×10^6 km^2 (or 4%) larger than that from the period 1948–1962; this is consistent with the results from other studies [*Feng and Fu*, 2013; *Ji et al.*, 2015]. Moreover, expansions of the dryland subtypes are 0.6×10^6 km^2, -0.1×10^6 km^2, 1.6×10^6 km^2, and 0.5×10^6 km^2 for the hyperarid, arid, semiarid, and dry subhumid regions, respectively. The largest dryland expansion has occurred in semiarid regions, where the area has expanded since the early 1960s (Figure 19d)
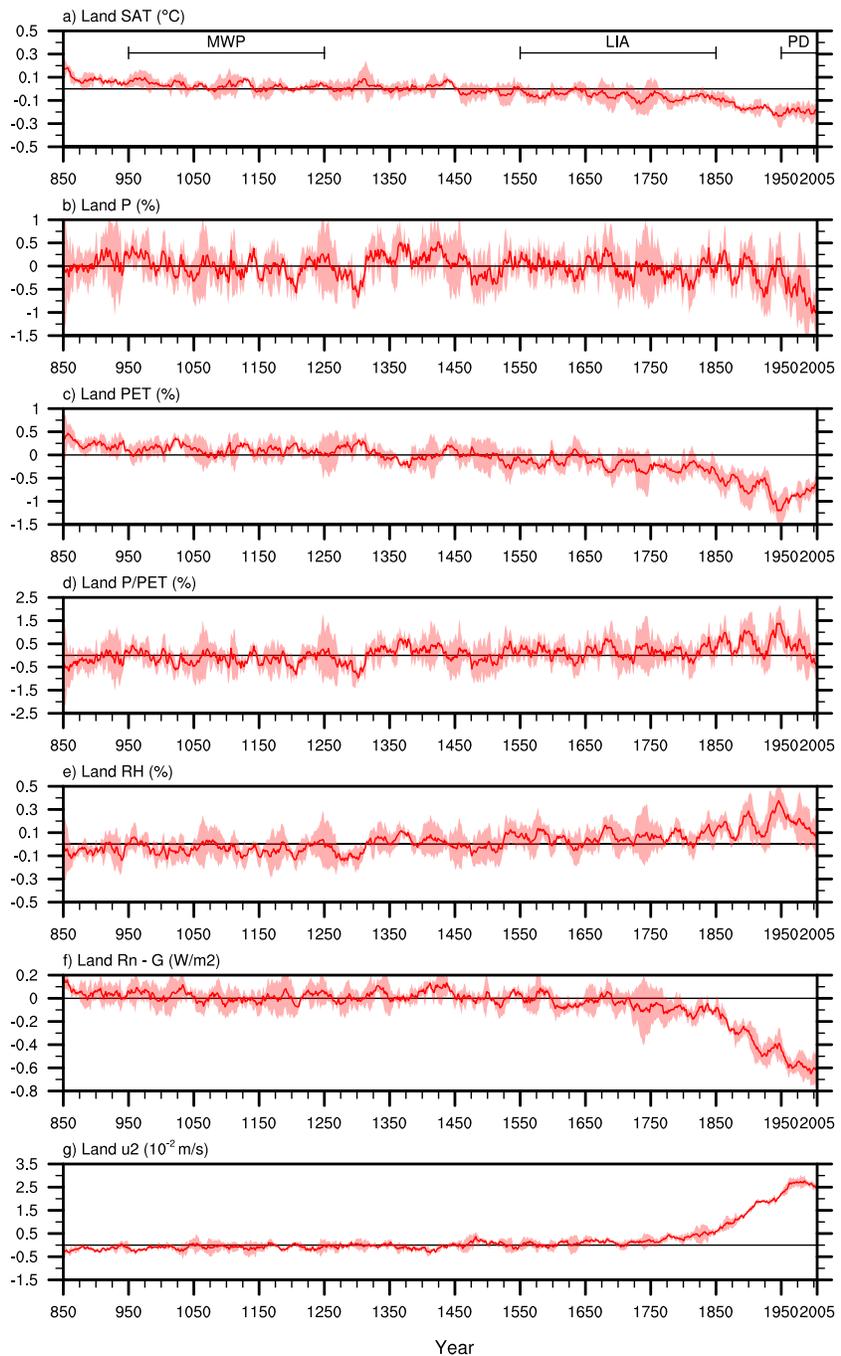
Figure 18. Temporal evolutions of annual mean anomalies in (a) surface air temperature (SAT), (b) precipitation (P), (c) potential evapotranspiration (PET), (d) aridity index (P/PET), (e) relative humidity (RH), (f) available energy (Rn-G), and (g) wind at 2 m above the surface (u2) due to land use, averaged over land, for 850 to 2005 A.D. from CESM-LME. The red lines are the ensemble average of the three simulations, and the shading denotes two standard deviations of the three ensembles. The units for P, PET, and P/PET are in percentage relative to the last millennium (850–1850) climatology. The periods of the Medieval Warm Period (MWP) (950–1250 A.D.), the Little Ice Age (LIA) (1550–1850 A.D.), and the present day (PD) (1950–2005 A.D.) are indicated in Figure 18a. Cited from *Fu et al.* [2016].

and accounts for more than half of the total dryland expansion (Figure 19b). The net change in the global semiarid regions (i.e., 1.6×10^6 km^2) is calculated by subtracting the reduced areas (transitions from semiarid to other subtypes) from the newly formed areas (transitions from other types to semiarid). Comparing the two types of shifts, semiarid areas that originated from subhumid/humid regions are nearly
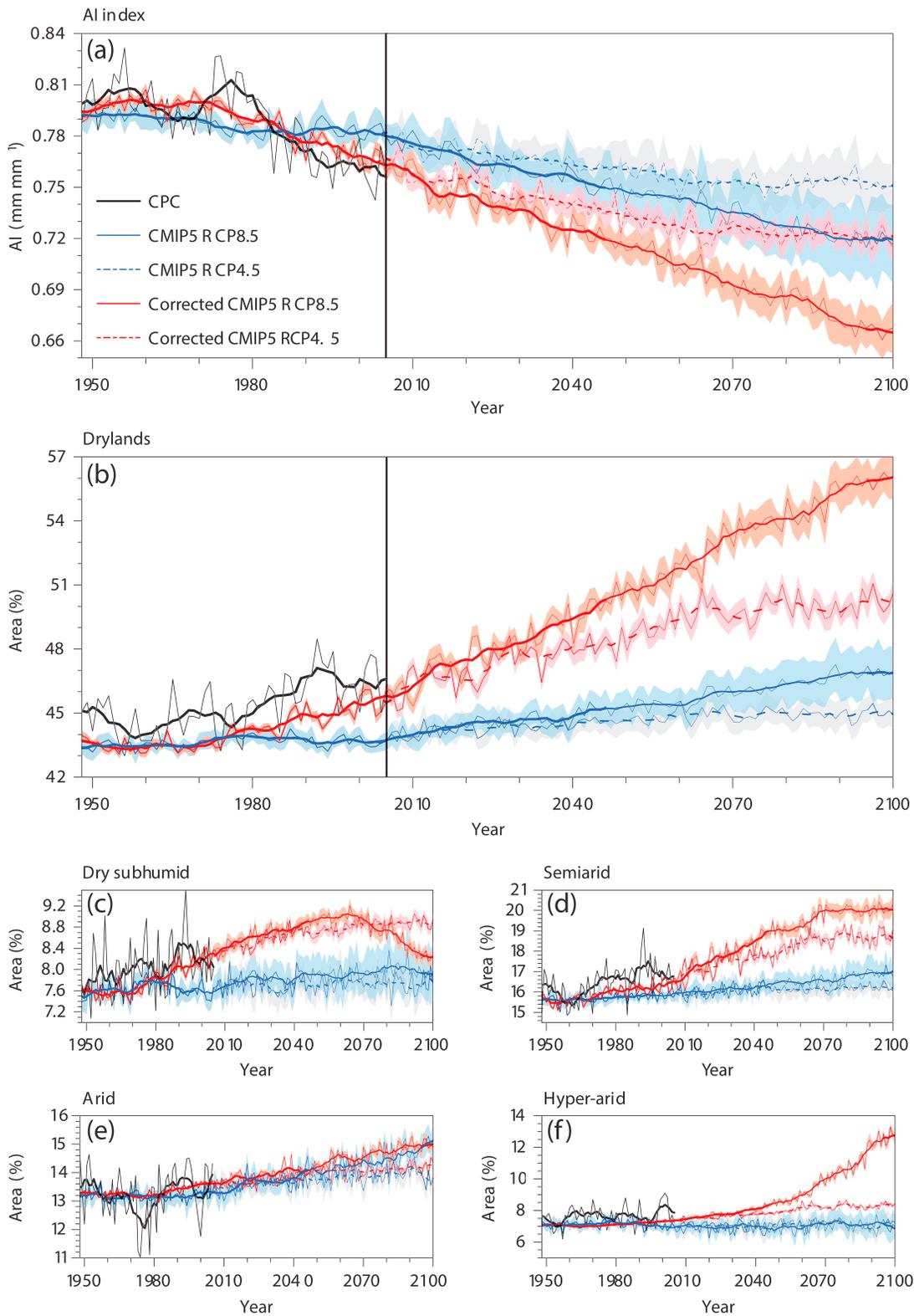
Figure 19. Temporal variations in the (a) global-mean AI and the areal coverage (% of global land area) of (b) total drylands, (c) dry subhumid regions, (d) semiarid regions, (e) arid regions and (f) hyperarid regions. The thin black lines are the CPC observations, and thin blue solid (dashed) lines are the CMIP5 multimodel ensemble mean (CMIP5-EM) from the historical and RCP8.5 (RCP4.5) projections. The thin red solid and dashed lines are the corrected CMIP5-EM results from the historical and RCP8.5 and RCP4.5 projections, respectively. The shading denotes 95% confidence intervals for the 20 models. The 7 year running means (thick colored lines) are shown to emphasize the aridity trends. Cited from *Huang et al.* [2017a].

3 times as large as those that originated from arid regions. This result indicates that the newly formed semi-arid regions primarily originated from subhumid and humid regions, which account for 73% of the newly formed semiarid regions. They also noted that the area transitioning from semiarid (subhumid/humid) to arid (semiarid) is much larger than that transitioning from arid (semiarid) to semiarid (subhumid/humid); there-fore, more semiarid (subhumid/humid) regions become drier [*Huang et al.*, 2016a].

Moreover, *Dai et al.* [2004] used the PDSI index to indicate the changes in the extremely dry/wet areas. They found that across the globe, very dry areas (defined as having a PDSI <-3.0) have more than doubled in size since the 1970s, with large increases in the early 1980s due to ENSO-induced precipitation decreases and later because of surface warming; by contrast, very wet areas (PDSI $>+3.0$) across the globe declined slightly during the 1980s. Together, the land areas characterized as very dry or very wet have increased in global extent from 20% to 38% since 1972, with surface warming as the primary cause after the mid-1980s. *Huang et al.* [2016a] examined the global distribution of semiarid regions and their transitions to other types and selected eight typical semiarid subregions. Results indicated that except for Central Asia and northern Africa, semiarid regions expanded in the other six subregions. The semiarid expansion in East Asia is the largest single expansion and accounts for nearly 50% of the global semiarid expansion. Moreover, relative to the six semiarid subregions in the Eastern Hemisphere, except for central/west Australia, the area that shifted to drier types is much larger than that shifted to wetter types, particularly in East Asia and northern Africa. In all eight semiarid subregions considered, two of the three ones that shifted to wetter types are within the American continents. *Feng et al.* [2014] suggested that the climate types will shift toward warmer and drier ones based on the Köppen-Trewartha climate classification. Specifically, the temperate, tropical, and dry climate types are projected to expand.

Based on the observations of dryland expansion from the historical period, many studies forecast future dryland expansion. By analyzing climate model simulations from CMIP5, *Feng and Fu* [2013] found that by the end of the 21st century (2071–2100), global drylands are projected to be 5.8×10^6 km^2 (or 11%) larger than in the 1961–1990 period, according to the RCP8.5. Furthermore, *Feng and Fu* [2013] predicted changes in coverage to drier and wetter types for 2071–2100 under RCP8.5 relative to 1961–1990. Major expansions of hyperarid areas are projected over northern Africa, parts of Saudi Arabia and Iraq, and southern Africa. Major expansions of arid regions will occur over southwest North America, the northern fringe of Africa, southern Africa, the Middle East, and Australia. Prime expansions of semiarid regions are projected over the north side of the Mediterranean, southern Africa, and North and South America. Focusing on North America, the arid regions are projected to occupy most of New Mexico, western Texas, and most of northern Mexico; the semi-arid regions are also projected to expand eastward by 2–3° of longitude in the Great Plains by the end of this century. Over the northern fringe of Africa, the arid and hyperarid climate is projected to expand into regions where the climate is currently semiarid. In southern Africa, the semiarid region is expected to expand north-ward and eastward while an arid climate is expected to cover most of Namibia and the majority of Botswana.

However, the above studies have indicated that the CMIP5 simulations have underestimated the dryland expansion (1948–2005), on the basis of observations [*Feng and Fu*, 2013; *Ji et al.*, 2015; *Huang et al.*, 2017a]. *Ji et al.* [2015] used both observations and CMIP5 simulations to investigate the changes in areal coverage over drylands and the four subtype regions across the globe; they found that the simulated expansion of total drylands (semiarid regions) from the most recent 15 years (1991–2005) was just one fourth (one tenth) of the observed one. This AI trend underestimation is mainly attributed to the underestimation of precipitation trend [*Feng and Fu*, 2013], and the AI or precipitation trend is far more negative than any CMIP5 ensemble member, which could be attributed to the model deficiencies of CMIP5 that is not internal but forced signal; thus, the dryland expansion is quite underestimated and needs to be corrected. *Huang et al.* [2017a] used observational data to correct the CMIP5 projections and investigated changes in dryland coverage under the high (RCP8.5) and moderate (RCP4.5) emission scenarios. The results showed that under RCP8.5 (RCP4.5), the world's drylands will expand by 23% (11%) relative to 1961–1990, which means 56% (50%) of the total land surface will be covered in drylands by 2100 (Figure 20). From the spatial distribution of future changes in the dryland subtypes, in the middle of 21st century, the areas that will become drier are mainly distributed in eastern Siberia, northeastern China, western Asia, central Africa, and Canada, which are much larger areas than those that will become wetter (Figure 20b). Moreover, 78% of the dryland expansion will occur in developing countries, making the dryland coverage rate in these countries reach 61% by the end of this century under RCP8.5 (Figure 20c).
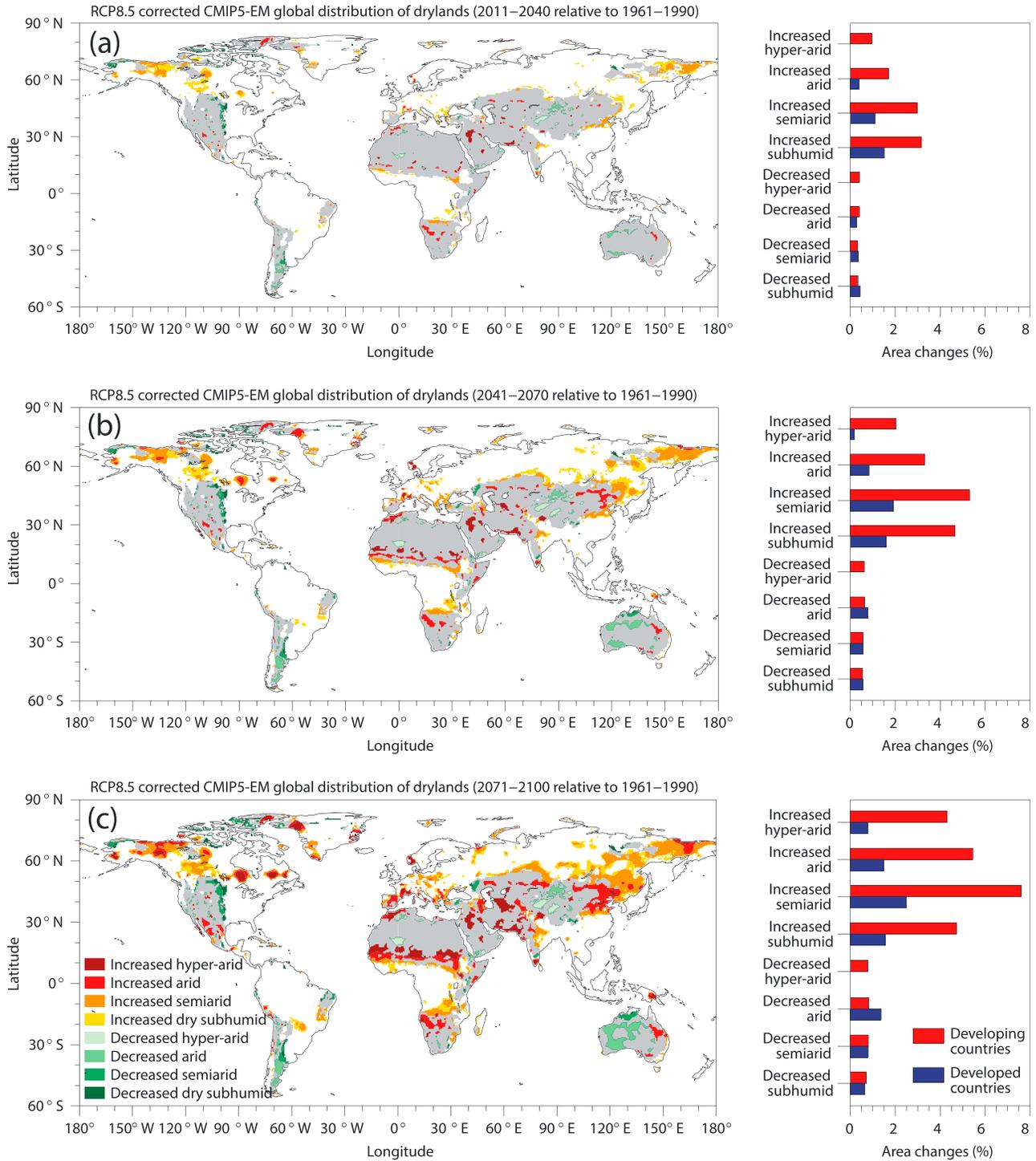
Figure 20. Global distribution of changes in the dryland subtypes from the corrected CMIP5 and RCP8.5 relative to the baseline (1961–1990), for the future periods of (a) 2011–2040, (b) 2041–2070, and (c) 2071–2100, and the corresponding changes in area (unit: percent of global land area) in developing and developed countries. The gray shading denotes the baseline drylands present in 1961–1990. Changes include any transition from adjacent and nonadjacent subtypes. For example, the "increased" category means that the indicated regions transitioned from any of the subtypes, i.e., semiarid, dry subhumid, and humid to a drier subtype; the "decreased" category refers to transitions from drier to wetter subtypes. Cited from *Huang et al.* [2017a].

8.2. Perspective of Dryland Desertification

Dryland expansion may lead to desertification, which will threaten the ecosystems and inhabitants of drylands [*Ohmura and Wild*, 2002; *Armah et al.*, 2010]. Desertification is an escalating concern over drylands [*White and Nackoney*, 2003], yet assessments to guide management and policy responses are limited by ambiguity concerning the definition of "desertification" and what processes are involved [*Bestelmeyer et al.*, 2015]. To improve clarity, *Kassas* [1995] identified the differences between drought (a natural hazard) and desertification (degradation of land resources). Desertification is defined as "land degradation in arid, semi-arid, and dry sub-humid areas resulting from various factors, including climatic variations and human activities", that is, it encompasses both biophysical and social factors [*Reynolds et al.*, 2007; *Spinoni et al.*, 2015]. Land degradation is in turn defined as the reduction or loss of the biological or economic productivity of drylands. It is a result of a long-term failure to balance demand for and supply of ecosystem services in drylands [*UNCCD*, 1994; *MEA*, 2005].

Assessment of the current status of desertification is the crucial first step in improving global food production and sustainably managing ecosystems in the context of climate change [*D'Odorico et al.*, 2013]. At the time of UNCOD (United Nations Conference on Desertification, 1977), the population in areas that had recently undergone severe desertification and were directly affected was estimated to be 78.5 million. The 1984 assessment (i.e., United Nations Plan of Action to Combat Desertification, PACD) confirmed that land continued to be irretrievably lost through desertification or degraded to desert-like conditions at a rate of 6 million ha annually [*Dregne et al.*, 1991]. The International Convention to Combat Desertification (CCD) secretariat indicated that desertification threatens approximately 30% of the Earth's terrestrial surface and already affects approximately 70% of the Earth's agricultural drylands, which are home to more than 250 million people in over 110 countries, with another 1 billion people at risk, and possible economic losses in the range of $42 billion annually [*Winslow et al.*, 2004]. *Bestelmeyer et al.* [2015] proposed that assessments of desertification and land transformation be placed within a state change-land use change(SC-LUC) framework and discuss how the SC-LUC perspective can guide more effective assessment of desertification and management of drylands.

Warren et al. [1996] indicated that major changes are likely to be experienced over arid and semiarid regions in the next few decades. The most important changes will be induced by increasing human pressures of various types, such as increasing population, in both rural and urban areas; continuing oil developments; and increased numbers of ambitious water infrastructure projects. Rural populations may be reaching the limits of cultivable land in many areas, which could impact soil and vegetation. According to UNEP's latest assessment (1991), 1.9 million ha of irrigated croplands (or 18% of the total area), 48.86 million ha of rain-fed croplands (or 61% of the total area), and 995.08 million ha of rangelands (or 74% of the total area) in Africa are affected by desertification at a moderate or higher level. Three distinct areas of the continent are at most risk: Mediterranean Africa, the Sudano-Sahelian region and the Kakahari-Namib region in southern Africa. Notably one third of Africa is affected by desertification and 73% of the total agriculturally used drylands are degraded [*Darkoh*, 1998].

However, some studies found that drylands were greening [*Fensholt et al.*, 2012; *Piao et al.*, 2015; *Zhang et al.*, 2015; *Mao et al.*, 2016] during the last three decades. *Fensholt et al.* [2012] analyzed the trends in vegetation greenness of semiarid regions across the globe using satellite-derived NDVI data sets during 1981–2007 and concluded that a slight increase in greenness over global semiarid regions. Moreover, *Piao et al.* [2015] used different satellite-derived LAI data sets and ecosystem models and detected the greening trend in China over the last 30 years and attributed it to increasing CO_2 concentrations and nitrogen deposition.

As one of the most seriously affected countries, China has made great efforts to combat desertification. Although improvements have been made in some areas, degradation continues to expand and is approaching sustainable water resource limits [*Feng et al.*, 2016]. Further land degradation assessments, such as assessments made by the Chinese Committee for Implementing UN Convention to Combat Desertification, will be necessary to ensure successful decision making, to combat increasing desertification and to implement Western strategies [*Yang et al.*, 2005]. *Xu et al.* [2009] developed a quantitative method for desertification assessment and assessed desertification of the Ordos Plateau in China by using Landsat data. They found that there was an overall decrease trend of desertification of the Ordos Plateau from 1980 to 2000.

Reynolds et al. [2007] reviewed recent lessons concerning the functioning of dryland ecosystems and the livelihoods systems of their human residents in which a new synthetic framework was introduced, the Drylands Development Paradigm (DDP). The DDP, which is supported by a growing and well-documented set of tools for policy and management action, helps to navigate the inherent complexity of desertification and dryland development, identifying and synthesizing the factors that are important for research, management, and policy communities [*Nahal*, 1995; *Qi et al.*, 2012].

8.3. Dryland Vulnerability and Adaptation

In climate change studies, vulnerability is defined as the degree to which a system is susceptible to, and unable to cope with, the adverse effects of climate change, including climate variability and extremes [*Intergovernmental Panel on Climate Change*, 2007], whereas hazard is defined as the potential occurrence of a natural or human-induced physical event or trend or physical impact that may cause various degrees of damage and loss [*IPCC*, 2014]. Thus, climate hazard (or forcing) and vulnerability of a system are jointly (but to different extents) responsible for natural disasters.

Drought is the most hazardous worldwide natural disaster in terms of the numbers of humans that are killed and/or those who are adversely affected [*Obasi*, 1994; *Guha-Sapir et al.*, 2004]. In general, high-impact climate-related hazards in drylands are characterized by drought, dust storms, and desertification. Drought acts as a background factor that influences dust storms as reported in section 4.1 [*Kurosaki et al.*, 2011b; *Nandintsetseg and Shinoda*, 2015], and the accumulated effect of multiyear droughts may lead to desertification. In addition to these phenomena, drylands at middle to high latitudes (such as those in Eurasia), with extreme cold in the winter, have long been jeopardized by repeated *dzud* (i.e., harsh cold-season conditions in Mongolian). Dzud is defined, biogeophysically, as anomalous climatic and/or land surface (i.e., snow/ice cover and lack of pasture) conditions that lead to reduced accessibility and/or availability of pastures and ultimately to significant livestock mortality during winter-spring [*Natsagdorj and Dulamsuren*, 2001]. Dzud occurs throughout central Asia and a similar phenomenon has previously been reported in inland Canada [*Shinoda*, 2017]. These drylands at middle to high latitudes are most likely to experience not only an intensified aridity but also a large degree of warming, especially during the cold season in semiarid regions [*Huang et al.*, 2012].

Recently, a new approach that focuses on multiple hazards has been evolving within disaster science [*ARMONIA*, 2007; *Kappes et al.*, 2012; *Gill and Malamud*, 2014], the call for "complete multihazard research" as a component of human settlement planning and management in disaster-prone areas originated within the UN Agenda 21 for sustainable development. Given this context, disaster management authorities, who are responsible for making countermeasure decisions for specific geographic areas, must consider all spatially relevant hazards. This interdisciplinary approach has been considered the "Applied Multi Risk Mapping of Natural Hazards for Impact Assessment" [*ARMONIA*, 2007] and "Integrating Dryland Disaster Science" [*Shinoda*, 2017] projects. The latter project aims to integrate studies on mechanisms of multidisasters over arid Eurasia and to develop comprehensive proactive countermeasures and policy recommendations in order to mitigate multidisaster impacts.

Multidisciplinary approaches to key linkages of complex natural and human systems have revealed that climate change impacts on such systems are often nonlinear, having a threshold or tipping point across which a catastrophic (and potentially nonresilient) change may occur in the system [see, e.g., *Scheffer et al.*, 2001]. For example, on the regional-continental scale, such changes or thresholds are detected in the response of vegetation to drought [*Shinoda et al.*, 2014], land-surface to wind erosion or dust emission (i.e., threshold wind speed) [*Kurosaki et al.*, 2011a], and livestock mortality to *dzud* [*Tachiiri et al.*, 2008; *Tachiiri and Shinoda*, 2012]. The satellite-derived threshold wind speed was used to produce a novel semi-real-time wind erodibility (i.e., soil susceptibility to wind erosion) map available for a dust early warning system [*Kimura and Shinoda*, 2010].

Shinoda et al. [2014] identified hot spots that exhibited nonresilient vegetation degradation after a multiyear megadrought in the Asian steppe using newly developed indices related to sensitivity and resilience (Figure 21). Temperate grasslands surrounding the desert dust source regions are likely to be sensitive to the ongoing and projected expansion of Asian drylands and are significant or potentially significant dust sources [*Shinoda et al.*, 2011; *Nandintsetseg and Shinoda*, 2015].
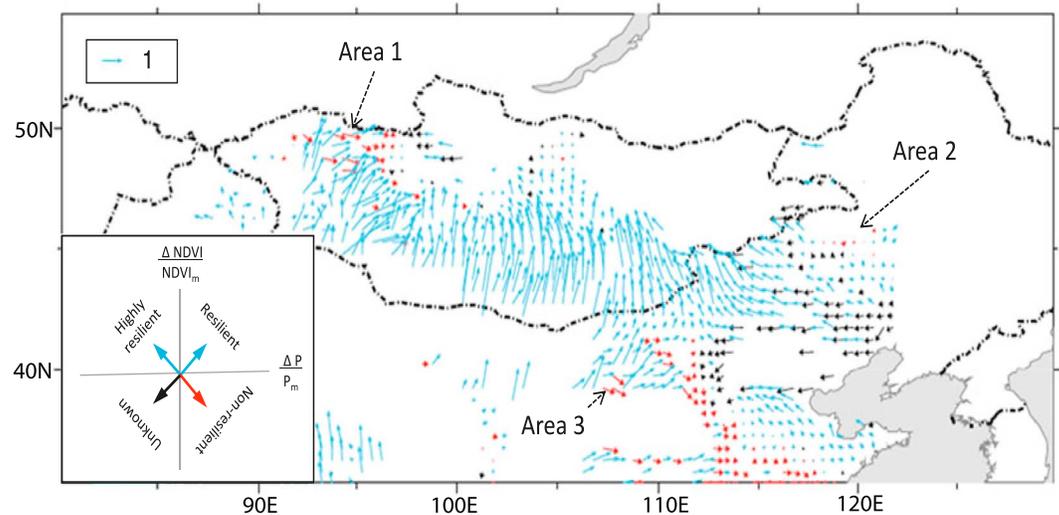
Figure 21. Spatial patterns in vectors of sensitivity and resiliency indices. See the details in *Shinoda et al.* [2014]. Nonresilient (potentially vulnerable) areas are denoted by red vectors indicating decreased vegetation despite increased precipitation during postdrought years, while resilient areas are indicated by blue vectors indicating increased vegetation during postdrought years.

In response to the dryland expansion discussed in section 8.1, adaptation actions must be taken based on projections of future climate hazards and insights into how and to what extent hazards and vulnerability of a local nature-society system will jointly result in disasters. Although disaster science employs quite a transdisciplinary approach that includes scientists and stakeholders, climate change scientists must take advantage of their modeling and analytical skills to identify catastrophic thresholds of the nature-society system.

9. Summary and Concluding Remarks

Drylands cover approximately 41% of the Earth's land surface and are home to more than 38% of the world's population [*White and Nackoney*, 2003; *Reynolds et al.*, 2007; *Mortimore et al.*, 2009; *UNDP*, 2014]. Drylands are particularly sensitive to climatic variability and change for several reasons. First, the relative scarcity of precipitation means that small changes can have large impacts. Second, most drylands exist along so-called "climate ecotones," the transition zones between a wet and a dry climatic regime often with sharp gradients in precipitation [*Nicholson*, 2011]. Compared to other regions, over drylands, the interactions among human activities, land surface, and climate change are more intense, especially in semiarid regions. Furthermore, perhaps more than anywhere else, the environments of drylands are the consequence of highly tuned feedback loops involving biological, geomorphological, hydrological, and human systems [*Nicholson*, 2011]. Changes in any of these systems can easily upset the feedback loops, creating serious environmental disturbances [*Graetz*, 1991; *Zimmerer*, 2014]. Determining how dryland climates will change in the future and how to create the strategies for regional sustainable development requires a deep understanding of the characteristics and mechanics of climate change over drylands. Therefore, investigating these issues will provide useful scientific knowledge for policymakers.

In this article, we provided an overview of the recent progress in dryland climate change research and systematically summarized the temporal and spatial characteristics of climate change over drylands. To better understand the dryland climate, scientists began to investigate the millennial climate over drylands using various paleoclimatic records. Results indicated that the dryland climate was warm and dry during the Middle Holocene in the western United States [*Grayson*, 2000; *Madsen et al.*, 2001; *Benson et al.*, 2002; *Jiang et al.*, 2007], whereas a relatively dry Medieval Warm Period and a wet Little Ice Age occurred in the last two millennia in Arid Central Asia [*Yang et al.*, 2009; *Chen et al.*, 2010]. Modern observations revealed that large increasing PET and decreasing precipitation have led to a drying trend, which is expected to affect a substantial portion of drylands [*Zhao and Dai*, 2015, 2016], leading to an approximately 10% increase in global dryland areas [*Feng and Fu*, 2013]. Results also indicated that the drying trend mainly occurred over
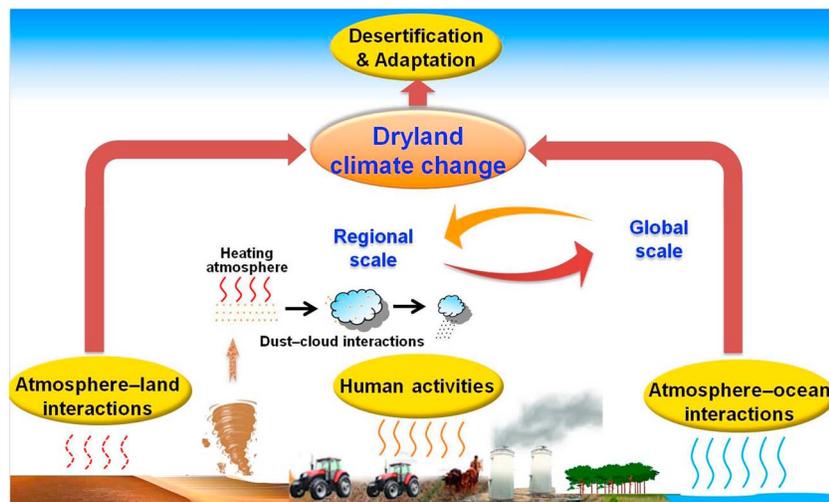
Figure 22. Major drivers of dryland climate system.

East Asia, the Sahel in West Africa, southern Africa, and eastern Australia beginning since 1950 [*Dai*, 2011a, 2011b, 2013b; *Dai and Zhao*, 2016; *Huang et al.*, 2016a; *Fu and Mao*, 2017]. Multimodel projections illustrated that drying is much more widespread than wetting in the tropics, subtropics, and midlatitudes because of ubiquitous PET increases [*Feng and Fu*, 2013; *Scheff and Frierson*, 2015]. Both observations and model simulations have indicated that precipitation changes played a relatively important role in climate shifts during the twentieth century. However, the projected temperature changes have become increasingly important and will dominate the shifts in climate types during the 21st century as warming becomes more pronounced [*Feng and Fu*, 2013; *Feng et al.*, 2014].

The temporal and spatial changes in the dryland climate may be caused by both regional and global-scale factors (Figure 22) via physical processes and dynamic mechanisms, including dust-cloud-precipitation interactions, atmosphere-land interactions, atmosphere-ocean interactions, and human activities. In terms of the local dust-cloud interactions, dust aerosols affect the dryland climate through direct, indirect and semidirect effects. These aerosols can absorb solar radiation and subsequently accelerate the evaporation of water droplets in lower atmosphere water clouds, thereby decreasing the cloud liquid water path. However, atmosphere-land interactions determine the intensity of the response to climate change over different regions. The land surface changes induced by drought in arid, semiarid, and subhumid regions appear to evoke a positive feedback loop that reinforces such droughts, prolonging and intensifying them. The atmosphere-ocean interactions mainly determine the decadal to interdecadal dryland climate changes on the global scale. Additionally, the decadal to interdecadal variability of SSTs can alter the overlying atmospheric circulation and influence drylands through teleconnection. Human beings have dramatically altered the global land surface and atmospheric composition through such activities as deforestation, agriculture, and the burning of fossil fuels. The effects of human activities will determine the long-term change trends, particularly those of temperature and precipitation. The progress regarding how these major processes affect dryland climate change is summarized in the following four paragraphs.

Arid and semiarid regions are the primary sources of mineral dust [*Penner et al.*, 2001; *Huang et al.*, 2015], which strongly impacts regional climate by modifying the energy balance and water cycles through aerosol-cloud-precipitation interactions. As global temperature increases, the dust amount increases because of decreases in wet deposition associated with decreased large-scale precipitation over land [*Allen et al.*, 2016]. Dust aerosols can alter the radiative energy of the Earth's surface atmosphere by directly attenuating solar radiation [e.g., *J. Huang et al.*, 2009] and indirectly modifying cloud macrophysical (areal coverage, structure, and altitude) and microphysical properties (droplet size and phase) in many different ways [e.g., *Huang et al.*, 2006a, 2006b]. The direct effects of dust aerosols over drylands lead to warming in the atmosphere, cooling at the surface, and, typically, warming or no change at the TOA because of higher surface albedo. Compared with the dust aerosols over the Sahara, Asian dust aerosols absorb more solar

radiation [*Ge et al.*, 2014]. Dust aerosols can evaporate clouds and, thereby, exert a warming effect on the climate [*J. Huang et al.*, 2010]. Furthermore, dust can inhibit or enhance precipitation under certain conditions, impacting the hydrological cycle. The issue of whether dust aggravates [*Huang et al.*, 2014] or alleviates [*Miller et al.*, 2004] desertification or plays an indiscernible role in the expansion of drylands [*Zhao et al.*, 2015] remains under debate. Although dust is often associated with drylands, significant dust events have also been reported at cold high latitudes [*Bullard et al.*, 2016]. Therefore, the impacts of high-latitude dust on the dryland climate should be evaluated in the future.

Enhanced dryland warming and decreased AI were identified [*Huang et al.*, 2012; *Berg et al.*, 2016] and amplified by atmosphere-land interactions through the responses of the energy cycle, water cycle, and carbon cycle under climate change. Enhanced dryland warming may aggravate dryland expansion by increasing the vapor pressure deficit and evaporative demand and decreasing soil moisture, possibly leading more energy to SH than to LH [*Seneviratne et al.*, 2010; *Sherwood et al.*, 2014]. The warming trends on global and regional scales are mainly attributable to radiatively forced temperature changes associated with stronger water vapor feedback over drier ecoregions in response to positive global-scale GHG forcing [*Guan et al.*, 2015; *Zhou et al.*, 2016]. In contrast, the heat from solar and infrared radiation is released primarily through sensible heat fluxes, and as a result, surface temperatures over drylands rise sharply and create an even stronger impact on temperature extremes [*Hirschi*, 2011; *Seneviratne et al.*, 2014]. Changes in temperature and soil moisture strongly impact the ecosystem carbon sequestration capacity over drylands, and the soil organic carbon storage decreases with increasing temperature and decreasing soil water content resulting from desertification [*Sharma et al.*, 2012; *Wu et al.*, 2013; *Sjögersten and Wookey*, 2016]. Therefore, enhanced dryland warming and atmosphere-land interactions result in a positive feedback loop that aggravates global warming [*Huang et al.*, 2017a].

Global-scale interdecadal aridity changes are controlled by continent-scale atmospheric and oceanic oscillations and by relevant global-scale factors, including planetary-scale changes in atmospheric circulations [*Ting and Wang*, 1997; *Dai and Wigley*, 2000; *Mo et al.*, 2009; *Schubert et al.*, 2009; *Hu and Feng*, 2012], SSTs [*Hoerling and Kumar*, 2003], and other external forcing [*Guan et al.*, 2015]. These influences can be demonstrated in terms of two aspects: First, Hadley cell expansion plays a crucial role in the global climate system, especially in subtropical drylands [*Fu et al.*, 2006; *Hu and Zhou*, 2009]. Second, the effects of these global-scale factors on dryland climate change with different regional performances are mainly determined by atmosphere-ocean interactions [*Feldl and Bordoni*, 2016]. These interaction effects on the decadal to interdecadal variability of SST in different ocean basins can trigger overlying atmospheric circulation anomalies on the corresponding timescales and, thereby, subsequently affects the climates over other regions via teleconnection [*Y. Zhang et al.*, 1997; *Mo et al.*, 2009; *Zhong et al.*, 2011; *Trenberth et al.*, 2014]. The compositions of different phases of the AMO, PDO, and ENSO [*Ma and Shao*, 2006; *Ma*, 2007; *Qian and Zhou*, 2014] will enhance or offset changes in land-sea and north-south thermal contrasts and, thus, affect the intensity of westerlies and planetary waves and the blocking frequency, accelerating or mitigating global warming and drying over a large scale [*Ma and Shao*, 2006; *Ma*, 2007].

Anthropogenic forcing from climate change has led to concerns regarding climate change in drylands [*Fu and Feng*, 2014; *Ji et al.*, 2015; *Donat et al.*, 2016; *Huang et al.*, 2016a, 2017a]. Many studies have projected drying trends over land during the 21st century in terms of different climate metrics because of high GHG emissions [*Held and Soden*, 2006; *Dai*, 2013b; *Feng and Fu*, 2013; *Fu and Feng*, 2014; *Cook et al.*, 2014a; *Scheff and Frierson*, 2015; *Huang et al.*, 2017a]. For example, according to CMIP5 transient CO_2 increase simulations, the AI value will decrease (i.e., drying) by 2.7%/°C global-mean SAT increase [*Taylor et al.*, 2002; *Fu and Feng*, 2014; *Lin et al.*, 2016a]. Additionally, anthropogenic SO_4 reduces precipitation and leads to a modest decrease in aridity index, at least in CESM [*Lin et al.*, 2016b]. Furthermore, BC has been demonstrated to result in a net decrease in the global-mean precipitation based on CESM and GFDL models [*Ocko et al.*, 2014; *Lin et al.*, 2016b]. Strongly nonlinear processing of anthropogenic pollutants occurs in urban areas. To date, human influences on drought and the potential feedbacks between drought and society remain somewhat uncertain [*Mahmood et al.*, 2014; *Berg et al.*, 2016; *Cook et al.*, 2016; *Fu et al.*, 2016; *Van Loon et al.*, 2016;], For example, land use was shown to result in a slight decrease in both precipitation (nonsignificant) and PET (significant), leading to nonsignificant changes in P/PET [*Fu et al.*, 2016], while *Cook et al.* [2016] suggested that land surface change might generate megadroughts in North America.

Global drylands have expanded over the last 60 years [*Feng and Fu*, 2013; *Huang et al.*, 2017a]. Global dryland expansion is projected to accelerate in the 21st century, and 78% of this expansion is expected to occur in developing countries [*Huang et al.*, 2016a]. The expanded drylands, along with extensive land use and rising temperatures, may exacerbate the risk of land degradation and desertification, posing a severe threat to ecosystems and the inhabitants of drylands and affecting approximately 30% of the Earth's terrestrial surface and approximately 70% of the Earth's agricultural drylands [*Winslow et al.*, 2004; *Milesi et al.*, 2010; *Jones*, 2011]. The most important changes will be induced by increasing human pressures of various types, such as increasing population, in both rural and urban areas, continuing oil developments, and increased numbers of ambitious water infrastructure projects [*Warren et al.*, 1996]. Therefore, in response to the drying climate and potential risk of desertification, proactive planning and adaption strategies should be developed; furthermore, climate disaster management and countermeasures must be implemented based on projections of future climate hazards and insights into how and to what extent hazards and vulnerability of a local nature-society system will jointly result in disasters. Some approaches have been used to detect dryland vulnerability [*Obasi*, 1994; *Guha-Sapir et al.*, 2004; *Shinoda et al.*, 2014], and some projects have been performed to develop comprehensive proactive countermeasures and policy recommendations to mitigate multidisaster impacts [*Applied Multi Risk Mapping of Natural Hazards for Impact Assessment (ARMONIA)*, 2007; *Shinoda*, 2017].

According to the above review, significant progress has been made in recent studies, but dryland climate change requires further investigation because of these regions' complex climates and relatively high sensitivity to climate change and the urgent demand for regional development. Additionally, increasing ground-based observations, improved satellite retrieval products and climatic proxies, increasingly reasonable parameterization schemes for modeling, and the advancement of data assimilation techniques are making "big data" possible, which will undoubtedly promote relevant research investigating dryland climates on multiple spatial and temporal scales. Many issues relating to the dryland climate remain to be investigated, and the data under a changing climate must be enriched. We suggest that future studies should focus on the following areas:

Determining the temporal and spatial characteristics of dryland climate change on different timescales. A better understanding of the temporal and spatial characteristics of dryland climate change on different timescales will provide the basis for accurate climate prediction and the development of scientific adaption strategies. Previous studies have mainly focused on specific types or regions of drylands, and few have systematically examined the temporal and spatial relationships of dryland climate change in different dryland regions worldwide. In the future, more studies should combine multisource data, such as climate reconstruction data and modern observational data, to investigate the spatial variation and spatiotemporal correlation of dryland climate change and create a complete picture of dry-wet oscillations on multiple time scales.

Combining ground-based measurements and satellite observations to study atmosphere-land interactions over drylands. Continuous and long-term observations of aerosols and the exchanges of energy, water, and materials are important for elucidating the characteristics of and differences in atmosphere-land interactions in different regions. High-quality data sets of ground-based measurements should be used to correct satellite remote sensing retrievals and construct a time series of key variables, such as the surface radiation budget, sensible heat flux, PET, surface temperature, and soil moisture. We need to establish gridded data sets of key parameters for atmosphere-land interactions by using all data sources. We should also study the interaction between human activities and atmosphere-land systems, especially the cycling of energy, water, and materials in different dryland regions.

Understanding the dynamic mechanisms of dryland climate change. Research focusing on climate drying mechanisms is lacking. Researchers should explore the dynamic mechanisms underlying the impacts of changes in atmospheric circulation on dryland climates by combining diagnostic analyses and numerical simulations. The responses of the key factors, such as clouds, radiation, precipitation, and evaporation, to changes in atmospheric circulation over drylands and the feedbacks between them should be investigated. The relative contributions of natural forcing (e.g., solar activities and volcanic eruptions) and human-induced perturbations (e.g., changes in GHG emissions, aerosols, and land use/land cover) to dryland climate change should be further evaluated.

Improving the capability of climate models to simulate aridity. Currently, precipitation remains poorly simulated and predicted by current state-of-the-art climate models, which is a barrier to study the variations and forecast aridity. Therefore, improvements are required. One of the most important reasons for the poor simulation of precipitation is the internal variability of climate systems. However, these uncertainties or influences have not been analyzed quantitatively in previous studies. Therefore, more attention should be paid to the influences and mechanisms of the internal variability of climate systems to improve the accuracy of aridity forecasts.

Understanding regional impacts and developing adaptive strategies. For climate disaster management, a practical and quantitative index of the vulnerability of a nature-society system should be developed to predict regional impacts of climate hazards. In particular, identification of a catastrophic threshold of the system is vital to provide an early warning of disasters, to take a proactive action, and finally to mitigate their impacts. This may form a central part of adaptive strategies.

10. Acronyms

ACA	Arid Central Asia
AD	*anno Domini*
AI	Aridity Index
AGCM	atmospheric general circulation model
AMO	Atlantic Multidecadal Oscillation
AO	Arctic oscillation
ARMONIA	Applied Multi Risk Mapping of Natural Hazards for Impact Assessment
ASM	Asian summer monsoon
BC	black carbon
CALIPSO	Cloud-Aerosol Lidar and Infrared Pathfinder Satellite Observation
CAM	Community Atmospheric Model
CCD	International Convention to Combat Desertification
CCICCD	Chinese Committee for Implementing UN Convention to Combat Desertification
CCSM4	Community Climate System Model, version 4
CESM	Community Earth System Model
CCN	cloud condensation nuclei
CGT	circumglobal teleconnection
CMIP5	Coupled Model Intercomparison Project Phase *5*
CMIP5-EM	CMIP5 multimodel ensemble mean
COWL	cold ocean-warm land
CONUS	contiguous United States
CPC	Climate Prediction Center
CRU	Climatic Research Unit
DDP	Drylands Development Paradigm
DRE	direct radiative effect
DMO	decadal modulated oscillation
EASM	East Asia summer monsoon
EAWM	East Asia winter monsoon
ENSO	El Niño–Southern Oscillation
EOF	empirical orthogonal function
Ep	potential evaporation
ESAW	enhanced semiarid warming
ET	*evapotranspiration*
G	ground heat flux
GCMs	general circulation models
GFDL	Geophysical Fluid Dynamics Laboratory
GHG	greenhouse gas
GLDAS	Global Land Data Assimilation System
GPP	gross primary production

HGT	geopotential height
ICTP-RegCM4	International Center for Theoretical Physics-Regional Climate Model
IGBP	International Geosphere-Biosphere Programme
IN	ice nuclei
IPCC	Intergovernmental Panel on Climate Change
IPO	interdecadal Pacific oscillation
ISLSCP	International Satellite Land-Surface Climatology Project
ITCZ	intertropical convergence zone
LH	latent heat flux
LAI	leaf area index
LIA	Little Ice Age
LSI	land-sea index
LUCC	land use/cover change
LULCC	land use-induced land cover change
LW	longwave
MCA	Medieval Climate Anomaly
MEEMD	multidimensional ensemble empirical mode decomposition
MODIS	Moderate-resolution Imaging Spectroradiometer
MTF	meridional thermal forcing
MWP	Medieval Warm Period
NDVI	normalized difference vegetation index
NH	Northern Hemisphere
NAO	North Atlantic Oscillation
P	precipitation
PACD	United Nations Plan of Action to Combat Desertification
PBL	planetary boundary layer
PD	present day
PET	potential evapotranspiration
PDO	Pacific Decadal Oscillation
PDOI	Pacific Decadal Oscillation index
PDSI	Palmer Drought Severity Index
R_n	net Radiation
RCP4.5	Representative Concentration Pathway 4.5
RCP8.5	Representative Concentration Pathway 8.5
RF	radiative forcing
RFFA	regional flood frequency analysis
RFT	radiatively forced temperature
RH	relative humidity
SAT	surface air temperature
SHADE	Saharan Dust Experiment
SH	sensible heat flux
SOC	soil organic carbon
SPEI	Standardized Precipitation Evapotranspiration Index
SSA	single scattering albedo
SST	sea surface temperature
SW	shortwave
SWI	surface wetness index
Tg	trillion grams
TOA	top of the atmosphere
U	wind speed
UB	Ural blocking
UN	United Nations
UNCCD	United Nations Convention to Combat Desertification
UNCOD	United Nations Conference on Desertification

UNEP	United Nations Environment Programme
WACL	warm Arctic and cold land
WOCL	warm ocean-cold land
ZTF	zonal thermal forcing

References

Ahlstrom, A., et al. (2015), The dominant role of semi-arid ecosystems in the trend and variability of the land CO_2 sink, *Science*, *348*(6237), 895–899, doi:10.1126/science.aaa1668.

Albrecht, B. A. (1989), Aerosols, cloud microphysics, and fractional cloudiness, *Science*, *245*(4923), 1227–1230, doi:10.1126/science.245.4923.1227.

Allen, M. R., and W. J. Ingram (2002), Constraints on future changes in climate and the hydrologic cycle, *Nature*, *419*(6903), 224–232, doi:10.1038/nature01092.

Allen, R. J., S. C. Sherwood, J. R. Norris, and C. S. Zender (2012), Recent Northern Hemisphere tropical expansion primarily driven by black carbon and tropospheric ozone, *Nature*, *485*(7398), 350–354, doi:10.1038/nature11097.

Allen, R. J., W. Landuyt, and S. T. Rumbold (2016), An increase in aerosol burden and radiative effects in a warmer world, *Nat. Clim. Chang.*, *6*(3), 269–274, doi:10.1038/nclimate2827.

An, Z., J. E. Kutzbach, W. L. Prell, and S. C. Porter (2001), Evolution of Asian monsoons and phased uplift of the Himalaya-Tibetan plateau since Late Miocene times, *Nature*, *411*(6833), 62–66.

Andreae, M. Q., D. Rosenfeld, P. Artaxo, A. A. Costa, G. P. Frank, K. M. Longo, and M. Silva-Dias (2004), Smoking rain clouds over the Amazon, *Science*, *303*(5662), 1337–1342, doi:10.1126/science.1092779.

Andreoli, R. V., and M. T. Kayano (2005), ENSO-related rainfall anomalies in South America and associated circulation features during warm and cold Pacific Decadal Oscillation regimes, *Int. J. Climatol.*, *25*(15), 2017–2030, doi:10.1002/joc.1222.

Angeler, D. G., C. R. Allen, H. E. Birgé, S. Drakare, B. G. Mckie, and R. K. Johnson (2014), Assessing and managing freshwater ecosystems vulnerable to environmental change, *Ambio*, *43*(1), 113–129, doi:10.1007/s13280-014-0566-z.

Armah, F. A., et al. (2010), Food security and climate change in drought-sensitive savanna zones of Ghana, *Mitig. Adapt. Strateg. Glob. Chang.*, *16*(3), 291–306, doi:10.1007/s11027-010-9263-9.

ARMONIA (2007), Assessing and mapping multiple risks for spatial planning, European Union 6th Framework Programme Reports, European Union.

Asseng, S., and D. J. Pannell (2013), Adapting dryland agriculture to climate change:Farming implications and research and development needs in Western Australia, *Clim. Change*, *118*(2), 167–181, doi:10.1007/s10584-012-0623-1.

Ault, A. P., C. R. Williams, A. B. White, P. J. Neiman, J. M. Creamean, C. J. Gaston, F. M. Ralph, and K. A. Prather (2011), Detection of Asian dust in California orographic precipitation, *J. Geophys. Res.*, *116*, D16205, doi:10.1029/2010JD015351.

Avila, F. B., A. J. Pitman, M. G. Donat, L. V. Alexander, and G. Abramowitz (2012), Climate model simulated changes in temperature extremes due to land cover change, *J. Geophys. Res.*, *117*, D04108, doi:10.1029/2011JD016382.

Bader, J., and M. Latif (2003), The impact of decadal-scale Indian Ocean sea surface temperature anomalies on Sahelian rainfall and the North Atlantic Oscillation, *Geophys. Res. Lett.*, *30*(22), 2169, doi:10.1029/2003GL018426.

Badreldin, N., and R. Goossens (2015), A satellite-based disturbance index algorithm for monitoring mitigation strategies effects on desertification change in an arid environment, *Mitig. Adapt. Strateg. Glob. Chang.*, *20*(2), 263–276, doi:10.1007/s11027-013-9490-y.

Ballantyne, A. P., C. B. Alden, J. B. Miller, P. P. Tans, and J. W. C. White (2012), Increase in observed net carbon dioxide uptake by land and oceans during the past 50 years, *Nature*, *488*(7409), 70–72, doi:10.1038/nature11299.

Ballantyne, A., et al. (2017), Accelerating net terrestrial carbon uptake during the warming hiatus due to reduced respiration, *Nat. Clim. Chang.*, *7*, 148–152, doi:10.1038/nclimate3204.

Barahona, D., J. Rodriguez, and A. Nenes (2010), Sensitivity of the global distribution of cirrus ice crystal concentration to heterogeneous freezing, *J. Geophys. Res.*, *115*, D23213, doi:10.1029/2010JD014273.

Barnett, J., and S. O'Neill (2010), Maladaptation, *Global Environ. Chang.*, *20*(2), 211–213, doi:10.1016/j.gloenvcha.2009.11.004.

Bates, B. C., Z. W. Kundzewicz, S. Wu, and J. Palutikof (2008), *Climate Change and Water: Technical Paper VI*, p. 210, UNT Digital Library, Geneva, Switzerland. [Available at http://digital.library.unt.edu/ark:/67531/metadc11958/.]

Benson, L., et al. (2002), Holocene multidecadal and multicentennial droughts affecting Northern California and Nevada, *Quat. Sci. Rev.*, *21*(4–6), 659–682, doi:10.1016/S0277-3791(01)00048-8.

Berg, A., et al. (2016), Land–atmosphere feedbacks amplify aridity increase over land under global warming, *Nat. Clim. Chang.*, *6*(9), 869–874, doi:10.1038/nclimate3029.

Berg, A., J. Sheffield, and P. Milly (2017), Divergent surface and total soil moisture projections under global warming, *Geophys. Res. Lett.*, *44*, 236–244, doi:10.1002/2016GL071921.

Bestelmeyer, B. T., G. S. Okin, M. C. Duniway, S. R. Archer, N. F. Sayre, J. C. Williamson, and J. E. Herrick (2015), Desertification, land use, and the transformation of global drylands, *Front. Ecol. Environ.*, *13*(1), 28–36, doi:10.1890/140162.

Birner, T. (2010), Recent widening of the tropical belt from global tropopause statistics: Sensitivities, *J. Geophys. Res.*, *115*, D23109, doi:10.1029/2010JD014664.

Blöschl, G., M. Sivapalan, T. Wagener, A. Viglione, and H. Savenije (2013), *Runoff Prediction in Ungauged Basins*, p. 465, Cambridge Univ. Press, Cambridge.

Bond, T. C., et al. (2013), Bounding the role of black carbon in the climate system: A scientific assessment, *J. Geophys. Res. Atmos.*, *118*, 5380–5552, doi:10.1002/jgrd.50171.

Breshears, D. D., and F. J. Barnes (1999), Interrelationships between plant functional types and soil moisture heterogeneity for semiarid landscapes within the grassland/forest continuum: A unified conceptual model, *Landsc. Ecol.*, *14*(5), 465–478, doi:10.1023/A:1008040327508.

Budyko, M. I. (1958), The heat balance of the Earth's surface, in *Natl. Weather Serv*, pp. 144–155, U.S. Department of Commerce, Washington, D. C.

Bullard, J. E., et al. (2016), High-latitude dust in the Earth system, *Rev. Geophys.*, *54*, 447–485, doi:10.1002/2016RG000518.

Burba, G. G., S. B. Verma, and J. Kim (1999), Surface energy fluxes of phragmites australis in a prairie wetland, *Agric. For. Meteorol.*, *94*(1), 31–51, doi:10.1016/s0168-1923(99)00007-6.

Burke, E. J., and S. J. Brown (2008), Evaluating uncertainties in the projection of future drought, *J. Hydrometeorol.*, *9*(2), 292–299, doi:10.1175/2007JHM929.1.

Burke, E. J. (2011), Understanding the sensitivity of different drought metrics to the drivers of drought under increased atmospheric CO_2, *J. Hydrometeorol.*, *12*(6), 1378–1394, doi:10.1175/2011JHM1386.1.

Byrne, M., and P. O'Gorman (2016), Understanding decreases in land relative humidity with global warming: Conceptual model and GCM simulations, *J. Clim.*, *29*(24), doi:10.1175/JCLI-D-16-0351.

Cai, W., T. Cowan, and M. Thatcher (2012), Rainfall reductions over Southern Hemisphere semi-arid regions: The role of subtropical dry zone expansion, *Sci. Rep.*, *2*, 702, doi:10.1038/srep00702.

Carslaw, K. S., et al. (2013), Large contribution of natural aerosols to uncertainty in indirect forcing, *Nature*, *503*(7474), 67–71, doi:10.1038/nature12674.

Chaboureau, J. P., P. Tulet, and C. Mari (2007), Diurnal cycle of dust and cirrus over West Africa as seen from Meteosat second generation satellite and a regional forecast model, *Geophys. Res. Lett.*, *34*, L02822, doi:10.1029/2006GL027771.

Charney, J. G. (1975), Dynamics of deserts and drought in the Sahel, *Q. J. R. Meteorol. Soc.*, *101*, 193–202.

Charney, J. G., and J. G. DeVore (1979), Multiple flow equilibria in the atmosphere and blocking, *J. Atmos. Sci.*, *36*(7), 1205–1216.

Che, H., et al. (2015), Ground-based aerosol climatology of China: Aerosol optical depth from the China Aerosol Remote Sensing Network (CARSNET) 2002-2013, *Atmos. Chem. Phys.*, *15*(13), 7619–7652, doi:10.5194/acp-15-7619-2015.

Chen, F., et al. (2008), Holocene moisture evolution in arid central Asia and its out-of-phase relationship with Asian monsoon history, *Quat. Sci. Rev.*, *27*(3–4), 351–364, doi:10.1016/j.quascirev.2007.10.017.

Chen, F., J. Wang, L. Jin, Q. Zhang, J. Li, and J. Chen (2009), Rapid warming in mid-latitude central Asia for the past 100 years, *Front. Earth Sci.*, *3*(1), 42–50, doi:10.1007/s11707-009-0013-9.

Chen, F., J. Chen, J. A. Holmes, I. Boomer, P. Austin, J. B. Gates, N. L. Wang, S. J. Brooks, and J. Zhang (2010), Moisture changes over the last millennium in the arid Central Asia: A review, synthesis and comparison with monsoon region, *Quat. Sci. Rev.*, *29*(7–8), 1055–1068, doi:10.1016/j.quascirev.2010.01.005.

Chen, F., W. Huang, L. Jin, J. Chen, and J. Wang (2011), Spatiotemporal precipitation variations in the arid Central Asia in the context of global warming, *Sci. China Earth Sci.*, *54*(12), 1812–1821, doi:10.1007/s11430-011-4333-8.

Chen, F., H. Wang, F. Chen, Y. Yuan, and R. Zhang (2015), Tree-ring reconstruction of July–May precipitation (AD 1816–2010) in the northwestern marginal zone of the East Asian summer monsoon reveals the monsoon-related climate signals, *Int. J. Climatol.*, *35*(8), 2109–2121, doi:10.1002/joc.4110.

Chen, F., Y. Yuan, T. Zhang, and H. W. Linderholm (2016a), Annual precipitation variation for the southern edge of the Gobi Desert (China) inferred from tree rings: Linkages to climatic warming of twentieth century, *Nat. Hazards.*, *81*(2), 939–955, doi:10.1007/s11069-015-2113-z.

Chen, F., R. Zhang, H. Wang, L. Qin, and Y. Yuan (2016b), Updated precipitation reconstruction (AD 1482–2012) for Huashan, North-Central China, *Theor. Appl. Climatol.*, *123*(3–4), 723–732, doi:10.1007/s00704-015-1387-0.

Cheng, S., and J. Huang (2016), Enhanced soil moisture drying in transitional regions under a warming climate, *J. Geophys. Res. Atmos.*, *121*, 2542–2555, doi:10.1002/2015JD024559.

Cheng, S., X. Guan, J. Huang, F. Ji, and R. Guo (2015), Long-term trend and variability of soil moisture over East Asia, *J. Geophys. Res. Atmos.*, *120*, 8658–8670, doi:10.1002/2015jd023206.

Choobari, O. A., P. Zawar-Reza, and A. Sturman (2014), The global distribution of mineral dust and its impacts on the climate system: A review, *Atmos. Res.*, *138*, 152–165, doi:10.1016/j.atmosres.2013.11.007.

Chou, C., J. D. Neelin, C. Chen, and J. Tu (2009), Evaluating the "rich-get-richer" mechanism in tropical precipitation change under global warming, *J. Clim.*, *22*(8), 1982–2005, doi:10.1175/2008JCLI2471.1.

Coats, S., J. E. Smerdon, B. I. Cook, R. Seager, E. R. Cook, and K. J. Anchukaitis (2016), Internal ocean-atmosphere variability drives megadroughts in Western North America, *Geophys. Res. Lett.*, *43*, 9886–9894, doi:10.1002/2016gl070105.

Conen, F., and J. Leifeld (2014), A new facet of soil organic matter, *Agric. Ecosyst. Environ.*, *185*, 186–187, doi:10.1016/j.agee.2013.12.024.

Cook, B. I., R. Seager, R. L. Miller, and J. A. Mason (2013), Intensification of North American Megadroughts through surface and dust aerosol forcing, *J. Clim.*, *26*(13), 4414–4430, doi:10.1175/JCLI-D-12-00022.1.

Cook, B. I., J. E. Smerdon, R. Seager, and S. Coats (2014a), Global warming and 21st century drying, *Clim. Dyn.*, *43*(9–10), 2607–2627, doi:10.1007/s00382-014-2075-y.

Cook, B. I., J. E. Smerdon, R. Seager, and E. R. Cook (2014b), Pan-continental droughts in North America over the last millennium, *J. Clim.*, *27*(1), 383–397, doi:10.1175/JCLI-D-13-00100.1.

Cook, B. I., E. R. Cook, J. E. Smerdon, R. Seager, A. P. Williams, S. Coats, D. W. Stahle, and J. V. Diaz (2016), North American megadroughts in the Common Era: Reconstructions and simulations, *Wiley Interdiscip, Rev.-Clim. Chang.*, *7*(3), 411–432, doi:10.1002/wcc.394.

Cook, E. R., D. M. Meko, D. W. Stahle, and M. K. Cleaveland (1999), Drought reconstructions for the continental United States, *J. Clim.*, *12*, 1145–1162.

Cook, E. R., K. J. Anchukaitis, B. M. Buckley, R. D. D'Arrigo, G. C. Jacoby, and W. E. Wright (2010), Asian monsoon failure and megadrought during the last millennium, *Science*, *328*, 486–489, doi:10.1126/science.1185188.

Cook, E. R., C. A. Woodhouse, C. M. Eakin, D. M. Meko, and D. W. Stahle (2004), Long-term aridity changes in the western United States, *Science*, *306*(5698), 1015–1018, doi:10.1126/science.1102586.

Costa, M. J., B. J. Sohn, V. Levizzani, and A. M. Silva (2006), Radiative forcing of Asian dust determined from the synergized GOME and GMS satellite data: A case study, *J. Meteorol. Soc. Jpn.*, *84*(1), 85–95, doi:10.2151/jmsj.84.85.

Creamean, J. M., et al. (2013), Dust and biological aerosols from the Sahara and Asia influence precipitation in the Western US, *Science*, *339*, 1572–1578, doi:10.1126/science.1227279.

Cudennec, C., C. Leduc, and D. Koutsoyiannis (2007), Dryland hydrology in Mediterranean regions—A review, *Hydrol. Sci. J.*, *52*(6), 1077–1087, doi:10.1623/hysj.52.6.1077.

D'Odorico, P., A. Bhattachan, K. F. Davis, S. Ravi, and C. W. Runyan (2013), Global desertification: Drivers and feedbacks, *Adv. Water Resour.*, *51*, 326–344, doi:10.1016/j.advwatres.2012.01.013.

Dai, A. (2011a), Drought under global warming: A review, *WIREs. Clim. Change*, *2*(1), 45–65, doi:10.1002/wcc.81.

Dai, A. (2011b), Characteristics and trends in various forms of the Palmer Drought Severity Index (PDSI) during 1900-2008, *J. Geophys. Res.*, *116*, D12115, doi:10.1029/2010JD015541.

Dai, A. (2013a), The influence of the Inter-decadal Pacific Oscillation on US precipitation during 1923–2010, *Clim. Dyn.*, *41*(3–4), 633–646, doi:10.1007/s00382-012-1446-5.

Dai, A. (2013b), Increasing drought under global warming in observations and models, *Nat. Clim. Chang.*, *3*(1), 52–58, doi:10.1038/NCLIMATE1633.

Dai, A., and T. M. L. Wigley (2000), Global patterns of ENSO-induced precipitation, *Geophys. Res. Lett.*, *27*(9), 1283–1286, doi:10.1029/1999GL011140.

Dai, A., and T. B. Zhao (2016), Uncertainties in historical changes and future projections of drought, Part I: Estimates of historical drought changes, *Clim. Change*, 1–15, doi:10.1007/s10584-016-1705-2.

Dai, A., I. Y. Fung, and A. D. Del Genio (1997), Surface observed global land precipitation variations during 1900–88, *J. Clim.*, *10*(11), 2943–2962, doi:10.1175/1520-0442(1997)010<2943:SOGLPV>2.0.CO;2.

Dai, A., K. E. Trenberth, and T. R. Karl (1998), Global variations in droughts and wet spells: 1900–1995, *Geophys. Res. Lett.*, *25*, 3367–3370.

Dai, A., K. E. Trenberth, and T. Qian (2004), A global dataset of Palmer Drought Severity Index for 1870–2002: Relationship with soil moisture and effects of surface warming, *J. Hydrometeorol.*, *5*(6), 1117–1130, doi:10.1175/JHM-386.1.

Darkoh, M. B. K. (1998), The nature, causes and consequences of desertification in the drylands of Africa, *Land Degradation and Development*, *9*, 1–20.

Das, R., A. T. Evan, and D. Lawrence (2013), Contributions of long-distance dust transport to atmospheric P inputs in the Yucatan Peninsula, *Global Biogeochem. Cycles*, *27*, 167–175, doi:10.1029/2012GB004420.

Davis, M. E., L. G. Thompson, T. Yao, and N. Wang (2005), Forcing of the Asian monsoon on the Tibetan Plateau: Evidence from high-resolution ice core and tropical coral records, *J. Geophys. Res.*, *110*, D04101, doi:10.1029/2004JD004933.

Davis, N., and T. Birner (2016), On the discrepancies in tropical belt expansion between reanalyses and climate models and among tropical belt width metrics, *J. Clim.*, *30*(4), doi:10.1175/JCLI-D-16-0371.1.

DeFlorio, M. J., I. D. Goodwin, D. R. Cayan, A. J. Miller, S. J. Ghan, D. W. Pierce, L. M. Russell, and B. Singh (2016), Interannual modulation of subtropical Atlantic boreal summer dust variability by ENSO, *Clim. Dyn.*, *46*(1–2), 585–599, doi:10.1007/s00382-015-2600-7.

Delgado-Baquerizo, M., et al. (2013), Decoupling of soil nutrient cycles as a function of aridity in global drylands, *Nature*, *502*, 672–676, doi:10.1038/nature12670.

DeMott, P. J., K. Sassen, M. R. Poellot, D. Baumgardner, D. C. Rogers, S. D. Brooks, A. J. Prenni, and S. M. Kreidenweis (2003), African dust aerosols as atmospheric ice nuclei, *Geophys. Res. Lett.*, *30*(14), 1732, doi:10.1029/2003GL017410.

Di Castri, F., A. J. Hansen, and M. M. Holland (1988), A new look at ecotones: Emerging international projects on landscape boundaries, *Biol. Int.*, *17*, 1–163.

Diaz, H. F., R. S. Bradley, and J. K. Eischeid (1989), Precipitation fluctuations over global land areas since the late 1800's, *J. Geophys. Res.*, *94*(1), 1195–1210.

Doherty, O. M., N. Riemer, and S. Hameed (2012), Control of Saharan mineral dust transport to Barbados in winter by the intertropical convergence zone over west Africa, *J. Geophys. Res.*, *117*, D19117, doi:10.1029/2012JD017767.

Doherty, O. M., and A. T. Evan (2014), Identification of a new dust-stratocumulus indirect effect over the tropical North Atlantic, *Geophys. Res. Lett.*, *41*, 6935–6942, doi:10.1002/2014GL060897.

Doherty, O. M., N. Riemer, and S. Hameed (2014), Role of the convergence zone over West Africa in controlling Saharan mineral dust load and transport in the boreal summer, *Tellus B.*, *66*, 23191, doi:10.3402/tellusb.v66.23191.

Donat, M., A. Lowry, L. Alexander, P. O'Gorman, and N. Maher (2016), More extreme precipitation in the world's dry and wet regions, *Nat. Clim. Chang.*, *6*, 508–513.

Dong, B., and A. Dai (2015), The influence of the Inter-decadal Pacific Oscillation on temperature and precipitation over the globe, *Clim. Dyn.*, *45*(9–10), 2667–2681, doi:10.1007/s00382-015-2500-x.

Dregne, H., M. Kassas, and B. Rozanov (1991), A new assessment of the world status of desertification, *Desertification Control Bulletin*, *20*, 6–18.

Dunion, J. P., and C. S. Velden (2004), The impact of the Saharan air layer on Atlantic tropical cyclone activity, *Bull. Am. Meteorol. Soc.*, *85*(3), 353–365, doi:10.1175/BAMS-85-3-353.

Dunstone, N. J., D. M. Smith, B. B. Booth, L. Hermanson, and R. Eade (2013), Anthropogenic aerosol forcing of Atlantic tropical storms, *Nat. Geosci.*, *6*(7), 534–539, doi:10.1038/NGEO1854.

El-Beltagy, A., and M. Madkour (2012), Impact of climate change on arid lands agriculture, *Agriculture and Food Security*, *1*, 3, doi:10.1186/2048-7010-1-3.

Engelstaedter, S., I. Tegen, and R. Wahsington (2006), North African dust emissions and transport, *Earth-Sci. Rev.*, *79*(1–2), 73–100, doi:10.1016/j.earscirev.2006.06.004.

Esper, J., E. R. Cook, and F. H. Schweingruber (2002a), Low-frequency signals in long treering chronologies for reconstructing past temperature variability, *Science*, *295*, 2250–2253, doi:10.1126/science.1066208.

Esper, J., F. H. Schweingruber, and M. Winiger (2002b), 1300 years of climatic history for Western Central Asia inferred from tree-rings, *Holocene*, *12*(3), 267–277, doi:10.1191/0959683602hl543rp.

Evan, A. T., D. J. Vimont, A. K. Heidinger, J. P. Kossin, and R. Bennartz (2009), The role of aerosols in the evolution of tropical North Atlantic Ocean temperature anomalies, *Science*, *324*(5928), 778–781, doi:10.1126/science.1167404.

Evan, A. T., and S. Mukhopadhyay (2010), African dust over the Northern tropical Atlantic: 1955–2008, *J. Appl. Meteorol. Climatol.*, *49*(11), 2213–2229, doi:10.1175/2010JAMC2485.1.

Fan, B., L. Guo, N. Li, J. Chen, H. Lin, X. Zhang, M. Shen, Y. Rao, C. Wang, and L. Ma (2014), Earlier vegetation green-up has reduced spring dust storms, *Sci. Rep.*, *4*, 6749, doi:10.1038/srep06749.

Fan, J., et al. (2014), Aerosol impacts on California winter clouds and precipitation during calwater 2011: Local pollution versus long-range transported dust, *Atmos. Chem. Phys.*, *14*(1), 81–101, doi:10.5194/acp-14-81-2014.

Feldl, N., and S. Bordoni (2016), Characterizing the Hadley circulation response through regional climate feedbacks, *J. Clim.*, *29*(2), 613–622, doi:10.1175/JCLI-D-15-0424.1.

Feng, S., and Q. Fu (2013), Expansion of global drylands under a warming climate, *Atmos. Chem. Phys.*, *13*(19), 10081–10094, doi:10.5194/acp-13-10081-2013.

Feng, S., Q. Hu, W. Huang, C. H. Ho, R. Li, and Z. Tang (2014), Projected climate regime shift under future global warming from multi-model, multi-scenario CMIP5 simulations, *Global and Planetary Change*, *112*, 41–52, doi:10.1016/j.gloplacha.2013.11.002.

Feng, X., et al. (2016), Revegetation in China's Loess Plateau is approaching sustainable water resource limits, *Nat. Clim. Chang.*, *6*(11), 1019–1022, doi:10.1038/nclimate3092.

Fensholt, R., et al. (2012), Greenness in semi-arid areas across the globe 1981–2007—An Earth Observing Satellite based analysis of trends and drivers, *Remote Sens. Environ.*, *121*, 144–158, doi:10.1016/j.rse.2012.01.017.

Findell, K. L., E. Shevliakova, P. C. D. Milly, and R. J. Stouffer (2007), Modeled impact of anthropogenic land cover change on climate, *J. Clim.*, *20*, 3621–3634, doi:10.1175/JCLI4185.1.

Fischer, E. M., and R. Knutti (2016), Observed heavy precipitation increase confirms theory and early models, *Nat. Clim. Chang.*, *6*(11), 986–991, doi:10.1038/nclimate3110.

Forzieri, G., R. Alkama, D. Miralles, and A. Cescatti (2017), Satellites reveal contrasting responses of regional climate to the widespread greening of Earth, *Science*, *356*(6343), 1180–1184, doi:10.1126/science.aal1727.

Fouquart, Y., B. Bonnel, G. Brogniez, J. C. Buriez, L. Smith, J. J. Morcrette, and A. Cerf (1987), Observations of Saharan aerosols: Results of ECLATS field experiment, Part II: Broadband radiative characteristics of the aerosols and vertical radiative flux divergence, *J. Clim. Appl. Meteorol.*, *26*, 38–52.

Frierson, D. M. W., I. M. Held, and P. Zurita-Gotor (2006), A gray-radiation aquaplanet moist GCM. Part I: Static stability and eddy scale, *J. Atmos. Sci.*, *63*(10), 2548–2566, doi:10.1175/jas3753.1.

Frierson, D. M. W., J. Lu, and G. Chen (2007), Width of the Hadley cell in simple and comprehensive general circulation models, *Geophys. Res. Lett.*, *34*, L18804, doi:10.1029/2007GL031115.

Fu, C. (1985), Studies on tropical rainforest climate-a suggested candidate for understanding the geosphere-biosphere interaction, in *Global Change*, edited by T. F. Malone and J. G. Roederer, pp. 496–497, Cambridge Univ. Press, Cambridge.

Fu, C. (1989), The effect of land use on the global change, in *The New Emergencies, The Scientific and Culture series*, edited by M. Dardo and K. Goebel, pp. 238–250, World Sci., Erice.

Fu, C. (1992), Transitional climate zone and biome boundaries, in *Landscape Boundaries: Consequences for Biotic Diversity and Ecological Flows*, edited by A. J. Hansen and F. di Castri, pp. 394–402, Springer, New York.

Fu, C., and Z. An (2002), Study of aridization in northern China—A global change issue facing directly the demand of nation, *Earth Science Frontiers*, *9*(2), 271–275.

Fu, C., and G. Wen (2002), Several issues on aridization in the northern China, *Clim. Environ. Res.*, *7*(1), 22–29.

Fu, C., and F. P. De Vries (2006), *Initial Science Plan of the Monsoon Asia Integrated Regional Study*, MAIRS-IPO, IAP-CAS, Beijing.

Fu, C., Z. Jiang, Z. Guan, J. He, and Z. Xu (2008), *Regional Climate Studies of China*, vol. 1, pp. 156–159, Springer, Berlin.

Fu, C., and H. Mao (Eds.) (2017), *Aridity Trend in Northern China*, World Sci., Singapore.

Fu, Q., and S. Feng (2014), Responses of terrestrial aridity to global warming, *J. Geophys. Res. Atmos.*, *119*, 7863–7875, doi:10.1002/2014JD021608.

Fu, Q., and P. Lin (2011), Poleward shift of subtropical jets inferred from satellite-observed lower stratospheric temperatures, *J. Clim.*, *24*, 5597–5603, doi:10.1175/JCLI-D-11-00027.1.

Fu, Q., C. M. Johanson, J. M. Wallace, and T. Reichler (2006), Enhanced mid-latitude tropospheric warming in satellite measurements, *Science*, *312*(5777), 1179–1179, doi:10.1126/science.1125566.

Fu, Q., L. Lin, J. Huang, S. Feng, and A. Gettelman (2016), Changes in terrestrial aridity for the period 850–2080 from the Community Earth System Model, *J. Geophys. Res. Atmos.*, *121*, 2857–2873, doi:10.1002/2015JD024075.

Fu, Y., et al. (2015), Declining global warming effects on the phenology of spring leaf unfolding, *Nature*, *526*(7571), 104–107, doi:10.1038/nature15402.

Gao, X., Y. Luo, W. Lin, Z. Zhao, and G. Filippo (2003), Simulation of effects of land use change on climate in China by a regional climate model, *Adv. Atmos. Sci.*, *6*, 224–230.

Garfinkel, C. I., D. W. Waugh, and L. M. Polvani (2015), Recent Hadley cell expansion: The role of internal atmospheric variability in reconciling modeled and observed trends, *Geophys. Res. Lett.*, *42*, 10,824–10,831, doi:10.1002/2015GL066942.

Gates, J. B., W. M. Edmunds, J. Ma, and P. R. Sheppard (2008), A 700-year history of groundwater recharge in the drylands of NW China, *Holocene*, *18*(7), 1045–1054, doi:10.1177/0959683608095575.

Ge, J., J. Su, Q. Fu, T. P. Ackerman, and J. Huang (2010), Dust aerosol forward scattering effects on ground-based aerosol optical depth retrievals, *J. Quant. Spectrosc. Radiat. Transfer*, *112*, 310–319, doi:10.1016/j.jqsrt.2010.07.006.

Ge, J., J. Huang, C. Xu, Y. Qi, and H. Liu (2014), Characteristics of Taklimakan dust emission and distribution: A satellite and reanalysis field perspective, *J. Geophys. Res. Atmos.*, *119*, 11772–11783, doi:10.1002/2014JD022280.

Ge, J., H. Liu, J. Huang, and Q. Fu (2016), Taklimakan Desert nocturnal low-level jet: Climatology and dust activity, *Atmos. Chem. Phys.*, *16*, 7773–7783, doi:10.5194/acp-16-7773-2016.

Gershunov, A., and T. P. Barnett (1998), Interdecadal modulation of ENSO teleconnections, *Bull. Am. Meteorol. Soc.*, *79*(12), 2715–2725, doi:10.1175/1520-0477(1998)079<2715:IMOET>2.0.CO;2.

Giannini, A., R. Saravanan, and P. Chang (2003), Oceanic forcing of Sahel rainfall on interannual to interdecadal time scales, *Science*, *302*(5647), 1027–1030, doi:10.1126/science.1089357.

Gibson, E. R., K. M. Gierlus, P. K. Hudson, and V. H. Grassian (2007), Generation of internally mixed insoluble and soluble aerosol particles to investigate the impact of atmospheric aging and heterogeneous processing on the CCN activity of mineral dust aerosol, *Aerosol Sci. Technol.*, *41*(10), 914–924, doi:10.1080/02786820701557222.

Gill, J. C., and B. D. Malamud (2014), Reviewing and visualizing the interactions of natural hazards, *Rev. Geophys.*, *52*, 680–722, doi:10.1002/2013RG000445.

Ginoux, P. A., J. M. Prospero, T. E. Gill, C. Hsu, and M. Zhao (2012), Global-scale attribution of anthropogenic and natural dust sources and their emission rates based on MODIS deep blue aerosol products, *Rev. Geophys.*, *50*, RG3005, doi:10.1029/2012RG000388.

GLP (2005), Global Land Project—Science Plan and Implementation Strategy, IGBP (International Geosphere Biosphere Program) report no. 53/International human dimensions programme report no. 19, IGBP secretariat, Stockholm.

Gong, D., and S. Wang (1999), Long-term variability of the Siberian high and the possible connection to global warming, *Acta Geographica Sinica*, *54*(2), 125–133.

Gong, D., P. Shi, and J. Wang (2004), Daily precipitation changes in the semi-arid region over Northern China, *J. Arid Environ.*, *59*(4), 771–784, doi:10.1016/j.jaridenv.2004.02.006.

Grace, J., J. San Jose, P. Meir, H. S. Miranda, and R. A. Montes (2006), Productivity and carbon fluxes of tropical savannas, *J. Biogeogr.*, *33*(3), 387–400, doi:10.1111/j.1365-2699.2005.01448.x.

Graetz, R. D. (1991), Desertification: A tale of two feedbacks, in *Ecosystem Experiments*, pp. 59–87, CSIRO's Research Publications Repository, Australia.

Grayson, D. K. (2000), Mammalian responses to Middle Holocene climatic change in the Great Basin of the western United States, *J. Biogeogr.*, *27*(1), 181–192, doi:10.1046/j.1365-2699.2000.00383.x.

Greve, P., and S. I. Seneviratne (2015), Assessment of future changes in water availability and aridity, *Geophys. Res. Lett.*, *42*, 5493–5499, doi:10.1002/2015GL064127.

Greve, P., B. Orlowsky, B. Mueller, J. Sheffield, M. Reichstein, and S. I. Seneviratne (2014), Global assessment of trends in wetting and drying over land, *Nat. Geosci.*, *7*(10), 716–721, doi:10.1038/NGEO2247.

Guan, X., J. Huang, R. Guo, H. Yu, P. Lin, and Y. Zhang (2015), Role of radiatively forced temperature changes in enhanced semi-arid warming in the cold season over East Asia, *Atmos. Chem. Phys.*, *15*(23), 13777–13786, doi:10.5194/acp-15-13777-2015.

Guha-Sapir, D., D. Hargitt, and P. Hoyois (2004) *Thirty Years of Natural Disasters 1974–2003: The Numbers*, Presses Universitaires de Louvain, Louvain-la-Neuve, Belgium.

Guo, W., X. Wang, J. Sun, A. Ding, and J. Zou (2016), Comparison of land-atmosphere interaction at different surface types in the mid- to lower reaches of the Yangtze River valley, *Atmos. Chem. Phys.*, 16(15), 9875–9890, doi:10.5194/acp-16-9875-2016.

Gutzler, D. S., D. M. Kann, and C. Thornbrugh (2002), Modulation of ENSO-based long-lead outlooks of southwestern US winter precipitation by the Pacific Decadal Oscillation, *Weather Forecasting*, 17(6), 1163–1172, doi:10.1175/1520-0434(2002)017<1163:MOEBLL>2.0.CO;2.

Hadgu, G., K. Tesfaye, and G. Mamo (2015), Analysis of climate change in Northern Ethiopia: Implications for agricultural production, *Theor. Appl. Climatol.*, 121(3–4), 733–747, doi:10.1007/s00704-014-1261-5.

Han, Z., J. Li, W. Guo, Z. Xiong, and W. Zhang (2013), A study of dust radiative feedback on dust cycle and meteorology over East Asia by a coupled regional climate-chemistry-aerosol model, *Atmos. Environ.*, 68, 54–63, doi:10.1016/j.atmosenv.2012.11.032.

Hansen, J. E., M. Sato, and R. Ruedy (1997), Radiative forcing and climate response, *J. Geophys. Res.*, 102(D6), 6831–6864, doi:10.1029/96JD03436.

Hartmann, K., and B. Wünnemann (2008), Hydrological changes and Holocene climate variations in NW China, inferred from lake sediments from Juyenze palaeolake by factor analysis, *Quatern. Int.*, 194, 28–44, doi:10.1016/j.quaint.2007.06.037.

Hawkins, E., and R. Sutton (2009), Decadal predictability of the Atlantic Ocean in a coupled GCM: Forecast skill and optimal perturbations using linear inverse modeling, *J. Clim.*, 22(14), 3960–3978, doi:10.1175/2009JCLI2720.1.

Haywood, J. M., P. Francis, S. Osborne, M. Glew, N. Loeb, E. Highwood, D. Tanré, G. Myhre, P. Formenti, and E. Hirst (2003), Radiative properties and direct radiative effect of Saharan dust measured by the C-130 aircraft during SHADE: 1. Solar spectrum, *J. Geophys. Res.*, 108(D18), 8577, doi:10.1029/2002JD002687.

He, Y., J. Huang, and M. Ji (2014), Impact of land-sea thermal contrast on interdecadal variation in circulation and blocking, *Clim. Dyn.*, 43(12), 3267–3279, doi:10.1007/s00382-014-2103-y.

Heim, R. R., Jr. (2002), A review of twentieth-century drought indices used in the United States, *Bull. Am. Meteorol. Soc.*, 83, 1149–1165.

Heintzenberg, J., K. Okada, and J. Strom (1996), On the composition of non-volatile material in upper tropospheric aerosols and cirrus crystals, *Atmos. Res.*, 41(1), 81–88, doi:10.1016/0169-8095(95)00042-9.

Held, I. M., and B. J. Soden (2006), Robust responses of the hydrological cycle to global warming, *J. Clim.*, 19(21), 5686–5699, doi:10.1175/JCLI3990.1.

Henderson, A. C. G., and J. A. Holmes (2008), Palaeolimnological evidence of environmental change over the past millennium from Lake Qinghai sediments: A review and future research perspective, *Quatern. Int.*, 194, 137–147, doi:10.1016/j.quaint.2008.09.008.

Hirschi, M. (2011), Observational evidence for soil-moisture impact on hot extremes in southeastern Europe, *Nat. Geosci.*, 4(1), 17–21, doi:10.1038/NGEO1032.

Hoerling, M., and A. Kumar (2003), The perfect ocean for drought, *Science*, 299(5607), 691–694, doi:10.1126/science.1079053.

Hoerling, M., J. Hurrell, J. Eischeid, and A. Phillips (2006), Detection and attribution of twentieth-century northern and southern African rainfall change, *J. Clim.*, 19(16), 3989–4008, doi:10.1175/JCLI3842.1.

Hoerling, M., J. Eischeid, and J. Perlwitz (2010), Regional precipitation trends: Distinguishing natural variability from anthropogenic forcing, *J. Clim.*, 23(8), 2131–2145, doi:10.1175/2009JCLI3420.1.

Hoover, D. L., M. C. Duniway, and J. Belnap (2015), Pulse-drought atop press-drought: Unexpected plant responses and implications for dryland ecosystems, *Oecologia*, 179(4), 1211–1221, doi:10.1007/s00442-015-3414-3.

Hu, Q., and S. Feng (2012), AMO-and ENSO-driven summertime circulation and precipitation variations in North America, *J. Clim.*, 25(19), 6477–6495, doi:10.1175/JCLI-D-11-00520.1.

Hu, Y., and Q. Fu (2007), Observed poleward expansion of the Hadley circulation since 1979, *Atmos. Chem. Phys.*, 7, 5229–5236.

Hu, Y., and C. Zhou (2009), Decadal changes in the Hadley circulation, in *Advances in Geosciences*, vol. 10, edited by J. H. Oh, p. 250, World Sci., Singapore.

Hu, Z. Z., and B. Huang (2009), Interferential impact of ENSO and PDO on dry and wet conditions in the US Great Plains, *J. Clim.*, 22(22), 6047–6065, doi:10.1175/2009JCLI2798.1.

Hu, Z., L. Wang, Z. Wang, Y. Hong, and H. Zheng (2015), Quantitative assessment of climate and human impacts on surface water resources in a typical semi-arid watershed in the middle reaches of the yellow river from 1985 to 2006, *Int. J. Climatol.*, 35(1), 97–113, doi:10.1002/joc.3965.

Huang, J. F., C. Zhang, and J. M. Prospero (2009), Large-scale effect of aerosols on precipitation in the West African monsoon region, *Q. J. R. Meteorol. Soc.*, 135(640), 581–594, doi:10.1002/qj.391.

Huang, J. F., C. Zhang, and J. M. Prospero (2010), African dust outbreaks: A satellite perspective of temporal and spatial variability over the tropical Atlantic Ocean, *J. Geophys. Res.*, 115, D05202, doi:10.1029/2009JD012516.

Huang, J., B. Lin, P. Minnis, T. Wang, X. Wang, Y. Hu, Y. Yi, and J. K. Ayers (2006a), Satellite-based assessment of possible dust aerosols semi-direct effect on cloud water path over East Asia, *Geophys. Res. Lett.*, 33, L19802, doi:10.1029/2006GL026561.

Huang, J., P. Minnis, B. Lin, T. Wang, Y. Yi, Y. Hu, S. Sun-Mack, and K. Ayers (2006b), Possible influences of Asian dust aerosols on cloud properties and radiative forcing observed from MODIS and CERES, *Geophys. Res. Lett.*, 33, L06824, doi:10.1029/2005GL024724.

Huang, J., Y. Wang, T. Wang, and Y. Yi (2006c), Dusty cloud radiative forcing derived from satellite data for middle latitude region of East Asia, *Prog. Nat. Sci.*, 16(10), 1084–1089.

Huang, J., P. Minnis, Y. Yi, Q. Tang, X. Wang, Y. Hu, Z. Liu, K. Ayers, C. Trepte, and D. Winker (2007), Summer dust aerosols detected from CALIPSO over the Tibetan Plateau, *Geophys. Res. Lett.*, 34, L18805, doi:10.1029/2007GL029938.

Huang, J., P. Minnis, B. Chen, Z. Huang, Z. Liu, Q. Zhao, Y. Yi, and J. K. Ayers (2008), Long-range transport and vertical structure of Asian dust from CALIPSO and surface measurements during PACDEX, *J. Geophys. Res.*, 113, D23212, doi:10.1029/2008JD010620.

Huang, J., Q. Fu, J. Su, Q. Tang, P. Minnis, Y. Hu, Y. Yi, and Q. Zhao (2009), Taklimakan dust aerosol radiative heating derived from CALIPSO observations using the Fu-Liou radiation model with CERES constraints, *Atmos. Chem. Phys.*, 9, 4011–4021, doi:10.5194/acp-9-4011-2009.

Huang, J., P. Minnis, H. Yan, Y. Yi, B. Chen, L. Zhang, and J. K. Ayers (2010), Dust aerosol effect on semi-arid climate over Northwest China detected from A-Train satellite measurements, *Atmos. Chem. Phys.*, 10(14), 6863–6872, doi:10.5194/acp-10-6863-2010.

Huang, J., X. Guan, and F. Ji (2012), Enhanced cold-season warming in semi-arid regions, *Atmos. Chem. Phys.*, 12(12), 5391–5398, doi:10.5194/acp-12-5391-2012.

Huang, J., T. Wang, W. Wang, Z. Li, and H. Yan (2014), Climate effects of dust aerosols over East Asian arid and semiarid regions, *J. Geophys. Res. Atmos.*, 119, 11398–11416, doi:10.1002/2014JD021796.

Huang, J., J. Liu, B. Chen, and S. L. Nasiri (2015), Detection of anthropogenic dust using CALIPSO lidar measurements, *Atmos. Chem. Phys.*, 15, 11653–11665, doi:10.5194/acp-15-11653-2015.

Huang, J., M. Ji, Y. Xie, S. Wang, Y. He, and J. Ran (2016a), Global semi-arid climate change over last 60 years, *Clim. Dyn.*, 46(3–4), 1131–1150, doi:10.1007/s00382-015-2636-8.

Huang, J., H. Yu, X. Guan, G. Wang, and R. Guo (2016b), Accelerated dryland expansion under climate change, *Nat. Clim. Chang.*, *6*(2), 166–171, doi:10.1038/nclimate2837.

Huang, J., Y. Xie, X. Guan, D. Li, and F. Ji (2017a), The dynamics of the warming hiatus over the Northern Hemisphere, *Clim. Dyn.*, *48*(1–2), 429–446, doi:10.1007/s00382-016-3085-8.

Huang, J., H. Yu, A. Dai, Y. Wei, and L. Kang (2017b), Potential threats over drylands behind 2°C global warming target, *Nat. Clim. Chang.*, *7*, 417–422, doi:10.1038/nclimate3275.

Huang, W., F. Chen, S. Feng, J. Chen, and X. Zhang (2013), Interannual precipitation variations in the mid-latitude Asia and their association with large scale atmospheric circulation, *Chin. Sci. Bul.*, *58*(32), 3962–3968, doi:10.1007/s11434-013-5970-4.

Huang, X., F. Chen, Y. Fan, and M. Yang (2008), Dry late-glacial and early Holocene climate in arid Central Asia indicated by lithological and palynological evidence from Bosten Lake, China, *Quatern. Int.*, *194*, 19–27, doi:10.1016/j.quaint.2007.10.002.

Hudson, R. D., M. F. Andrade, M. B. Follette, and A. D. Frolov (2006), The total ozone field separated into meteorological regimes—Part II: Northern Hemisphere mid-latitude total ozone trends, *Atmos. Chem. Phys.*, *6*, 5183–5191.

Hughes, L. (2011), Climate change and Australia: Key vulnerable regions, *Reg. Environ. Change*, *11*, S189–S195, doi:10.1007/s10113-010-0158-9.

Hughes, M. K., and L. J. Graumlich (1996), Climatic variations and forcing mechanisms of the last 2000 years, in *Multi-Millennial Dendroclimatic Studies from the Western United States*, NATO ASI Series, vol. 141, pp. 109–124, Springer, Berlin.

Hulme, M., R. Marsh, and P. Jones (1992), Global changes in a humidity index between 1931–60 and 1961–90, *Clim. Res.*, *2*, 1–22.

Hulme, M. (1996), Recent climatic change in the world's drylands, *Geophys. Res. Lett.*, *23*(1), 61–64, doi:10.1029/95GL03586.

Huntington, T. G. (2006), Evidence for intensification of the global water cycle: Review and synthesis, *J. Hydrol.*, *319*(1–4), 83–95, doi:10.1016/j.jhydrol.2005.07.003.

Intergovernmental 732 Panel on Climate Change (2007), Working group III, in *Climate Change 2007: Mitigation of Climate Change*, Cambridge Univ. Press, Cambridge.

Intergovernmental Panel on Climate Change (2013), Working group I, in *Climate Change 2013: The Physical Science Basis*, Cambridge Univ. Press, Cambridge.

Intergovernmental Panel on Climate Change (2014), Working group II, in *Climate Change 2014: Impacts, Adaptation, and Vulnerability*, Cambridge Univ. Press, Cambridge.

Islam, M. N., and M. Almazroui (2012), Direct effects and feedback of desert dust on the climate of the Arabian Peninsula during the wet season: A regional climate model study, *Clim. Dyn.*, *39*(9–10), 2239–2250, doi:10.1007/s00382-012-1293-4.

Ji, F., Z. Wu, J. Huang, and E. P. Chassignet (2014), Evolution of land surface air temperature trend, *Nat. Clim. Chang.*, *4*(6), 462–466, doi:10.1038/nclimate2223.

Ji, M., J. Huang, Y. Xie, and J. Liu (2015), Comparison of dryland climate change in observations and CMIP5 simulations, *Adv. Atmos. Sci.*, *32*(11), 1565–1574, doi:10.1007/s00376-015-4267-8.

Jia, X., T. Zha, J. Gong, B. Wu, Y. Zhang, S. Qin, G. Chen, W. Feng, S. Kellomaki, and H. Peltola (2016), Energy partitioning over a semi-arid shrubland in northern China, *Hydrol. Process.*, *30*(6), 972–985, doi:10.1002/hyp.10685.

Jiang, J., X. Gu, and J. Ju (2007), Significant changes in subseries means and variances in an 8000-year precipitation reconstruction from tree rings in the southwestern USA, *Ann. Geophys.*, *25*(7), 1519–1530.

Jin, L., B. Schneider, W. Park, M. Latif, V. Khon, and X. Zhang (2014), The spatial-temporal patterns of Asian summer monsoon precipitation in response to Holocene insolation change: A model-data synthesis, *Quat. Sci. Rev.*, *85*, 47–62.

Johanson, C. M., and Q. Fu (2009), Hadley cell widening: Model simulations versus observations, *J. Clim.*, *22*(10), 2713–2725, doi:10.1175/2008JCLI2620.1.

Jones, N. (2011), Heating up tensions, *Nat. Clim. Chang.*, *1*(7), 327–329, doi:10.1038/nclimate1236.

Jones, P. D., and A. Moberg (2003), Hemispheric and large-scale surface air temperature variations: An extensive revision and an update to 2001, *J. Clim.*, *16*(2), 206–223, doi:10.1175/1520-0442(2003)016<0206:HALSSA>2.0.CO;2.

Jones, P. D., K. R. Briffa, T. P. Barnett, and S. F. B. Tett (1998), High-resolution palaeoclimatic records for the last millennium: Interpretation, integration and comparison with General Circulation Model control-run temperatures, *Holocene*, *8*(4), 455–471, doi:10.1191/095968398667194956.

Junkermann, W., J. Hacker, T. Lyons, and U. Nair (2009), Land use change suppresses precipitation, *Atmos. Chem. Phys.*, *9*(17), 6531–6539, doi:10.5194/acp-9-6531-2009.

Kala, J., M. Kauwe, A. Pitman, B. Medlyn, Y.-P. Wang, R. Lorenz, and S. Perkins-Kirkpatrick (2016), Impact of the representation of stomatal conductance on model projections of heatwave intensity, *Sci. Rep.*, *6*, 23418, doi:10.1038/srep23418.

Kappes, M. S., M. Keiler, K. Von Elverfeldt, and T. Glade (2012), Challenges of analyzing multi-hazard risk: A review, *Nat. Hazards*, *64*(2), 1925–1958, doi:10.1007/s11069-012-0294-2.

Kassas, M. (1995), Desertification: A general review, *J. Arid Environ.*, *30*(2), 115–128, doi:10.1016/S0140-1963(05)80063-1.

Kaufman, Y. J., I. Koren, L. A. Remer, D. Tanré, P. Ginoux, and S. Fan (2005), Dust transport and deposition observed from the Terra-Moderate Resolution Imaging Spectroradiometer (MODIS) spacecraft over the Atlantic Ocean, *J. Geophys. Res.*, *110*, D10S12, doi:10.1029/2003JD004436.

Kawamoto, K., T. Nakajima, D. Streets, and J. H. Woo (2004), Examining the aerosol indirect effect over China using an SO_2 emission inventory, *Atmos. Res.*, *72*(1–4), 353–363, doi:10.1016/j.atmosres.2004.03.028.

Keenan, T. F., I. C. Prentice, J. G. Canadell, C. A. Williams, H. Wang, M. Raupach, and G. J. Collatz (2016), Recent pause in the growth rate of atmospheric CO_2 due to enhanced terrestrial carbon uptake, *Nat. Commun.*, *7*, 13428, doi:10.1038/ncomms13428.

Kerr, Y. H. (2007), Soil moisture from space: Where are we?, *Hydrogeol. J.*, *15*(1), 117–120.

Keyantash, J., and J. A. Dracup (2002), The quantification of drought: An evaluation of drought indices, *Bull. Am. Meteorol. Soc.*, *83*(8), 1167–1180.

Kim, H., and M. Choi (2015), Impact of soil moisture on dust outbreaks in East Asia: Using satellite and assimilation data, *Geophys. Res. Lett.*, *42*, 2789–2796, doi:10.1002/2015GL063325.

Kim, Y., K. Y. Kim, and J. G. Jhun (2013), Seasonal evolution mechanism of the East Asian winter monsoon and its interannual variability, *Clim. Dyn.*, *41*(5–6), 1213–1228, doi:10.1007/s00382-012-1491-0.

Kimura, R., and M. Shinoda (2010), Spatial distribution of threshold wind speeds for dust outbreaks in Northeast Asia, *Geomorphology*, *114*, 319–325, doi:10.1016/j.geomorph.2009.07.014.

Klein, C., J. Bliefernicht, D. Heinzeller, U. Gessner, I. Klein, and H. Kunstmann (2017), Feedback of observed interannual vegetation change: A regional climate model analysis for the West African monsoon, *Clim. Dyn.*, *48*(9–10), 2837–2858, doi:10.1007/s00382-016-3237-x.

Knippertz, P., and M. C. Todd (2012), Mineral dust aerosols over the Sahara: Meteorological controls on emission and transport and implications for modeling, *Rev. Geophys.*, *50*, RG1007, doi:10.1029/2011RG000362.

Konaré, A., A. S. Zakey, F. Solmon, F. Giorgi, S. Rauscher, S. Ibrah, and X. Bi (2008), A regional climate modeling study of the effect of desert dust on the West African monsoon, *J. Geophys. Res.*, *113*, D12206, doi:10.1029/2007JD009322.

Kool, D., W. P. Kustas, A. Ben-Gal, N. Lazarovitch, J. L. Heitmand, T. J. Sauer, and N. Agam (2016), Energy and evapotranspiration partitioning in a desert vineyard, *Agric. For. Meteorol.*, *218*, 277–287, doi:10.1016/j.agrformet.2016.01.002.

Köppen, W. (1884), Die Wärmezonen der Erde, nach der Dauer der heissen, gemässigten und kalten Zeit und nach der Wirkung der Wärme auf die organische Welt betrachtet (The thermal zones of the Earth according to the duration of hot, moderate and cold periods and to the impact of heat on the organic world), −Meteorol. Z. 1, 215–226. (translated and edited by E. Volken and S. Brönnimann, -Meteorol. Z. 20(2011), 351–360).

Koren, I., Y. J. Kaufman, D. Rosenfeld, L. A. Remer, and Y. Rudich (2005), Aerosol invigoration and restructuring of Atlantic convective clouds, *Geophys. Res. Lett.*, *32*, L14828, doi:10.1029/2005GL023187.

Koren, I., L. A. Remer, O. Altaratz, J. V. Martins, and A. Davidi (2010), Aerosol-induced changes of convective cloud anvils produce strong climate warming, *Atmos. Chem. Phys.*, *10*(10), 5001–5010, doi:10.5194/acp-10-5001-2010.

Koster, R. D., et al. (2004), Regions of strong coupling between soil moisture and precipitation, *Science*, *305*(5687), 1138–1140, doi:10.1126/science.1100217.

Kullman, L. (2006), Tree line population monitoring of Pinus sylvestris in the Swedish scandes, 1973–2005: Implications for tree line theory and climate change ecology, *J. Ecol.*, *95*(1), 41–52, doi:10.1111/j.1365-2745.2006.01190.x.

Kumar, K. S. K., and J. Parikh (2001), Indian agriculture and climate sensitivity, *Global Environ. Chang.*, *11*(2), 147–154, doi:10.1016/S0959-3780(01)00004-8.

Kurosaki, Y., M. Shinoda, and M. Mikami (2011a), What caused a recent increase in dust outbreaks over East Asia?, *Geophys. Res. Lett.*, *38*, L11702, doi:10.1029/2011GL047494.

Kurosaki, Y., M. Shinoda, M. Mikami, and B. Nandintsetseg (2011b), Effects of soil and land surface conditions in summer on dust outbreaks in the following spring in a Mongolian grassland, *SOLA*, *7*(1), 69–72, doi:10.2151/sola.2011-018.

Lal, A. (2003), Carbon sequestration in dryland ecosystems, *Environ. Manage.*, *33*(4), 528–544, doi:10.1007/s00267-003-9110-9.

Lambert, F. H., and M. J. Webb (2008), Dependency of global mean precipitation on surface temperature, *Geophys. Res. Lett.*, *35*, L16706, doi:10.1029/2008GL034838.

Lau, K. M., and K. M. Kim (2006), Observational relationships between aerosol and Asian monsoon rainfall, and circulation, *Geophys. Res. Lett.*, *33*, L21810, doi:10.1029/2006GL027546.

Lau, K. M., M. K. Kim, and K. M. Kim (2006), Asian summer monsoon anomalies induced by aerosol direct forcing: The role of the Tibetan Plateau, *Clim. Dyn.*, *26*(7–8), 855–864, doi:10.1007/s00382-006-0114-z.

Lau, K. M., K. M. Kim, Y. C. Sud, and G. K. Walker (2009), A GCM study of the response of the atmospheric water cycle of West Africa and the Atlantic to Sahara dust radiative forcing, *Ann. Geophys.*, *27*, 4023–4037, doi:10.5194/angeo-27-4023-2009.

Lau, W., and K. M. Kim (2015), Robust Hadley Circulation changes and increasing global dryness due to CO2 warming from CMIP5 model projections, *Proc. Natl. Acad. Sci.*, *112*(12), 3630–3635, doi:10.1073/pnas.1418682112.

Lawrimore, J. H., et al. (2001), Climate assessment for 2000, *Bull. Am. Meteorol. Soc.*, *82*(6), S1–S55.

Levin, Z., A. Teller, E. Ganor, and Y. Yin (2005), On the interactions of mineral dust, sea-salt particles, and clouds: A measurement and modeling study from the Mediterranean Israeli dust experiment campaign, *J. Geophys. Res.*, *110*, D20202, doi:10.1029/2005JD005810.

Levine, X. J., and T. Schneider (2011), Response of the Hadley circulation to climate change in an aquaplanet GCM coupled to a simple representation of ocean heat transport, *J. Atmos. Sci.*, *68*(4), 769–783, doi:10.1175/2010jas3553.1.

Levy, H., L. W. Horowitz, M. D. Schwarzkopf, Y. Ming, J. C. Golaz, V. Naik, and V. Ramaswamy (2013), The roles of aerosol direct and indirect effects in past and future climate change, *J. Geophys. Res. Atmos.*, *118*, 4521–4532, doi:10.1002/jgrd.50192.

Li, C., B. Stevens, and J. Marotzke (2015a), Eurasian winter cooling in the warming hiatus of 1998–2012, *Geophys. Res. Lett.*, *42*, 8131–8139, doi:10.1002/2015GL065327.

Li, C., T. Zhao, and K. Ying (2015b), Effects of anthropogenic aerosols on temperature changes in China during the twentieth century based on CMIP5 models, *Theor. Appl. Climatol.*, *125*(3–4), 529–540, doi:10.1007/s00704-015-1527-6.

Li, H., A. Dai, T. Zhou, and J. Lu (2010), Responses of East Asian summer monsoon to historical SST and atmospheric forcing during 1950–2000, *Clim. Dyn.*, *34*(4), 501–514, doi:10.1007/s00382-008-0482-7.

Li, J., X. Gou, E. R. Cook, and F. Chen (2006), Tree-ring based drought reconstruction for the central Tien Shan area in Northwest China, *Geophys. Res. Lett.*, *33*, L07715, doi:10.1029/2006GL025803.

Li, J., E. R. Cook, F. Chen, X. Gou, and Y. Zhang (2007), Drought reconstruction for North Central China from tree rings: The value of the Palmer drought severity index, *Int. J. Climatol.*, *27*(7), 903–909, doi:10.1002/joc.1450.

Li, J., Z. Liu, C. He, W. Tu, and Z. Sun (2016), Are the drylands in northern China sustainable? A perspective from ecological footprint dynamics from 1990 to 2010, *Sci. Total Environ.*, *553*, 223–231, doi:10.1016/j.scitotenv.2016.02.088.

Li, M., and Z. Ma (2013), Soil moisture-based study of the variability of dry-wet climate and climate zones in China, *Chin. Sci. Bull.*, *58*, 531–544.

Li, Y., and X. Zhao (2012), An empirical study of the impact of human activity on long-term temperature change in China: A perspective from energy consumption, *J. Geophys. Res.*, *117*, D17117, doi:10.1029/2012JD018132.

Li, Y., J. Huang, M. Ji, and J. Ran (2015), Dryland expansion in Northern China from 1948 to 2008, *Adv. Atmos. Sci*, *32*(6), 870–876, doi:10.1007/s00376-014-4106-3.

Li, Z., K.-H. Lee, J. Xin, Y. Wang, and W.-M. Hao (2010), First observation-based estimates of aerosol radiative forcing at the top, bottom and inside of the atmosphere, *J. Geophys. Res.*, *115*, D00K18, doi:10.1029/2009JD013306.

Li, Z., F. Niu, J. Fan, Y. Liu, D. Rosenfeld, and Y. Ding (2011), Long-term impacts of aerosols on the vertical development of clouds and precipitation, *Nat. Geosci.*, *4*(12), 888–894, doi:10.1038/ngeo1313.

Li, Z., et al. (2016), Aerosol and monsoon climate interactions over Asia, *Rev. Geophys.*, *54*, 866–929, doi:10.1002/2015RG000500.

Lin, L., A. Gettelman, S. Feng, and Q. Fu (2015), Simulated climatology and evolution of aridity in the 21st century, *J. Geophys. Res. Atmos.*, *120*, 10,214–10,228, doi:10.1002/2015JD023657.

Lin, L., A. Gettelman, Y. Xu, and Q. Fu (2016a), Simulated differences in 21st century aridity due to different scenarios of greenhouse gases and aerosols, *Clim. Change*, doi:10.1007/s10584-016-1615-3.

Lin, L., A. Gettelman, Y. Xu, and Q. Fu (2016b), Simulated responses of terrestrial aridity to black carbon and sulfate aerosols, *J. Geophys. Res. Atmos.*, *121*, 785–794, doi:10.1002/2015JD024100.

Liu, J., B. Wang, H. Wang, X. Kuang, and R. Ti (2011a), Forced response of the East Asian summer rainfall over the past millennium: Results from a coupled model simulation, *Clim. Dyn.*, *36*(1–2), 323–336, doi:10.1007/s00382-009-0693-6.

Liu, J., Y. Zheng, Z. Li, C. Flynn, E. J. Welton, and M. Cribb (2011b), Transport, vertical structure and radiative properties of dust events in Southeast China determined from ground and space sensors, *Atmos. Environ.*, *45*(35), 6469–6480, doi:10.1016/j.atmosenv.2011.04.031.

Liu, J., J. Chen, K. Selvaraj, Q. Xu, Z. Wang, and F. Chen (2014), Chemical weathering over the last 1200 years recorded in the sediments of Gonghai Lake, Lvliang Mountains, North China: A high-resolution proxy of past climate, *Boreas*, *43*(4), 914–923, doi:10.1111/bor.12072.

Liu, Y., W. Guo, and Y. Song (2015), Estimation of key surface parameters in semi-arid region and their impacts on improvement of surface fluxes simulation, *Science China Earth Sciences*, *59*(2), 307–319, doi:10.1007/s11430-015-5140-4.

Liu, Z., et al. (2008), Airborne dust distributions over the Tibetan Plateau and surrounding areas derived from the first year of CALIPSO lidar observations, *Atmos. Chem. Phys.*, *8*(16), 5045–5060, doi:10.5194/acp-8-5045-2008.

Lohmann, U., and J. Feichter (2005), Global indirect aerosol effects: A review, *Atmos. Chem. Phys.*, *5*, 715–737, doi:10.5194/acp-5-715-2005.

Lohmann, U. (2006), Aerosol effects on clouds and climate, *Space Sci. Rev.*, *125*(1–4), 129–137, doi:10.1007/s11214-006-9051-8.

Lowenthal, D. H., R. D. Borys, W. Cotton, S. Saleeby, S. A. Cohn, and W. O. J. Brown (2011), The altitude of snow growth by riming and vapor deposition in mixed-phase orographic clouds, *Atmos. Environ.*, *45*(2), 519–522, doi:10.1016/j.atmosenv.2010.09.061.

Lu, J. (2009), The dynamics of the Indian Ocean sea surface temperature forcing of Sahel drought, *Clim. Dyn.*, *33*(4), 445–460, doi:10.1007/s00382-009-0596-6.

Lu, J., and T. L. Delworth (2005), Oceanic forcing of the late 20th century Sahel drought, *Geophys. Res. Lett.*, *32*, L22706, doi:10.21029/22005GL023316.

Lu, J., G. A. Vecchi, and T. Reichler (2007), Expansion of the Hadley cell under global warming, *Geophys. Res. Lett.*, *34*, L06805, doi:10.1029/2006GL028443.

Lu, J., G. Chen, and D. Frierson (2008), Response of the zonal mean atmospheric circulation to el Nino versus global warming, *J. Clim.*, *21*(22), 5835–5851, doi:10.1175/2008JCLI2200.1.

Lu, X., L. Wang, and M. F. McCabe (2016), Elevated CO_2 as a driver of global dryland greening, *Sci. Rep.*, *6*, 20716, doi:10.1038/srep20716.

Luo, D., Y. Xiao, Y. Yao, A. Dai, I. Simmonds, and C. Franzke (2016a), Impact of Ural blocking on winter warm Arctic–cold Eurasian anomalies. Part I: Blocking-induced amplification, *J. Clim.*, *29*(11), 3925–3947, doi:10.1175/JCLI-D-15-0611.1.

Luo, D., Y. Xiao, Y. Diao, A. Dai, C. Franzke, and I. Simmonds (2016b), Impact of Ural blocking on winter warm Arctic–cold Eurasian anomalies. Part II: The link to the North Atlantic oscillation, *J. Clim.*, *29*(11), 3949–3971, doi:10.1175/JCLI-D-15-0612.1.

Luo, D., Y. Yao, A. Dai, I. Simmonds, and L. Zhong (2017), Increased quasi-stationarity and persistence of winter Ural blocking and Eurasian extreme cold events in response to Arctic warming. Part II: A theoretical explanation, *J. Clim.*, *30*(10), 3569–3587, doi:10.1175/JCLI-D-16-0262.1.

Lynn, B., A. Khain, D. Rosenfeld, and W. L. Woodley (2007), Effects of aerosols on precipitation from orographic clouds, *J. Geophys. Res.*, *112*, D10225, doi:10.1029/2006JD007537.

Ma, Z. (2007), The interdecadal trend and shift of dry/wet over the central part of North China and their relationship to the Pacific Decadal Oscillation (PDO) [in Chinese], *Chinese Sci. Bullet.*, *52*(10), 1199–1206.

Ma, Z., and L. Dan (2005), Dry/wet variation and its relationship with regional warming in arid-regions of Northern China, *Chinese J. of Geophys.*, *48*(5), 1091–1099, doi:10.1002/cjg2.752.

Ma, Z., and C. Fu (2003), Interannual characteristics of the surface hydrological variables over the arid and semi-arid areas of Northern China, *Global Planet. Change*, *37*(3–4), 189–200, doi:10.1016/S0921-8181(02)00203-5.

Ma, Z., and C. Fu (2006), Some evidences of drying trend over North China from 1951 to 2004, *Chinese Sci. Bullet.*, *51*, 2913–2925.

Ma, Z., and C. Fu (2007), Evidences of drying trend in the global during the later half of 20th century and their relationship with large scale climate background, *Sci. China Earth Sci.*, *50*(5), 776–788.

Ma, Z., and L. Shao (2006), Relationship between dry/wet variation and the Pacific Decadal Oscillation (PDO) in Northern China during the last 100 years [in Chinese], *Chinese J. Atmos Sci.*, *30*, 464–474.

Madsen, D. B., et al. (2001), Late Quaternary environmental change in the Bonneville basin, western USA, *Palaeogeogr. Palaeoclimatol. Palaeoecol.*, *167*(3–4), 243–271, doi:10.1016/S0031-0182(00)00240-6.

Maestre, F. T., et al. (2013), Changes in biocrust cover drive carbon cycle responses to climate change in drylands, *Global Change Biol.*, *19*(12), 3835–3847, doi:10.1111/gcb.12306.

Mahmood, R., et al. (2014), Land cover changes and their biogeophysical effects on climate, *Int. J. Climatol.*, *34*(4), 929–953, doi:10.1002/joc.3736.

Mainguet, M. (1999), *Aridity-Droughts and Human Development*, Springer, New York.

Malone, S. L., C. L. Staudhammer, H. W. Loescher, P. Olivas, S. F. Oberbauer, M. G. Ryan, J. Schedlbauer, and G. Starr (2014), Seasonal patterns in energy partitioning of two freshwater marsh ecosystems in the Florida Everglades, *J. Geophys. Res. Biogeosci.*, *119*, 1487–1505, doi:10.1002/2014JG002700.

Mann, M. E., and P. D. Jones (2003), Global surface temperatures over the past two millennia, *Geophys. Res. Lett.*, *30*(15), 1820, doi:10.1029/2003GL017814.

Mann, M. E., Z. Zhang, M. K. Hughes, R. S. Bradley, S. K. Miller, S. Rutherford, and F. Ni (2008), Proxy-based reconstructions of hemispheric and global surface temperature variations over the past two millennia, *Proc. Natl. Acad. Sci.*, *105*(36), 13,252–13,257, doi:10.1073/pnas.0805721105.

Mao, J., et al. (2016), Human-induced greening of the northern extratropical land surface, *Nat. Clim. Chang.*, *6*(10), 959–963, doi:10.1038/nclimate3056.

Mason, J. A., J. B. Swinehart, R. J. Goble, and D. B. Loope (2004), Late-Holocene dune activity linked to hydrological drought, Nebraska sand hills, USA, *Holocene*, *14*(2), 209–217, doi:10.1191/0959683604hl677rp.

May, W., M. Rummukainen, F. Chéruy, S. Hagemann, and A. Meier (2016), Contributions of soil moisture interactions to future precipitation changes in the GLACE-CMIP5 experiment, *Clim. Dynam.*, *45*(11–12), 1–24, doi:10.1007/s00382-016-3408-9.

McAlpine, C. A., et al. (2010), More than CO_2: A broader paradigm for managing climate change and variability to avoid ecosystem collapse, *Curr. Opin. Environ. Sustain.*, *2*(5–6), 334–346, doi:10.1016/j.cosust.2010.10.001.

McCabe, G. J., M. A. Palecki, and J. L. Betancourt (2004), Pacific and Atlantic Ocean influences on multidecadal drought frequency in the United States, *Proc. Natl. Acad. Sci.*, *101*(12), 4136–4141, doi:10.1073/pnas.0306738101.

McCusker, K. E., J. C. Fyfe, and M. Sigmond (2016), Twenty-five winters of unexpected Eurasian cooling unlikely due to Arctic sea-ice loss, *Nat. Geosci.*, *1*, 1–6, doi:10.1038/ngeo2820.

McKee, T. B., N. J. Doesken, and J. Kleist (1993), The relationship of drought frequency and duration to time scales. In: 8th Conference on Applied Climatology, Anaheim, 179–184.

McMahon, T. A. (1979), *Hydrological Characteristics of Arid Zones*, Proc. Symposium on the hydrology of areas of low precipitation, IAHS, Canberra.

MEA (2005), *Millennium Ecosystem Assessment Ecosystems and Human Well-Being: Desertification Synthesis*, World Resources Institute, Washington, D. C.

Meehl, G. A., et al. (2012), Climate system response to external forcings and climate change projections in CCSM4, *J. Clim.*, *25*(11), 3661–3683, doi:10.1175/JCLI-D-11-00240.1.

Middleton, N., and D. Thomas (1997), *World Atlas of Desertification*, 2nd ed., Copublished in the US, Central and South America by John Wiley, Arnold.

Milesi, C., A. Samanta, H. Hashimoto, K. K. Kumar, S. Ganguly, P. S. Thenkabail, A. N. Srivastava, R. R. Nemani, and R. B. Myneni (2010), Decadal variations in NDVI and food production in India, *Remote Sens.*, *2*(3), 758–776, doi:10.3390/rs2030758.

Miller, R. L., I. Tegen, and J. Perlwitz (2004), Surface radiative forcing by soil dust aerosols and the hydrologic cycle, *J. Geophys. Res.*, *109*, D04203, doi:10.1029/2003JD004085.

Milly, P. C. D., and K. A. Dunne (2016), Potential evapotranspiration and continental drying, *Nat. Clim. Chang.*, *6*(10), 946–949, doi:10.1038/nclimate3046.

Mitas, C. M., and A. Clement (2006), Recent behavior of the Hadley cell and tropical thermodynamics in climate models and reanalyses, *Geophys. Res. Lett.*, *33*, L01810, doi:10.1029/2005GL024406.

Mitchell, J. F. B., C. A. Wilson, and W. M. Cunnington (1987), On CO_2 climate sensitivity and model dependence of results, *Q. J. R. Meteorol. Soc.*, *113*(475), 293–322, doi:10.1256/smsqj.47516.

Mo, K. C., J. K. E. Schemm, and S. H. Yoo (2009), Influence of ENSO and the Atlantic Multidecadal Oscillation on drought over the United States, *J. Clim.*, *22*(22), 5962–5982, doi:10.1175/2009JCLI2966.1.

Moberg, A., D. M. Sonechkin, K. Holmgren, N. M. Datsenko, and W. Karlen (2005), Highly variable Northern Hemisphere temperatures reconstructed from low- and high-resolution proxy data, *Nature*, *433*(7026), 613–617, doi:10.1038/nature03265.

Mori, M., M. Watanabe, H. Shiogama, J. Inoue, and M. Kimoto (2014), Robust Arctic sea-ice influence on the frequent Eurasian cold winters in past decades, *Nat. Geosci.*, *7*(12), 869–873, doi:10.1038/ngeo2277.

Mortimore, M. (2009), *Dryland Opportunities*, IUCN, Gland, Switzerland, HED, London, UK and UNDP, New York, USA.

Moulin, C., C. E. Lambert, F. Dulac, and U. Dayan (1997), Control of atmospheric export of dust from North Africa by the North Atlantic oscillation, *Nature*, *387*(6634), 691–694.

Mullan, A. B. (1995), On the linearity and stability of Southern Oscillation-climate relationships for New Zealand, *Int. J. Climatol.*, *15*(12), 1365–1386, doi:10.1002/joc.3370151205.

Nahal, I. (1995), Desertification and its effects in the Arabian peninsula, in *United Nations Environment Programme*, pp. 53–57, Nairobi.

Nair, V. S., S. S. Babu, K. K. Moorthy, and S. S. Prijith (2013), Spatial gradients in aerosol-induced atmospheric heating and surface dimming over the oceanic regions around India: Anthropogenic or natural?, *J. Clim.*, *26*(19), 7611–7621, doi:10.1175/JCLI-D-12-00616.1.

Nandintsetseg, B., and M. Shinoda (2015), Land surface memory effects on dust emission in a Mongolian temperate grassland, *J. Geophys. Res. Biogeosci.*, *120*, 414–427, doi:10.1002/2014JG002708.

Neelin, J. D., C. Chou, and H. Su (2003), Tropical drought regions in global warming and El Niño teleconnections, *Geophys. Res. Lett.*, *30*(24), 2275, doi:10.1029/2003GL018625.

Nguyen, H., A. Evans, C. Lucas, I. Smith, and B. Timbal (2013), The Hadley circulation in reanalyses: Climatology, variability, and change, *J. Clim.*, *26*(10), 3357–3376, doi:10.1175/jcli-d-12-00224.1.

Nguyen, H., C. Lucas, A. Evans, B. Timbal, and L. Hanson (2015), Expansion of the Southern Hemisphere Hadley cell in response to greenhouse gas forcing, *J. Clim.*, *28*(20), 8067–8077, doi:10.1175/jcli-d-15-0139.1.

Nicholson, S. E. (2011), *Dryland Climatology*, Cambridge Univ. Press, Cambridge.

Novick, K., et al. (2016), The increasing importance of atmospheric demand for ecosystem water and carbon fluxes, *Nat. Clim. Chang.*, *6*(11), 1023–1027, doi:10.1038/nclimate3114.

Nyamadzawo, G., et al. (2009), Land-use and land-use change effects on nitrous oxide emissions in the seasonally dry ecosystems of Zimbabwe: A review, *Actas Urológicas Españolas*, *33*(3), 249–257.

O'Gorman, P. A., R. P. Allan, M. P. Byrne, and M. Previdi (2012), Energetic constraints on precipitation under climate change, *Surv. Geophys.*, *33*(3–4), 585–608, doi:10.1007/s10712-011-9159-6.

Obasi, G. O. P. (1994), WMO's role in the international decade for natural disaster reduction, *Bull. Am. Meteorol. Soc.*, *75*(9), 1655–1661.

Ocko, I. B., V. Ramaswamy, and Y. Ming (2014), Contrasting climate responses to the scattering and absorbing features of anthropogenic aerosol forcings, *J. Clim.*, *27*(14), 5329–5345, doi:10.1175/JCLI-D-13-00401.1.

Ohmura, A., and M. Wild (2002), Is the hydrological cycle accelerating?, *Science*, *298*(5597), 1345–1345, doi:10.1126/science.1078972.

Okin, G. S., et al. (2011), Impacts of atmospheric nutrient deposition on marine productivity: Roles of nitrogen, phosphorus, and iron, *Global Biogeochem. Cycles*, *25*, GB2022, doi:10.1029/2010GB003858.

Olson, J. M., et al. (2008), Integrating diverse methods to understand climate-land interactions in East Africa, *Geoforum*, *39*(2), 898–911.

Osmond, B., et al. (2004), Changing the way we think about global climate change research: Scaling up in ecosystem experimental science, *Global Change Biol.*, *10*, 393–407.

Otto-Bliesner, B. L., E. C. Brady, J. Fasullo, A. Jahn, L. Landrum, S. Stevenson, N. Rosenbloom, A. Mai, and G. Strand (2015), Climate variability and change since 850 CE: An ensemble approach with the Community Earth System Model, *Bull. Am. Meteorol. Soc.*, *97*(5), 735–754, doi:10.1175/BAMS-D-14-00233.1.

Ou, T., and W. Qian (2006), Vegetation variations along the monsoon boundary zone in East Asia, *Chin. J. Geophys.*, *49*(3), 627–636.

Overland, J. E., K. R. Wood, and M. Wang (2011), Warm Arctic-cold continents: Climate impacts of the newly open Arctic Sea, *Polar Res.*, *30*, 15787, doi:10.3402/polar.v30i0.15787.

Palmer, W. C. (1965), *Meteorological Drought*, *U.S. Weather Bur. Res. Pap*, vol. 45, p. 58, U.S. Department of Commerce, Washington, D. C.

Parkes, S., M. McCabe, A. Griffiths, L. Wang, S. Chambers, A. Ershadi, A. Williams, J. Strauss, and A. Element (2017), Response of water vapour D-excess to land–atmosphere interactions in a semi-arid environment, *Hydrol. Earth Syst. Sci.*, *21*(1), 533–548, doi:10.5194/hess-21-533-2017.

Pavia, E. G., F. Graef, and J. Reyes (2006), PDO-ENSO effects in the climate of Mexico, *J. Clim.*, *19*(24), 6433–6438, doi:10.1175/JCLI4045.1.

Pendergrass, A. G., and D. L. Hartmann (2014), The atmospheric energy constraint on global-mean precipitation change, *J. Clim.*, *27*(2), 757–768, doi:10.1175/jcli-d-13-00163.1.

Peng, S., et al. (2013), Asymmetric effects of daytime and night-time warming on Northern Hemisphere vegetation, *Nature*, *501*(7465), 88–92, doi:10.1038/nature12434.

Penman, H. L. (1948), Natural evaporation from open water, bare soil and grass, proceedings of, *Proc. R. Soc. London, Ser. A*, *193*(1032), 120–145.

Penner, J. E., et al. (2001), *Aerosols: Their Direct and Indirect Effects, Climate Change 2001: The Scientific Basis, Contribution of Working Group I to IPCC*, pp. 291–336, Cambridge Univ. Press, Cambridge.

Piao, S., et al. (2015), Detection and attribution of vegetation greening trend in China over the last 30 years, *Global Change Biol.*, *21*(4), 1601–1609, doi:10.1111/gcb.12795.

Pilgrim, D. H., T. G. Chapman, and D. G. Doran (1988), Problems of rainfall runoff modeling in arid and semi-arid regions, *Hydrol. Sci. J.*, *33*(4), 379–400.

Polvani, L. M., D. W. Waugh, G. J. P. Correa, and S. W. Son (2011), Stratospheric ozone depletion: The main driver of twentieth-century atmospheric circulation changes in the Southern Hemisphere, *J. Clim.*, *24*(3), 795–812, doi:10.1175/2010jcli3772.1.

Poulter, B., et al. (2014), Contribution of semi-arid ecosystems to interannual variability of the global carbon cycle, *Nature*, *509*(7502), 600–603, doi:10.1038/nature13376.

Power, P. P. (1999), π-bonding and the lone pair effect in multiple bonds between heavier main group elements, *Chem. Rev.*, *99*(12), 3463–3503, doi:10.1021/cr9408989.

Prenni, A. J., M. D. Petters, S. M. Kreidenweis, C. L. Heald, S. T. Martin, P. Artaxo, R. M. Garland, A. G. Wollny, and U. Poschl (2009), Relative roles of biogenic emissions and Saharan dust as ice nuclei in the Amazon basin, *Nat. Geosci.*, *2*(6), 401–404, doi:10.1038/ngeo517.

Previdi, M., and B. G. Liepert (2007), Annular modes and Hadley cell expansion under global warming, *Geophys. Res. Lett.*, *34*, L22701, doi:10.1029/2007GL031243.

Prospero, J. M., and P. J. Lamb (2003), African droughts and dust transport to the Caribbean: Climate change implications, *Science*, *302*(5647), 1024–1027, doi:10.1126/science.1089915.

Prudhomme, C., et al. (2014), Hydrological droughts in the 21st century, hotspots and uncertainties from a global multimodel ensemble experiment, *Proc. Natl. Acad. Sci.*, *111*, 3262–3267, doi:10.1073/pnas.1222473110.

Qi, J., J. Chen, S. Wan, and L. Ai (2012), Understanding the coupled natural and human systems in dryland East Asia, *Environ. Res. Lett.*, *7*(1), 015202), doi:10.1088/1748-9326/7/1/015202.

Qian, C., and T. Zhou (2014), Multidecadal variability of North China aridity and its relationship to PDO during 1900–2010, *J. Clim.*, *27*(3), 1210–1222, doi:10.1175/JCLI-D-13-00235.1.

Qian, T., A. Dai, K. E. Trenberth, and K. W. Oleson (2006), Simulation of global land surface conditions from 1948–2004. Part I: Forcing data and evaluation, *J. Hydrometeorol.*, *7*, 953–975.

Qian, T., A. Dai, and K. E. Trenberth (2007), Hydroclimatic trends in the Mississippi river basin from 1948–2004, *J. Clim.*, *20*, 4599–4614.

Qian, W., T. Ding, H. Hu, X. Lin, and A. Qin (2009), An overview of dry-wet climate variability among monsoon-westerly regions and the monsoon northernmost marginal active zone in China, *Adv. Atmos. Sci.*, *26*, 630–641.

Quan, X., H. F. Diaz, and M. P. Hoerling (2004), *Change in the Tropical Hadley Cell Since 1950*, pp. 85–120, Springer, Dordrecht, doi:10.1007/978-1-4020-2944-8_3

Reich, P. B., K. M. Sendall, A. Stefanski, X. Wei, R. L. Rich, and R. A. Montgomery (2016), Boreal and temperate trees show strong acclimation of respiration to warming, *Nature*, *531*(7596), 633–636, doi:10.1038/nature17142.

Reynolds, J. F., et al. (2007), Global desertification: Building a science for dryland development, *Science*, *316*(5826), 847–851, doi:10.1126/science.1131634.

Rietkerk, M., S. C. Dekker, P. C. de Ruiter, and J. van de Koppel (2004), Self-organized patchiness and catastrophic shifts in ecosystems, *Science*, *305*(5692), 1926–1929, doi:10.1126/science.1101867.

Roderick, M., P. Greve, and G. Farquhar (2015), On the assessment of aridity with changes in atmospheric CO_2, *Water Resour. Res.*, *51*, 5450–5463, doi:10.1002/2015WR017031.

Rodwell, M. J., and B. J. Hoskins (1996), Monsoons and the dynamics of deserts, *Q. J. R. Meteorol. Soc.*, *122*(534), 1385–1404.

Rodwell, M. J., and B. J. Hoskins (2001), Subtropical anticyclones and summer monsoons, *J. Clim.*, *14*(15), 3192–3211.

Rosenfeld, D., Y. Rudich, and R. Lahav (2001), Desert dust suppressing precipitation: A possible desertification feedback loop, *Proc. Natl. Acad. Sci.*, *98*(11), 5975–5980, doi:10.1073/pnas.101122798.

Rosenfeld, D., W. L. Woodley, A. Khain, W. R. Cotton, G. Carrio, I. Ginis, and J. H. Golden (2012), Aerosol effects on microstructure and intensity of tropical cyclones, *Bull. Am. Meteorol. Soc.*, *93*(7), 987–1001, doi:10.1175/BAMS-D-11-00147.1.

Rosenfeld, D., R. Wood, L. J. Donner, and S. C. Sherwood (2013), Aerosol cloud-mediated radiative forcing: Highly uncertain and opposite effects from shallow and deep clouds, in *Climate Science for Serving Society: Research, Modeling and Prediction Priorities*, pp. 105–149, Springer, New York.

Rotenberg, E., and D. Yakir (2010), Contribution of semi-arid forests to the climate system, *Science*, *327*(5964), 451–454, doi:10.1126/science.1179998.

Ryan, C., and P. Elsner (2016), The potential for sand dams to increase the adaptive capacity of East African drylands to climate change, *Reg. Environ. Change*, *16*(7), 2087–2096, doi:10.1007/s10113-016-0938-y.

Saber, M., T. Hamaguchi, T. Kojiri, K. Tanaka, and T. Sumi (2015), A physically based distributed hydrological model of wadi system to simulate flash floods in arid regions, *Arab. J. Geosci.*, *8*(1), 143–160, doi:10.1007/s12517-013-1190-0.

Safriel, U., et al. (2005), Dryland systems, in *Ecosystems and Human Wellbeing, Current State and Trends*, edited by R. Hassan, R. Scholes, and N. Ash, pp. 623–662, Island Press, Washington, D. C.

Sakaeda, N., R. Wood, and P. J. Rasch (2011), Direct and semi-direct aerosol effects of southern African biomass burning aerosol, *J. Geophys. Res.*, *116*, D12205, doi:10.1029/2010JD015540.

Sassen, K. (2002), Indirect climate forcing over the Western US from Asian dust storms, *Geophys. Res. Lett.*, *29*(10), 1465, doi:10.1029/2001GL014051.

Sassen, K., P. J. DeMott, J. M. Prospero, and M. R. Poellot (2003), Saharan dust storms and indirect aerosol effects on clouds: CRYSTAL-FACE results, *Geophy. Res. Lett.*, *30*(12), 1633, doi:10.1029/2003GL017371.

Scheff, J., and D. M. W. Frierson (2012a), Robust future precipitation declines in CMIP5 largely reflect the poleward expansion of model subtropical dry zones, *Geophys. Res. Lett.*, *39*, L18704, doi:10.1029/2012GL052910.

Scheff, J., and D. M. W. Frierson (2012b), Twenty-first-century multimodel subtropical precipitation declines are mostly midlatitude shifts, *J. Clim.*, *25*(12), 4330–4347, doi:10.1175/JCLI-D-11-00393.1.

Scheff, J., and D. M. W. Frierson (2014), Scaling potential evapotranspiration with greenhouse warming, *J. Clim.*, *27*(4), 1539–1558, doi:10.1175/JCLI-D-13-00233.1.

Scheff, J., and D. M. W. Frierson (2015), Terrestrial aridity and its response to greenhouse warming across CMIP5 climate models, *J. Clim.*, *28*(14), 5583–5600, doi:10.1175/JCLI-D-14-00480.1.

Scheffer, M., S. Carpenter, J. A. Foley, C. Folke, and B. Walker (2001), Catastrophic shifts in ecosystems, *Nature*, *413*(6856), 591–596, doi:10.1038/35098000.

Schlaepfer, D. R., et al. (2017), Climate change reduces extent of temperate drylands and intensifies drought in deep soils, *Nat. Commun.*, *8*, 14196.

Schneider, B. (1977), Quantitative assessment of the effect of individual flow obstacles on the dispersion of air pollution, *Z. Gesamte Hyg.*, *23*(9), 646–648.

Schneider, U., A. Becker, P. Finger, A. Meyer-Christoffer, M. Ziese, and B. Rudolf (2014), GPCC's new land surface precipitation climatology based on quality-controlled in situ data and its role in quantifying the global water cycle, *Theor. Appl. Climatol.*, *115*(1), 15–40.

Schubert, S., et al. (2009), A US CLIVAR project to assess and compare the responses of global climate models to drought-related SST forcing patterns: Overview and results, *J. Clim.*, *22*(19), 5251–5272, doi:10.1175/2009JCLI3060.1.

Seager, R., Y. Kushnir, C. Herweijer, N. Naik, and J. Velez (2005), Modeling of tropical forcing of persistent droughts and pluvial over western North America: 1856–2000, *J. Clim.*, *18*, 4065–4088.

Seager, R., et al. (2007), Model projections of an imminent transition to a more arid climate in southwestern North America, *Science*, *316*(5828), 1181–1184, doi:10.1126/science.1139601.

Seager, R., N. Naik, and G. A. Vecchi (2010), Thermodynamic and dynamic mechanisms for large-scale changes in the hydrological cycle in response to global warming, *J. Clim.*, *23*(17), 4651–4668, doi:10.1175/2010JCLI3655.1.

Seddon, A. W. R., M. Macias-Fauria, P. R. Long, D. Benz, and K. J. Willis (2016), Sensitivity of global terrestrial ecosystems to climate variability, *Nature*, *531*(7593), 229–232, doi:10.1038/nature16986.

Seidel, D. J., Q. Fu, W. J. Randel, and T. J. Reichler (2008), Widening of the tropical belt in a changing climate, *Nat. Geosci.*, *1*(1), 21–24, doi:10.1038/ngeo.2007.38.

Seidel, T. M., A. N. Grant, A. A. P. Pszenny, and D. J. Allman (2007), Dewpoint and humidity measurements and trends at the summit of Mount Washington, New Hampshire, 1935–2004, *J. Clim.*, *20*(22), 5629–5641, doi:10.1175/2007jcli1604.1.

Seisel, S., C. Borensen, R. Vogt, and R. Zellner (2005), Kinetics and mech- anism of the uptake of N_2O_5 on mineral dust at 298 K, *Atmos. Chem. Phys.*, *5*, 3423–3432, doi:10.5194/acp-5-3423-2005.

Seneviratne, S. I., T. Corti, E. L. Davin, M. Hirschi, E. B. Jaeger, I. Lehner, B. Orlowsky, and A. J. Teuling (2010), Investigating soil moisture-climate interactions in a changing climate: A review, *Earth-Sci. Rev.*, *99*(3–4), 125–161, doi:10.1016/j.earscirev.2010.02.004.

Seneviratne, S. I., M. Donat, B. Mueller, and L. V. Alexander (2014), No pause in the increase of hot temperature extremes, *Nat. Clim. Chang.*, *4*(3), 161–163.

Sharma, P., V. Abrol, S. Abrol, and R. Kumar (2012), Resource management for sustainable agriculture, Ch. 6. InTech.

Sheffield, J., and E. F. Wood (2008), Global trends and variability in soil moisture and drought characteristics, 1950–2000, from observation-driven simulations of the terrestrial hydrologic cycle, *J. Clim.*, *21*(3), 432–458.

Sheffield, J., E. F. Wood, and M. L. Roderick (2012), Little change in global drought over the past 60 years, *Nature*, *491*(7424), 435–438.

Sherwood, S., and Q. Fu (2014), A drier future?, *Science*, *343*(6172), 737–739, doi:10.1126/science.1247620.

Shi, Y., Y. Shen, E. Kang, D. Li, Y. Ding, G. Zhang, and R. Hu (2007), Recent and future climate change in Northwest China, *Clim. Change*, *80*, 379–393, doi:10.1007/s10584-006-9121-7.

Shi, Z., L. Zhang, and G. Sui (1994), Natural disasters and their formation causes on Chinese monsoon marginal belt [in Chinese], *J. Catastophol.*, *9*(4), 59–64.

Shi, Z. (1996), Regional characters of natural disaster in marginal monsoon belt of China [in Chinese], *Arid Land Resour. Environ.*, *10*(4), 1–7.

Shin, S. H., I. U. Chung, and H. J. Kim (2012), Relationship between the expansion of drylands and the intensification of Hadley circulation during the late twentieth century, *Meteorol. Atmos. Phys.*, *118*(3), 117–128.

Shinoda, M., J. A. Gillies, M. Mikami, and Y. Shao (2011), Temperate grasslands as a dust source: Knowledge, uncertainties, and challenges, *Aeolian Res.*, *3*(3), 271–293, doi:10.1016/j.aeolia.2011.07.001.

Shinoda, M., B. Nandintsetseg, U. G. Nachinshonhor, and H. Komiyama (2014), Hotspots of recent drought in Asian steppes, *Reg. Environ. Change*, *14*(1), 103–117, doi:10.1007/s10113-013-0464-0.

Shinoda, M. (2017), Evolving a multi-hazard focused approach for arid Eurasia, in *Climate Hazard Crises in Asian Societies and Environments*, edited by T. Sternberg, pp. 73–102, Routledge, Oxon, U. K.

Sjögersten, S., and P. A. Wookey (2016), The impact of climate change on ecosystem carbon dynamics at the Scandinavian mountain birch forest–tundra heath ecotone, *Ambio*, *38*(1), 2–10.

Smoliak, B. V., J. M. Wallace, P. Lin, and Q. Fu (2015), Dynamical adjustment of the Northern Hemisphere surface air temperature field: Methodology and application to observations, *J. Clim.*, *28*, 1613–1629, doi:10.1175/JCLI-D-14-00111.1.

Solmon, F., N. Elguindi, and M. Mallet (2012), Radiative and climatic effects of dust over West Africa, as simulated by a regional climate model, *Clim. Res.*, *52*(1), 97–113, doi:10.3354/cr01039.

Solmon, F., V. S. Nair, and M. Mallet (2015), Increasing Arabian dust activity and the Indian summer monsoon, *Atmos. Chem. Phys.*, *15*(14), 8051–8064, doi:10.5194/acp-15-8051-2015.

Solomina, O., and K. Alverson (2004), High latitude Eurasian paleoenvironments: Introduction and synthesis, *Palaeogeogr. Palaeoclimatol. Palaeoecol.*, *209*(1–4), 1–18, doi:10.1016/j.palaeo.2004.02.027.

Solomon, S., D. Qin, M. Manning, Z. Chen, M. Marquis, K. B. Averyt, M. Tignor, and H. K. Miller (2007), *Climate Change, 2007: The Physical Science Basis*, Cambridge Univ. Press, Cambridge.

Song, Y., W. Guo, and Y. Zhang (2009), Numerical study of impacts of soil moisture on the diurnal and seasonal cycles of sensible/latent heat fluxes over semi-arid region, *Adv. Atmos. Sci.*, *26*(2), 319–326.

Sorrel, P., S. M. Popescu, M. J. Head, J. P. Suc, S. Klotz, and H. Oberhansli (2006), Hydrographic development of the Aral Sea during the last 2000 years based on a quantitative analysis of dinoflagellate cysts, *Palaeogeogr. Palaeoclimatol. Palaeoecol.*, *234*(2–4), 304–327, doi:10.1016/j.palaeo.2005.10.012.

Spinoni, J., J. Vogt, G. Naumann, H. Carrao, and P. Barbosa (2015), Towards identifying areas at climatological risk of desertifcation using the Köppen–Geiger classifcation and FAO aridity index, *Int. J. Climatol.*, *35*(9), 2210–2222, doi:10.1002/joc.4124.

Stadler, S. J. (2005), Aridity indices, in *Encyclopedia of World Climatology*, vol. 89-94, edited by J. E. Oliver et al., Springer, Berlin.

Stephens, G. L., and T. D. Ellis (2008), Controls of global-mean precipitation increases in global warming GCM experiments, *J. Clim.*, *21*(23), 6141–6155, doi:10.1175/2008jcli2144.1.

Sterling, S. M., A. Ducharne, and J. Polcher (2013), The impact of global land-cover change on the terrestrial water cycle, *Nat. Clim. Chang.*, *3*(4), 385–390, doi:10.1038/nclimate1690.

Stine, S. (1994), Extreme and persistent drought in California and Patagonia during mediaeval time, *Nature*, *369*(6481), 546–549, doi:10.1038/369546a0.

Su, J., J. Huang, Q. Fu, P. Minnis, J. Ge, and J. Bi (2008), Estimation of Asian dust aerosol effect on cloud radiation forcing using Fu-Liou radiative model and CERES measurements, *Atmos. Chem. Phys.*, *8*, 2763–2771, doi:10.5194/acp-8-2763-2008.

Sun, H., Z. Pan, and X. Liu (2012), Numerical simulation of spatial-temporal distribution of dust aerosol and its direct radiative effects on East Asian climate, *J. Geophys. Res.*, *117*, D13206, doi:10.1029/2011JD017219.

Sun, L., J. Perlwitz, and M. Hoerling (2016), What caused the recent "Warm Arctic, Cold Continents" trend pattern in winter temperatures?, *Geophys. Res. Lett.*, *43*, 5345–5352, doi:10.1002/2016GL069024.

Sun, Q., S. Wang, J. Zhou, J. Shen, P. Cheng, X. Xie, and F. Wu (2009), Lake surface fluctuations since the late glaciation at Lake Daihai, North Central China: A direct indicator of hydrological process response to East Asian monsoon climate, *Quatern. Int.*, *194*, 45–54, doi:10.1016/j.quaint.2008.01.006.

Swann, A., F. Hoffman, C. Koven, and J. Randerson (2016), Plant responses to increasing CO_2 reduce estimates of climate impacts on drought severity, *Proc. Natl. Acad. Sci.*, *113*(36), 10019–10024, doi:10.1073/pnas.1604581113.

Sylla, M. B., J. S. Pal, G. Wang, and P. J. Lawrence (2015), Impact of land cover characterization on regional climate modeling over West Africa, *Clim. Dyn.*, *46*(1–2), 637–650, doi:10.1007/s00382-015-2603-4.

Tachiiri, K., M. Shinoda, B. Klinkenberg, and Y. Morinaga (2008), Assessing Mongolian snow disaster risk using livestock and satellite data, *J. Arid Environ.*, *72*(12), 2251–2263, doi:10.1016/j.jaridenv.2008.06.015.

Tachiiri, K., and M. Shinoda (2012), Quantitative risk assessment for future meteorological disasters reduced livestock mortality in Mongolia, *Clim. Change*, *113*(3–4), 867–882, doi:10.1007/s10584-011-0365-5.

Takemura, T., Y. J. Kaufman, L. A. Remer, and T. Nakajima (2007), Two competing pathways of aerosol effects on cloud and precipitation formation, *Geophys. Res. Lett.*, *34*, L04802, doi:10.1029/2006GL028349.

Tanaka, H. L., N. Ishizaki, and D. Nohara (2005), Intercomparison of the intensities and trends of Hadley, Walker and monsoon circulations in the global warming projections, *SOLA*, *1*, 77–80, doi:10.2151/sola.2005.021.

Tarnavsky, E., M. Mulligan, M. Ouessar, A. Faye, and E. Black (2013), Dynamic hydrological modeling in drylands with TRMM based rainfall, *Remote Sens.*, *5*(12), 6691–6716, doi:10.3390/rs5126691.

Taylor, C. M., E. F. Lambin, N. Stephenne, R. J. Harding, and R. L. H. Essery (2002), The influence of land use change on climate in the Sahel, *J. Clim.*, *15*, 3615–3629.

Teller, A., and Z. Levin (2006), The effects of aerosols on precipitation and dimensions of subtropical clouds: A sensitivity study using a numerical cloud model, *Atmos. Chem. Phys.*, *6*, 67–80, doi:10.5194/acp-6-67-2006.

Thompson, L. G., E. Mosley-Thompson, M. E. Davis, P. Lin, K. A. Henderson, J. Cole-Dai, J. F. Bolzan, and K. Liu (1995), A 1000 year climate ice-core record from the Guliya ice cap, China: Its relationship to global climate variability, *Ann. Glaciol.*, *21*, 175–181.

Thornthwaite, C. W. (1948), An approach toward a rational classification of climate, *Geogr. Rev.*, *38*(1), 55–94.

Ting, M., and H. Wang (1997), Summertime US precipitation variability and its relation to Pacific sea surface temperature, *J. Clim.*, *10*(8), 1853–1873, doi:10.1175/1520-0442(1997)010<1853:SUSPVA>2.0.CO;2.

Trenberth, K. E., A. Dai, G. van der Schrier, P. D. Jones, J. Barichivich, K. R. Briffa, and J. Sheffield (2014), Global warming and changes in drought, *Nat. Clim. Chang.*, *4*(1), 17–22, doi:10.1038/nclimate2067.

Treydte, K., G. H. Schleser, G. Helle, D. C. Frank, M. Winiger, G. H. Haug, and J. Esper (2006), Millennium-long precipitation record from tree ring oxygen isotopes in northern Pakistan, *Nature*, *440*, 1179–1182.

Twomey, S. (1977), The influence of pollution on the shortwave albedo of clouds, *J. Atmos. Sci.*, *34*, 1149–1152, doi:10.1175/1520-0469(1977)034<1149:TIOPOT>2.0.CO;2.

Ukkola, A. M., I. C. Prentice, T. F. Keenan, A. van Dijk, N. R. Viney, R. B. Myneni, and J. Bi (2015), Reduced streamflow in water-stressed climates consistent with CO_2 effects on vegetation, *Nat. Clim. Chang.*, *6*(1), 75–78, doi:10.1038/NCLIMATE2831.

United Nations Convention to Combat Desertification (UNCCD) (1994), *United Nations Convention to Combat Desertification*, p. 58, United Nations, Geneva, Switzerland.

United Nations Development Programme (UNDP) (2014), Environment and energy, drylands development centre, where we work, Accessed 19 Jan 2014.

Uno, I., K. Eguchi, K. Yumimoto, T. Takemura, A. Shimizu, M. Uematsu, Z. Liu, Z. Wang, Y. Hara, and N. Sugimoto (2009), Asian dust transported one full circuit around the globe, *Nat. Geosci.*, *2*(8), 557–560, doi:10.1038/ngeo583.

Valizadeh, J., S. M. Ziaei, and S. M. Mazloumzadeh (2014), Assessing climate change impacts on wheat production (a case study), *J. Saudi Soc. Agric. Sci.*, *13*(2), 107–115, doi:10.1016/j.jssas.2013.02.002.

Vallejo, V. R., A. Smanis, E. Chirino, D. Fuentes, A. Valdecantos, and A. Vilagrosa (2012), Perspectives in dryland restoration: Approaches for climate change adaptation, *New Forests*, *43*(5–6), 561–579, doi:10.1007/s11056-012-9325-9.

van der Schrier, G., P. D. Jones, and K. R. Briffa (2011), The sensitivity of the PDSI to the Thornthwaite and Penman-Monteith parameterizations for potential evapotranspiration, *J. Geophys. Res.*, *116*, D03106, doi:10.1029/2010JD015001.

Van Loon, A. F., et al. (2016), Drought in the anthropocene, *Nat. Geosci.*, *9*(2), 89–91, doi:10.1038/ngeo2646.

Vecchi, G. A., and B. J. Soden (2007), Global warming and the weakening of the tropical circulation, *J. Clim.*, *20*(17), 4316–4340, doi:10.1175/jcli4258.1.

Verstraete, M. M., A. B. Brink, R. J. Scholes, M. Beniston, and M. S. Smith (2008), Climate change and desertification: Where do we stand, where should we go?, *Global Planet. Change*, *64*(3–4), 105–110, doi:10.1016/j.gloplacha.2008.09.003.

Vicente-Serrano, S. M., S. Beguería, J. I. López-Moreno, M. Angulo, and A. El Kenawy (2010), A new global 0.5° gridded dataset (1901–2006) of a multiscalar drought index: Comparison with current drought index datasets based on the Palmer drought severity index, *J. Hydrometeol.*, *11*, 1033–1043.

Vicente-Serrano, S. M., S. Beguería, J. Lorenzo-Lacruz, J. J. Camarero, J. I. López-Moreno, C. Azorin-Molina, J. Revuelto, E. Morán-Tejeda, and A. Sanchez-Lorenzo (2012), Performance of drought indices for ecological, agricultural, and hydrological applications, *Earth Interact.*, *16*(10), 1–27.

Vinoj, V., P. J. Rasch, H. Wang, J. Yoon, P. Ma, K. Landu, and B. Singh (2014), Short-term modulation of Indian summer monsoon rainfall by West Asian dust, *Nat. Geosci.*, *7*(4), 308–313, doi:10.1038/NGEO2107.

Vogel, M. M., R. Orth, F. Cheruy, S. Hagemann, R. Lorenz, B. J. J. M. van den Hurk, and S. I. Seneviratne (2017), Regional amplification of projected changes in extreme temperatures strongly controlled by soil moisture-temperature feedbacks, *Geophys. Res. Lett.*, *44*, 1511–1519, doi:10.1002/2016GL071235.

Walker, C. C., and T. Schneider (2006), Eddy influences on Hadley circulations: Simulations with an idealized GCM, *J. Atmos. Sci.*, *63*(12), 3333–3350, doi:10.1175/jas3821.1.

Wallace, J. M., Y. Zhang, and L. Bajuk (1996), Interpretation of interdecadal trends in Northern Hemisphere surface air temperature, *J. Clim.*, *9*(2), 249–259, doi:10.1175/1520-0442(1996)009<0249:IOITIN>2.0.CO;2.

Wallace, J. M., Q. Fu, B. V. Smoliak, P. Lin, and C. M. Johanson (2012), Simulated versus observed patterns of warming over the extratropical Northern Hemisphere continents during the cold season, *Proc. Natl. Acad. Sci.*, *109*, 14337–14342, doi:10.1073/PNAS.1204875109.

Wallén, C. C. (1967), Aridity definitions and their applicability, *Geografiska Annaler, Series A, Physical Geography*, *49*(2/4), 367–384, doi:10.2307/520903.

Wang, G. (2005), Agricultural drought in a future climate: Results from 15 global climate models participating in the IPCC 4th assessment, *Clim. Dyn.*, *25*(7), 739–753, doi:10.1007/s00382-005-0057-9.

Wang, G., J. Huang, W. Guo, J. Zuo, J. Wang, J. Bi, Z. Huang, and J. Shi (2010), Observation analysis of land-atmosphere interactions over the Loess Plateau of Northwest China, *J. Geophys. Res.*, *115*, D00K17, doi:10.1029/2009JD013372.

Wang, H., Y. Chen, and Z. Chen (2013), Spatial distribution and temporal trends of mean precipitation and extremes in the arid region, northwest of China, during 1960—2010, *Hydrol. Process.*, *27*(12), 1807–1818, doi:10.1002/hyp.9339.

Wang, K., and R. E. Dickinson (2013), Contribution of solar radiation to decadal temperature variability over land, *Proc. Natl. Acad. Sci.*, *110*(37), 14877–14882, doi:10.1073/pnas.1311433110.

Wang, L., W. Chen, and R. Huang (2008), Interdecadal modulation of PDO on the impact of ENSO on the east Asian winter monsoon, *Geophys. Res. Lett.*, *35*, L20702, doi:10.1029/2008GL035287.

Wang, L., P. D'Odorico, J. P. Evans, D. J. Eldridge, M. F. McCabe, K. K. Caylor, and E. G. King (2012), Dryland ecohydrology and climate change: Critical issues and technical advances, *Hydrol. Earth Syst. Sci.*, *16*(8), 2585–2603, doi:10.5194/hess-16-2585-2012.

Wang, L., C. Wei, and G. Huang (2016), Changes of the transitional climate zone in East Asia: Past and future, *Clim. Dyn.*, doi:10.1007/s00382-016-3400-4.

Wang, N., X. Jiang, L. G. Thompson, and M. E. Davis (2007), Accumulation rates over the past 500 years recorded in ice cores from the Northern and Southern Tibetan Plateau, China, *Arct. Antarct. Alp. Res.*, *39*(4), 671–677, doi:10.1657/1523-0430(07-507)[WANG]2.0.CO;2.

Wang, S., J. Huang, Y. He, and Y. Guan (2014), Combined effects of the Pacific Decadal Oscillation and El Niño-Southern Oscillation on global land dry-wet changes, *Sci. Rep.*, *4*, 6651, doi:10.1038/srep06651.

Wang, W., J. Huang, P. Minnis, Y. Hu, J. Li, Z. Huang, J. K. Ayers, and T. Wang (2010), Dusty cloud properties and radiative forcing over dust source and downwind regions derived from A-train data during the Pacific dust experiment, *J. Geophys. Res.*, *115*, D00H35, doi:10.1029/2010JD014109.

Wang, W., A. Evan, C. Flamant, and C. Lavaysse (2015), On the decadal scale correlation between African dust and Sahel rainfall: The role of Saharan heat low-forced winds, *Sci. Adv.*, *1*(9), e1500646, doi:10.1126/sciadv.1500646.

Wang, Y., et al. (2005), The Holocene Asian Monsoon: Links to solar changes and North Atlantic climate, *Science*, *308*(5723), 854–857.

Wang, Y., K. -H. Lee, Y. Lin, M. Levy, and R. Zhang (2014), Distinct effects of anthropogenic aerosols on tropical cyclones, *Nat. Clim. Chang.*, *4*(5), 368–373, doi:10.1038/nclimate2144.

Waple, A. M., et al. (2002), Climate assessment for 2001, *Bull. Am. Meteorol. Soc.*, *83*(6), S1–S62.

Wardle, D. A. (2013), Ecology: Drivers of decoupling in drylands, *Nature*, *502*, 628–629, doi:10.1038/502628a.

Warren, A., Y. C. Sud, and B. Rozanov (1996), The future of deserts, *J. Arid Environ.*, *32*(1), 75–89, doi:10.1006/jare.1996.0007.

Wells, N., S. Goddard, and M. J. Hayes (2004), A self-calibrating Palmer Drought Severity Index, *J. Clim.*, *17*, 2335–2351.

Wen, G., and C. Fu (2000), Defination of climate and ecological transitional zones with satellite data sets [in Chinese], *Chinese J. Atmos. Sci.*, *24*(3), 324–332.

Wentz, F. J., L. Ricciardulli, K. Hilburn, and C. Mears (2007), How much more rain will global warming bring?, *Science*, *317*(5835), 233–235, doi:10.1126/science.1140746.

White, R. P., and J. Nackoney (2003), *Drylands, People and Ecosystem Goods and Services*, World Resources Institute, Washington.

Winslow, M., B. I. Shapiro, R. Thomas, and S. V. R. Shetty (2004), Desertification, drought, poverty and agriculture: Research lessons and opportunities, Aleppo, Syria. [Available at https://www.researchgate.net/publication/237508819.]

Woollings, T., B. Harvey, and G. Masato (2014), Arctic warming, atmospheric blocking and cold European winters in CMIP5 models, *Environ. Res. Lett.*, *9*(1), 468–475, doi:10.1088/1748-9326/9/1/014002.

Wu, G., G. Ren, D. Wang, Z. Shi, and D. Warrington (2013), Above- and below-ground response to soil water change in an alpine wetland ecosystem on the Qinghai-Tibetan Plateau, China, *J. Hydrol.*, *476*, 120–127, doi:10.1016/j.jhydrol.2012.10.031.

Wu, M., G. Schurgers, M. Rummukainen, B. Smith, P. Samuelsson, C. Jansson, J. Siltberg, and W. May (2016), Vegetation-climate feedbacks modulate rainfall patterns in Africa under future climate change, *Earth Syst. Dyn.*, *7*(3), 627–647, doi:10.5194/esd-7-627-2016.

Wu, Q., and D. M. Straus (2004), AO, COWL, and observed climate trends, *J. Clim.*, *17*(11), 2139–2156, doi:10.1175/1520-0442(2004)017<2139:ACAOCT>2.0.CO;2.

Wu, Z., N. Huang, J. M. Wallace, B. V. Smoliak, and X. Chen (2011), On the time-varying trend in global-mean surface temperature, *Clim. Dyn.*, *37*(3–4), 759–773, doi:10.1007/s00382-011-1128-8.

Xi, X., and I. N. Sokolik (2016), Quantifying the anthropogenic dust emission from agricultural land use and desiccation of the Aral Sea in Central Asia, *J. Geophys. Res. Atmos.*, *121*, 12,270–12,281, doi:10.1002/2016JD025556.

Xia, X., et al. (2016), Ground-based remote sensing of aerosol climatology in China: Aerosol optical properties, direct rdiative effect and its parameterization, *Atmos. Environ.*, *124*, 243–251, doi:10.1016/j.atmosenv.2015.05.071.

Xie, Y., J. Huang, and Y. Liu (2016), From accelerated warming to warming hiatus in China, *Int. J. Climatol.*, *37*, 1758–1773, doi:10.1002/joc.4809.

Xu, D., X. Kang, D. Qiu, D. Zhuang, and J. Pan (2009), Quantitative assessment of desertification using landsat data on a regional scale—A case study in the Ordos Plateau, China, *Sensors*, *9*(3), 1738–1753, doi:10.3390/s90301738.

Xu, L., H. Zhou, L. Du, H. Yao, and H. Wang (2015), Precipitation trends and variability from 1950 to 2000 in arid lands of Central Asia, *J. Arid Land.*, *7*(4), 514–526, doi:10.1007/s40333-015-0045-9.

Xue, Y., and J. Shukla (1993), The influence of land-surface properties on Sahel climate. 1. Desertification, *J. Clim.*, *6*, 2232–2245.

Yan, H., Z. Li, J. Huang, M. Cribb, and J. Liu (2014), Long-term aerosol-mediated changes in cloud radiative forcing of deep clouds at the top and bottom of the atmosphere over the southern Great Plains, *Atmos. Chem. Phys.*, *14*, 7113–7124, doi:10.5194/acpd-14-7113-2014.

Yang, B., J. Wang, A. Braeuning, Z. Dong, and J. Esper (2009), Late Holocene climatic and environmental changes in arid Central Asia, *Quatern. Int.*, *194*, 68–78, doi:10.1016/j.quaint.2007.11.020.

Yang, X., K. Zhang, B. Jia, and L. Ci (2005), Desertification assessment in China: An overview, *J. Arid Environ.*, *63*(2), 517–531, doi:10.1016/j.jaridenv.2005.03.032.

Yao, Y., D. Luo, A. Dai, and I. Simmonds (2017), Increased quasi-stationarity and persistence of winter Ural blocking and Eurasian extreme cold events in response to Arctic warming. Part I: Insights from observational analyses, *J. Clim.*, *30*, 3549–3568, doi:10.1175/JCLI-D-16-0261.1.

Yeh, T. C., and C. Fu (1984), Climatic change—A global and multidisciplinary themes, in *Global Change*, edited by T. F. Malone and J. G. Roederer, pp. 236–244, Cambridge Univ. Press, Cambridge.

Yin, D., M. L. Roderick, G. Leech, F. Sun, and Y. Huang (2014), The contribution of reduction in evaporative cooling to higher surface air temperatures during drought, *Geophys. Res. Lett.*, *41*, 7891–7897, doi:10.1002/2014GL062039.

Yin, J. H. (2005), A consistent poleward shift of the storm tracks in simulations of 21st century climate, *Geophys. Res. Lett.*, *32*, L18701, doi:10.1029/2005GL023684.

Yoshioka, M., N. M. Mahowald, A. J. Conley, W. D. Collins, D. W. Fillmore, C. S. Zender, and D. B. Coleman (2007), Impact of desert dust radiative forcing on Sahel precipitation: Relative importance of dust compared to sea surface temperature variations, vegetation changes, and greenhouse gas warming, *J. Clim.*, *20*(8), 1445–1467, doi:10.1175/JCLI4056.1.

Yu, M., G. Wang, and J. S. Pal (2015), Effects of vegetation feedback on future climate change over West Africa, *Clim. Dyn.*, *46*(11–12), 3669–3688, doi:10.1007/s00382-015-2795-7.

Zaman, M. A., A. Rahman, and K. Haddad (2012), Regional flood frequency analysis in arid regions: A case study for Australia, *J. Hydrol.*, *475*, 74–83, doi:10.1016/j.jhydrol.2012.08.054.

Zeng, N., and J. Yoon (2009), Expansion of the world's deserts due to vegetation-albedo feedback under global warming, *Geophys. Res. Lett.*, *36*, L17401, doi:10.1029/2009GL039699.

Zhai, P., X. Zhang, H. Wan, and X. Pan (2005), Trends in total precipitation and frequency of daily precipitation extremes over China, *J. Clim.*, *18*(7), 1096–1108, doi:10.1175/JCLI-3318.1.

Zhang, G., M. Cai, and A. Hu (2013), Energy consumption and the unexplained winter warming over Northern Asia and North America, *Nat. Clim. Chang.*, *3*(5), 466–470, doi:10.1038/nclimate1803.

Zhang, H., G. M. McFarquhar, S. M. Saleeby, and W. R. Cotton (2007), Impacts of Saharan dust as CCN on the evolution of an idealized tropical cyclone, *Geophys. Res. Lett.*, *34*, L14812, doi:10.1029/2007GL029876.

Zhang, J., J. A. Holmes, F. Chen, M. Qiang, A. Zhou, and S. Chen (2008), An 850-year ostracod-shell trace-element record from Sugan Lake on the northern Tibetan Plateau: Implications for interpreting the shell chemistry in high-Mg/Ca waters, *Quatern. Int.*, *194*, 119–133, doi:10.1016/j.quaint.2008.05.003.

Zhang, J., J. Niu, A. Buyantuev, and J. Wu (2014), A multilevel analysis of effects of land use policy on land-cover change and local land use decisions, *J. Arid Environ.*, *108*, 19–28, doi:10.1016/j.jaridenv.2014.04.006.

Zhang, K., J. Kimball, R. Nemani, S. Running, Y. Hong, J. Gourley, and Z. Yu (2015), Vegetation greening and climate change promote multidecadal rises of global land evapotranspiration, *Sci. Rep.*, *5*, 15956, doi:10.1038/srep15956.

Zhang, X., R. Arimoto, and Z. An (1997), Dust emission from Chinese desert sources linked to variations in atmospheric circulation, *J. Geophys. Res.*, *102*(D23), 28041–28047, doi:10.1029/97JD02300.

Zhang, X., and L. Jin (2016), Association of the Northern Hemisphere circumglobal teleconnection with the Asian summer monsoon during the Holocene in a transient simulation, *Holocene*, *26*(2), 290–301, doi:10.1177/0959683615608689.

Zhang, Y., J. M. Wallace, and D. S. Battisti (1997), ENSO-like interdecadal variability: 1900–93, *J. Clim.*, *10*(5), 1004–1020, doi:10.1175/1520-0442(1997)010<1004:ELIV>2.0.CO;2.

Zhang, Y., and L. Zhang (2005), Preipitation and temperature probability characteristic in climatic and ecological transition zone of Northeast China in recent 50 years [in Chinese], *Scientia Geographica Sinica*, *25*(5), 561–599.

Zhao, S., H. Zhang, S. Feng, and Q. Fu (2015), Simulating direct effects of dust aerosol on arid and semi-arid regions using an aerosol-climate coupled system, *Int. J. Climatol.*, *35*(8), 1858–1866, doi:10.1002/joc.4093.

Zhao, T., L. Chen, and Z. Ma (2014), Simulation of historical and projected climate change in arid and semiarid areas by CMIP5 models, *Chin. Sci. Bull.*, *59*, 414–429.

Zhao, T., and A. Dai (2015), The magnitude and causes of global drought changes in the 21st century under a low-moderate emissions scenario, *J. Clim.*, *28*, 4490–4512, doi:10.1175/JCLI-D-14-00363.1.

Zhao, T., and A. Dai (2016), Uncertainties in historical changes and future projections of drought, Part II: Model-simulated historical and future drought changes, *Clim. Change*, 1–14, doi:10.1007/s10584-016-1742-x.

Zhao, Y., Z. Yu, and F. Chen (2008), Spatial and temporal patterns of Holocene vegetation and climate changes in arid and semi-arid China, *Quatern. Int.*, *194*, 6–18.

Zhao, Y., S. Peth, P. Hallett, X. Wang, M. Giese, Y. Gao, and R. Horn (2011), Factors controlling the spatial patterns of soil moisture in a grazed semi-arid steppe investigated by multivariate geostatistics, *Ecohydrology*, *4*(1), 36–48, doi:10.1002/eco.121.

Zhao, Y., and H. Zhang (2015), Impacts of SST warming in tropical Indian Ocean on CMIP5 model-projected summer rainfall changes over Central Asia, *Clim. Dyn.*, *46*(9–10), 3223–3238, doi:10.1007/s00382-015-2765-0.

Zhong, Y., Z. Liu, and M. Notaro (2011), A GEFA assessment of observed global ocean influence on US precipitation variability: Attribution to regional SST variability modes, *J. Clim.*, *24*(3), 693–707, doi:10.1175/2010JCLI3663.1.

Zhou, L., H. Chen, and Y. Dai (2015), Stronger warming amplification over drier ecoregions observed since 1979, *Environ. Res. Lett.*, *10*(6), 064012), doi:10.1088/1748-9326/10/6/064012.

Zhou, L., H. Chen, W. Hua, Y. Dai, and N. Wei (2016), Mechanisms for stronger warming over drier ecoregions observed since 1979, *Clim. Dyn.*, *47*(9), 2955–2974, doi:10.1007/s00382-016-3007-9.

Zhu, G., L. Lu, Y. Su, X. Wang, X. Cui, J. Ma, J. He, K. Zhang, and C. Li (2014), Energy flux partitioning and evapotranspiration in a sub-alpine spruce forest ecosystem, *Hydrol. Process.*, *28*(19), 5093–5104, doi:10.1002/hyp.9995.

Zinyengere, N., O. Crespo, S. Hachigonta, and M. Tadross (2014), Local impacts of climate change and agronomic practices on dry land crops in southern Africa, *Agric. Ecosyst. Environ.*, *197*, 1–10, doi:10.1016/j.agee.2014.07.002.